ÇUKUROVA UNIVERSITY
INSTITUTE OF NATURAL AND APPLIED SCIENCES

MSc. THESIS

Leila NAJAFI

NUMERICAL AND EXPERMENTAL INVESTIGATION OF FLOW AROUND YAWED CYLINDERS IN TANDEM ARRANGEMENT

DEPARTMENT OF MECHANICAL ENGINEERING

ADANA, 2014

ÇUKUROVA ÜNİVERSİTESİ
FEN BİLİMLERİ ENSTİTÜSÜ

NUMERICAL AND EXPERMENTAL INVESTIGATION OF FLOW AROUND YAWED CYLINDERS IN TANDEM ARRANGEMENT

Leila NAJAFI

MASTER TEZİ

MAKİNA MÜHENDİSLİĞİ ANABİLİM DALI

Bu Tez ..../..../2014 Tarihinde Aşağıdaki Jüri Üyeleri Tarafından Oybirliği/Oyçokluğu İle Kabul Edilmiştir.

……...	…….	……
Prof. Dr. Hüseyin AKILLI	Prof. Dr. Beşir ŞAHİN	Doç. Dr. Sami AKÖZ
DANIŞMAN	ÜYE	ÜYE

Bu Tez Enstitümüz Makina Mühendisliği Anabilim Dalında Hazırlanmıştır.
Kod No:

Prof. Dr. Mustafa GÖK
Enstitü Müdürü

ABSTRACT

MSc THESIS

NUMERICAL AND EXPERMENTAL INVESTIGATION OF FLOW AROUND YAWED CYLINDERS IN TANDEM ARRANGEMENT

Leila NAJAFI

ÇUKUROVA UNIVERSITY
INSTITUTE OF NATURAL AND APPLIED SCIENCES
DEPARTMENT OF MECHANICAL ENGINEERING

Supervisor : Prof. Dr. Hüseyin AKILLI
Year : 2014, Pages: 123
Jury : Prof. Dr. Hüseyin AKILLI
: Prof. Dr. Beşir ŞAHİN
: Assoc.Prof. Dr. M. Sami AKÖZ

The aim of present research is to investigate the flow structure around a single yawed cylinder and two yawed cylinders both numerically and experimentally. In this purpose, the main circular was 50 mm in diameter and 60 cm in length is set against the fluid flow for the single cylinder case at a Reynolds number = 5000.The paricle imaging velocimetry (PIV) technique is used to investigate the wake structure experimentally. Single yawed cylinder was investigated in the water tunnel under steady upstream cross-flow conditions with angle configurations from $\alpha = 0^o$ to 60^o with 5^o increments. For the case of two yawed cylinders, in order to understand the effects of gap ratio and yaw angle on the flow structure around two yawed cylinders in tandem, nine different gap ratios from L/D = 1 to 5 with 0.5 increments and five different yaw angles of α = 0, 15, 20, 25 and 30 were considered. ANSYS CFX software was used for numerical studies. The results obtained from CFX were compared with PIV results. SST turbulence model that was based on $k - \omega$ was used for the turbulence modeling.

Key Words: Circular cylinder**,** Yaw angle, PIV, Ansys CFX, Vortex shedding,

ÖZ

YKSEK LISANS TEZİ

EĞİK DURUMDAKİ ARKA ARKAYA İKİ SİLİNDİR ARDINDAKİ AKIŞ YAPISININ EĞİM AÇISIYLA DEĞİŞİMİNİN SAYISAL

Leila NAJAFI

ÇUKUROVA ÜNİVERSİTESİ
FEN BİLİMLERİ ENSTİTÜSÜ
MAKİNA MÜHENDİSLİĞİ ANABİLİM DALI

Danışman : Prof. Dr.Hüseyin AKILLI
Yıl: 2014, Sayfa:123
Jüri : Prof. Dr.Hüseyin AKILLI
: Prof. Dr. Beşir ŞAHİN
: Doç. Dr. M. Sami AKÖZ

Bu çalışmanın amacı, eğik durumdaki tek silindir ve iki silindir arasındaki mesafenin ve eğim açısının akış yapısının nümerik ve deneysel olarak araştırılmasıdır. Bu maksatla, çapı 50 mm olan ve 60 cm uzunluğunda dairesel silindir kullanılmıştır ve silindir çapına bağlı Reynolds sayısı Re_D=5000 olarak belirlenmiştir. Art izibölgesindeki akış yapısını incelemek için yapılan deneylerde Parçacık Görüntülemeli Hız Ölçüm Tekniği (PIV) sistemi kullanılmıştır. Tek silindir, farklı eğim açıları konfigürasyonunda (α =0^o'den 60^o'ye kadar 5^o'lik artımla) derin su kanalı içerisinde incelenmiştir. İki silindir durumu için ise, art arda yerleşmiş eğik iki silindir arasındaki mesafenin etkisini anlamak için, dokuz farklı boşluk oranı (L/D= 1'den 5'e kadar, 0.5 artımla) ve beş farklı eğim açısı (a=0 ,15 ,20 ,25 ve 30) göz önüne alınmıştır. Nümerik simülasyon için ANSYS CFX programı kullanılmıştır. Nümerik simülasyonda elde edilen sonuçlar, PIV sonuçları ile karşılaştırılmıştır. Çalışmada, k – ω yöntemine dayalı SST türbülans modeli kullanılmıştır.

Anahtar Kelimeler: Dairesel silindir, eğim açısı, PIV, Ansys CFX, Girdap kopması

ACKNOWLEDGEMENTS

I would never have been able to finish my dissertation without the guidance of my advisor, help from friends, and support from my family .

I would like to express my deepest gratitude to my advisor Prof. Dr. Hüseyin AKILLI, for his excellent guidance, caring, patience, and providing me with an excellent atmosphere for doing research. Knowing and feeling his support during my thesis helped me a lot.

I would also like to thank Professor.Dr. Beşir ŞAHİN for their very useful comments.

My heartfelt thanks go to Research Assistant Erhan FIRAT. My research would not have been possible without their helps in PIV lab and for excellant friendship.

Many thanks go to my freinds Assistant prof Dr.Bengi GOZMEN for her help and moral support and excellant freindship.

I would like to thank to Assistant prof. Dr Çetin Canpolat, , Assistant prof. Engin PINAR ,Research Assistant Göktürk ÖZKAN , Research Assistant Tahir DURHASAN and Research Assistant Vali ÖZBOLAT for helping in my study and for their friendship.

Last but not least, I am greatly indebted to my father Hossein NAJAFI, my mother Zahra NAJAFI. My parents, brother and sister have given me their unequivocal support throughout, as always, for which my mere expression of thanks likewise does not suffice.

CONTENTS **PAGE**

LIST OF FIGURES PAGE

LIST OF TABLES PAGE

LIST OF ABBREVIATONS

D : Cylinder diameter

H : Depth of the water in the channel

ν : Kinematic viscosity

Re : Reynolds number

U : Free stream velocity

$< u'u' >$: Streamwise Reynolds normal stress

$< v'v' >$: Transverse Reynolds normal stress

$< u'v' >$: Reynolds shear stress

$< u >$: Streamwise velocity

TKE : Turbulent Kinetic Energy

h_D : Submerged height from the free surface for cylinders

Dt : Time interval

Sp : Saddle point

L/D : Gap ratio

S_t : Strouhal number

f : Frequency

L_c : Length of the cylinder

α :yaw angle

1. INTRODUCTION

The flow around circular cylinders has been extensively studied due to its practical importance in engineering and scientific relevance in fluid mechanics. On the engineering side, there are a number of devices in mechanical, civil and naval engineering where circular-cylindrical structures are used. Samples of such devices are heat exchangers, chimneys and offshore platforms. In scientific terms, the flow around circular cylinders exhibits various important physical phenomena, such as separation, vortex shedding and turbulence in the wake, at relatively low flow speed. When circular cylinders are grouped in close proximity, the flow field and the forces experienced by the cylinders are entirely different from those observed when the bodies are isolated in the fluid stream. The effect of the presence of other bodies in the flow is called flow interference, and it has crucial importance in aerodynamics and hydrodynamics. For example, in all the devices mentioned at the beginning of this chapter it is common to have circular-cylindrical structures grouped together.

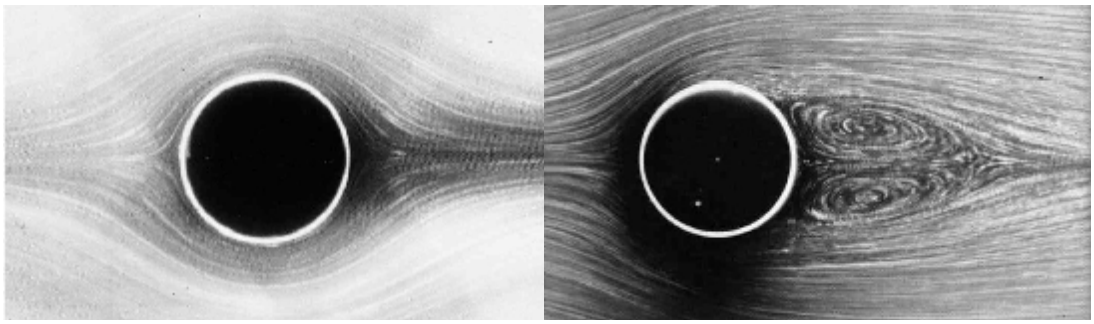

(a) Re = 0.16 (b) Re = 26

Figure 1.1 .Visualization of low Reynolds number flows around a circular cylinder. (a) creeping flow, (b) steady symmetric separated flow. Flow is from left to right. Adapted from Van Dyke (1982).

Flow over bluff bodies, in association with the flow over an obstacle or the movement of a body, are commonly encountered in nature and engineering applications. Typical examples within the context of marine applications are the flows past a submarine, a ship, the legs of an oil platform, and a riser. The three-dimensional complexity that these flows possess makes them a significant topic of

research by means of experiments and numerical simulations, being perhaps the flow past a circular cylinder the bluff-body configuration that have received most of the attention during the 20th century (see for instance the work by Zdravkovich, 1997). In many cases, however, cylindrical geometries are non-uniform, introducing further complexities into the flow features that are interesting to study.

1.1. APPLICATION

For most objects whose are in against of flow, there is a possibility of creating fluctuations and vibrations which is induced by the fluid flow. Phenomena associated are known as a flow induced vibration (FIV) with fluid flow. This phenomenon occurs in many engineering fields, as a instance, it can be cited to design of structures such as bridges, chimneys, electrical transmission lines (electrical current cables), airplane wings, offshore structures, risers on oil platforms extraction, heat exchangers, pipelines, marine cables and submarine components.

These uncontrolled vibrations can be a reason of damage to building. One of the inherent reasons of creating vibrations in these cases, induced of occurring flow separation and forming vortex structures on the wake. The vortex structure makes body vibration by fluctuating of aerodynamics forces on body. The group of vibrations induced by fluid flow wake is called Vortex Induced Vibration (VIV) ,which the inherent factor of their happening due to create vortex structures in downstream of body .

Because of cylindrical structures were used in most structures widely, Study of fluid flow around them and forces on these structures has a specific importance.Therefore in recent decades and With progression of measurement equipment and revealing fluid flow structure in the other hand ,also development of computers as tools for calculation and simulation of fluid flow, Several studies has been done on this filed.

One of the most important fields, is oil and gas extraction risers from Sea depth. These risers have cylindrical structures , and the vibrations problems are the

most challenge. Various methods to reduce and eliminate these fluctuations have been proposed by studying the flow around the cylinder.

Figure 1.2. (a)Oil platform - (b) Oil and gas extraction risers

1.2. Flow past circular cylinders

One of the most popular problems in fluid mechanics is the flow around a uniform circular cylinder. The fact that there is a huge amount of available literature on this subject is not surprising, since flow past cylinders has been a topic of theoretical, experimental and numerical research for many years. In the extensive review made by Zdravkovich (1997), three main components of the flow past a circular cylinder (and past a bluff body in general) are mentioned: the boundary layer, the separated shear layers and the wake (see figures 1.4). In the absence of surface roughness and blockage effects, these interacting components undergo a transition process towards turbulence that depends on only one parameter of the flow, namely the Reynolds number, Re, which is defined as

$$\mathrm{Re} = \frac{UD}{\nu}$$

with U the characteristic velocity of the incoming flow, D the cylinder diameter and v the kinematic viscosity of the fluid. Some stages of this transition process as Re increases are summarized in this section.

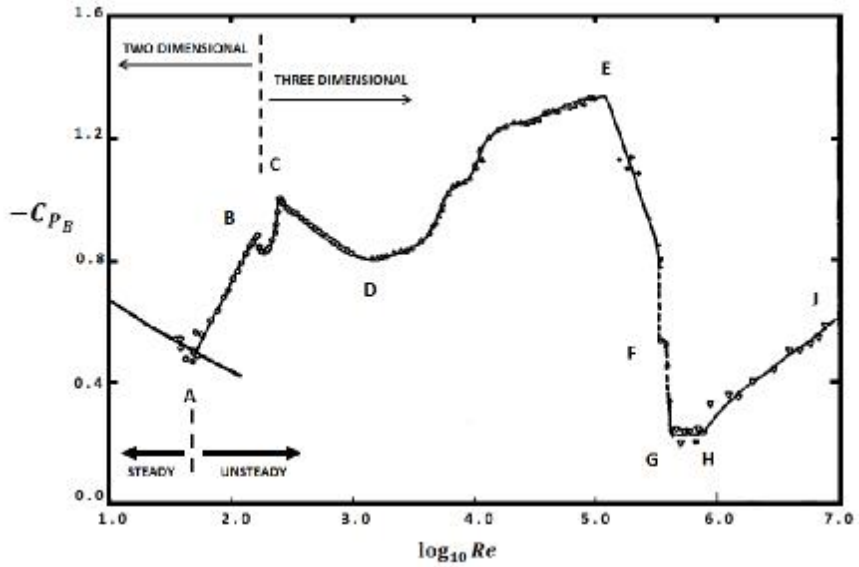

Figure 1.3. Classification of flow regimes according to the plot of base suction coefficients (CPB) over a large range of Reynolds numbers (Williamson, 1996)

For Re < 6, the flow is steady and two-dimensional with only one separation point at the rear stagnation point. For the range of 6 < Re <49, the flow is still steady, two-dimensional and flow separates from the trailing edge of the cylinder. In addition, stationary vortex pair (Figure 1.4) occur in the wake whose recirculation length grows as the Reynolds number increases.

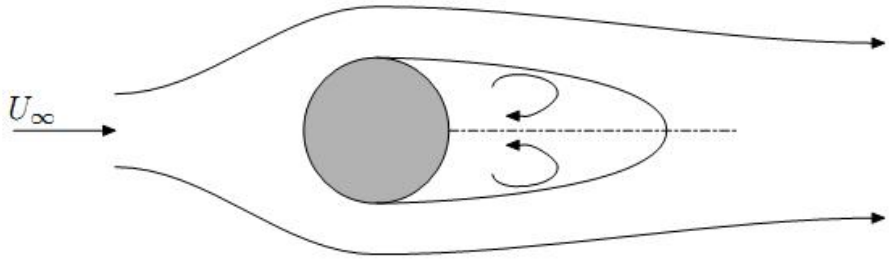

Figure 1.4. Schematic of Steady wake

At the critical number (Re≈ 49), although all the imposed conditions are being held steady, instability increases suddenly and vortex shedding forms downstream of the circular cylinder, resulting in the well-known von Karman vortex street.

The mechanism of vortex shedding proposed by Gerrard (1964) was presented in Figure 1.5. The main reason of the formation of vortex-street wake is commutual

interaction between the two separating shear layers. A vortex, named as upper vortex, goes on to grow by feeding with circulation from its connected shear layer until it draws the opposing shear layer across the near wake. This drawn shear layer (forming lower vortex) transports fluid with oppositely signed vorticity along with it and exterminates and cuts off supply of circulation to the upper vortex which results in the shedding of the upper vortex. In the next turn, this lower vortex grows sufficiently, it would draw the upper shear layer across the wake and a result of extermination, lower vortex would be shed and moves off downstream.

This cycle repeats and alternates shedding of vortices from either side forming a vortex street downstream of the body. Gerrrard's vortex-formation model observes that entrainment has an important role to form a vortex street which is mentioned above. In Figure 1.5, Gerrard indicates entrainment flows in vortex formation. At this model, entrained fluid "a" is pulled into the growing vortex while fluid "b" moves into the developing shear layer. And some fluid "c" is temporarily entrained into the oscillating wake region between the base of the body and the growing vortex.

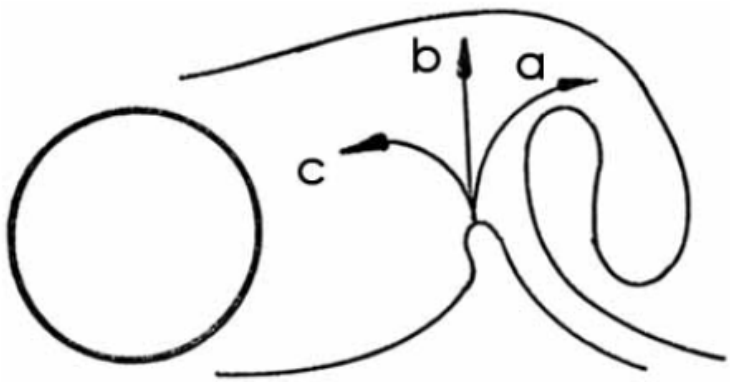

Figure 1.5. The vortex shedding mechanism by Gerrard (1964)

For 49 < Re < 194 (regime A-B: laminar vortex shedding regime in Figure (1.3)the recirculation region develops instabilities whose strength and amplification grow with Re resulting in alternating high and low pressure regions on the lee side of the body. As the instability of wake becomes amplified, the effects of Reynolds stresses in the near wake region improve, the formation length shortens, the base suction increases consistently.

For 190 < Re < 260 (regime B-C: 3D wake transition regime), the wake first develops a secondary instability and intrinsic three dimensionality which seems in a regular spanwise structure in Williamson's (1988) flow visualization. In the case of higher Reynolds values, i.e. Re > 200, the flow becomes three dimensional and turbulent.

For regime C-D (increasing disorder in the fine-scale three dimensionalities: 260 < Re < 1000), at Re = 260, the peak Reynolds stresses and a particular ordered 3-D streamwise vortex structure in the near wake are effective on the base section. As Re is increased towards point D, three dimensionality starts to be disordered. Hence, reduction in the two-dimensional Reynolds stresses, a consistent reduction in base section and an increasing length of the formation region are observed.

In the shear layer transition regime (D-E: 103 < Re < 2x105), the base section and the 2-D Reynolds stresses increase, whereas the strouhal number and the formation length of the mean recirculation region decrease. And there is an increase in base suction and drag as the turbulent transition point in the separating shear layers moves upstream and Re increases. In addition, for this regime, it is thought that three dimentional structures on the scale of the shear layer vortices develop as well as three dimensionality on the scale of the Karman vortices.

Critical transition (E-G) regime is called "critical transition" in which base suction and drag diminish significantly, because of a separation-reattachment bubble. This bubble revitalizes the boundary layer and it moves the final separation point further downstream on the cylinder to about 140°. This transition continues until point F. At this point, a separation- reattachment bubble forms on only one side of the body, causing a large mean lift forces (CL= 1).

In the supercritical regime (G-H), the flow is symmetric again with two separation-reattachment bubbles. Some fluctuations are discovered in the wake at large Strouhal numbers of around 0.4. The Reynolds stresses of the boundary layer following the separation bubble are considerably higher and this causes the boundary layer to survive a greater adverse pressure gradient than in the post critical regime, where transition finally exists before separation.

For regime H-J (Boundary-layer transition regime or post-critical regime), the boundary layer is fully turbulent and the separation occurs further forward on the cylinder at about 100°, yielding higher drag and base section and a wider downstream wake than in the previous regime.

1.2.1. Flow Separation

The appearance of the fluid viscosity retardeds the fluid particles very close to the solid surface and takes shape like a thin fluid layer called a boundary layer. The flow velocity is zero at the surface because of the no-slip boundary condition.

Due to the flow exposes to a strong viscous flow resistance, flow momentum is substantially low within the boundary layer. Because of this occurance, the boundary layer flow is sensitive to the external pressure gradient which is the form of a pressure force effecting fluid particles.

When the pressure decreases in the direction of the flow, the pressure gradient is said to be favourable. In this position, the pressure force can help the fluid movement and the flow doesn't slow down. But, when the pressure is rising in the direction of the flow, opposite the pressure gradient condition as so it is called exist. Furthermore, the presence of a strong viscous force, the fluid particles have to act opposite of the increasing pressure force. As a result, the fluid particles could be stopped or reversed, causing the neighbouring particles to move away from the surface. This phenomenon is called the boundary layer separation. Consequently, when the velocity at the wall is zero or negative and an inflection point exists in the velocity profile and a positive or adverse pressure gradient occurs in the direction of flow, flow separation is appeared. Figure 1.6 exhibits flow separation.

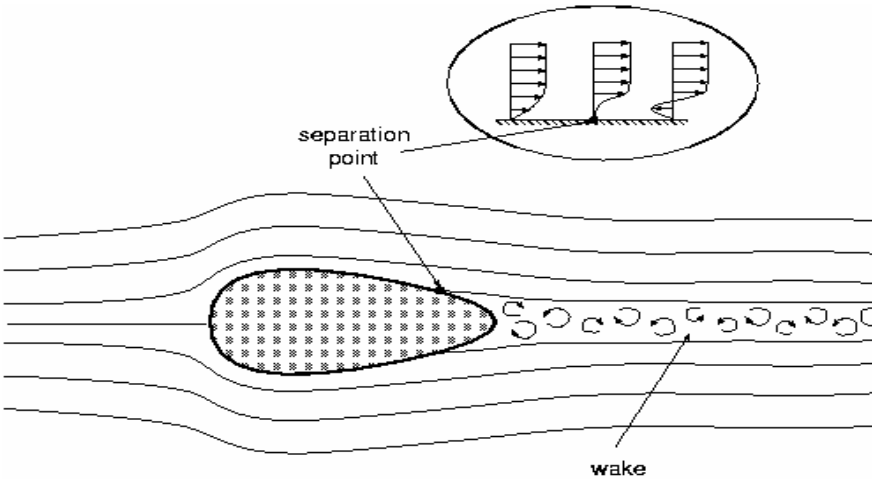

Figure 1.6. Flow Separation

1.3. Flow past Yawed Circular Cylinders

The description given in the previous section applies for cylinders with their axes perpendicular to the free-stream direction. In many engineering applications, however, circular cylinders are positioned at a certain yaw angle a, which is defined as that between the cylinder axis and the normal to the free-stream velocity. A typical flow configuration of the flow past a yawed cylinder is shown in figure 1.7. The response of a yawed cylinder in terms of vortex shedding frequency, base pressure and hydrodynamic forces may differ from the normal incidence case. According to Zdravkovich (2003), the following features are associated to flow past yawed cylinders:

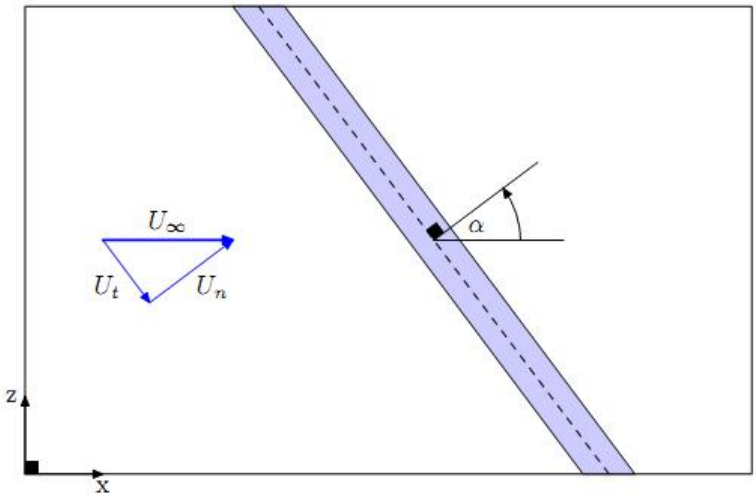

Figure 1.7.Schematic view of the flow past a yawed cylinder. Here α is the yaw angle and U∞ is the inflow velocity, which is decomposed in its normal Un and tangential Ut components. For the configuration shown here, α = 0◦ corresponds to cross flow and α = 90◦ corresponds to axial flow

i. The cross-section of a yawed circular cylinder becomes elliptical, being the ratio of the major-to-minor axis of the ellipse proportional to the yaw angle.

ii. The free stream velocity has two components, one normal to the cylinder axis Un = U∞ cos α, and the other parallel to the cylinder axis Ut = U∞ sin α. From this two, it has been argued that Un has a larger effect on the flow.

A common approach to modelling the hydrodynamics of the flow past yawed cylinders is to use the Independence Principle (IP), also known as the Cosine Law. In this formulation the projected flow in the normal plane, based on the component of the free-stream velocity normal to the cylinder axis Un, is similar to the normal incidence case. Zdravkovich (2003) mentions the following limitations of the IP:

i. Originally the IP was derived from the laminar boundary layer theory, which becomes invalid beyond separation.

ii. As the flow past yawed cylinders is subjected to end effects, the mathematical idealization of two-dimensional flow past cylinders of infinite aspect ratio cannot be realized in practice. This is especially relevant for experimental studies.

iii. The transition around separation for unyawed cylinders occurs at a certain Reynolds number due to instability of the boundary layers. It may be expected that the instability would occur at the same Re for a yawed cylinder, but the spanwise flow is likely to modify the disturbances and the Re value at which separation occurs.

Early attempts to experimentally verify the IP in the laminar regime were done by Hanson (1966). He measured the frequency of the wake trail oscillations, and subsequently the eddy shedding in the range 40 < Re < 150 for the yaw angles 0° < a < 72. It was reported that a has an effect upon the onset of the laminar vortex shedding regime Reosc, based on the free stream velocity Hanson noted that Reosc rises with increasing a. However, when using the local Reynolds number Ren = UnD/u, the critical Reynolds number at which vortex shedding initiates was constant up to a = 50°. Hanson (1966) also studied vortex shedding for low Reynolds number from vibrating yawed hot wires in an air stream. Using the Roshko's number (Ro = fD2/u), Hanson obtained different straight lines of Ro vs. Re for various values of a in the low Reynolds number range 40-150. Scaling this data by Ren gave evidence that the following linear relationship derived for uniform cylinders could be extended for yawed cylinders.

$$Ro_n = 0.212Re_n - 4.5, \qquad \text{for } \alpha \leq 50°.$$

For a = 72°, however, Hanson (1966) noted that the shedding frequencies values (or values of Ro) departed from equation.

In an attempt to explain the apparent discontinuity reported by Hanson (1966) for a in the range 50° < a < 75°, Van Atta (1968) carried out careful measurements of the vortex shedding frequency. For constant Ren, he reported a steady decrease of St as the yaw angle a increases. He concluded that the discontinuity observed by Hanson was not due to the large a, but to the existence of locked-in modes depending on the value of the wire tension. He also reported that for a given tension, the wire does not necessarily vibrate with the frequency of the harmonic that is nearest to the natural shedding frequency, but always locks-in to the frequency that is lower than the natural shedding frequency. In the case of non-vibrating yawed cylinders, Van Atta (1968) showed that for a < 35° the vortex shedding frequency decreases nearly like the IP, whereas for

larger angles the decrease with increasing angle of yaw a is slower than the proposed IP.

Ramberg (1983) studied the effect of yaw angle (a = 0-60°) and end-conditions for stationary and forced vibrating circular cylinders (with aspect ratio 20-100) in the Reynolds number range 150-1000. He found that the results were very sensitive to end-conditions especially at the lower Reynolds numbers, showing that slantwise shedding at angles other than the cylinder yaw angle is intrinsic to stationary inclined cylinders in the absence of end-effects. Ramberg (1983) suggested that the IP fails in the case of stationary yawed cylinders because the shedding frequency is always greater than that expected from the IP, while the shedding angle, the vortex-formation length, the base pressure and the wake width are all less than expected. Nevertheless, he concluded that locked-in vortex wakes of vibrating yawed cylinders can be described successfully by the IP. In this case, frequency lock-in between the vortex wake and the cylinder motion was accompanied by vortex shedding parallel to the cylinder axis.

A numerical study using DNS at Re = 1000 and a yaw angle range 0-60° was conducted by Zhao et al. (2009), showing that the Strouhal frequency at various yaw angles followed the Independence Principle. In this case, the use of DNS allowed for better visualization of additional flow features in the streamlines and the vortical structures. The streamlines approached the leading edge of the cylinder with an increasing bending and sliding along the cylinder, followed by a deflection in the main flow direction. After passing the cylinder, a fraction of the streamlines are retained inside the recirculation region and move in the spanwise direction of the cylinder in helical tracks, while others move in the free stream direction. Once the primary vortex is shed from the cylinder surface, the trapped streamlines are released and their directions change back to the aerodynamics flow direction. The spanwise vortices in this study were identified as isosurfaces of spanwise vorticity uz. At a = 45° the spanwise vortices were shed parallel to the cylinder axis, whereas at a = 60° the shedding angle was less defined. This was in good agreement with a previous study by Lucor and Karniadakis (2003), in which they observed that the spanwise wake vortices are oriented at a smaller angle than the yaw angle of the cylinder for a > 45°. Zhao et al.

(2009) also noticed that the mean pressure coefficient Cp along the surface of the cylinder decreases with increasing a, reducing the difference in pressure between the front and rear stagnation lines as well. The validity of the IP was obtained by normalizing the pressures coefficients by Un, in this case the pressure coefficient curves for different a's collapsed into a single curve. The frequency spectra were obtained for different values of a, no variation in the peak locations with a was detected. Moreover, the peak region for a = 60° was broader than that for the unyawed cylinder, indicating that with the increase of the yaw angle, the rate of the breakdown of the vortical structures is increased.

Using a phase averaged technique, Zhou et al. (2010) investigated the dependence of the wake vortical structures on cylinder yaw angle 0-45°. All three-velocity and vorticity components were measured simultaneously using an eight-hot wire vorticity probe in the intermediate region x/D = 10 of a yawed stationary circular cylinder wake.

It was found that when a < 15°, the maximum coherent concentrations of the three vorticity components do not change with a. However, when a is increased to 45°, the maximum concentrations of the coherent transverse and spanwise vorticity components decrease by about 33% and 50%, respectively, while that of the streamwise vorticity increases by about 70%, suggesting that the strength of the primary vortices shed from the yawed cylinder decreases and the three dimensionality of the flow is enhanced.

2. PRELIMINARY WORK

2.1. Experimentally Investigated

2.1.1. Experimentally Investigated for Flow Past Yawed or Un yawed Bluff Bodies

Flow past yawed or unyawed bluff bodies in widely encountered in engineering applications, such as cable suspension bridges, overhead cables, tow cables, chimney stacks, towers, offshore structures, etc.

How to fully understand the complicated flow phenomena around a yawed cylindrical cable and how to reduce their bodies drag and fluctuating lift are important problems for engineering design. In fundamental research, flow of past circular cylinders have been extensively investigated both experimentally and numerically. Many important physical phenomena were observed. For flow past yawed circular cylinders, Bursnall and Loftin (1951) experimentally investigated the pressure distribution of a yawed circular cylinder in the critical Reynolds number range. They showed that at critical Reynolds number, the flow and force characteristics of a yawed cylinder cannot be determined only by the component of flow normal to the axis of the cylinder when the yaw angle is greater than 45°. Hanson (1966).investigated the vortex shedding frequency of a yawed cylinder at low Reynolds number. Van Atta (1968) found that the Independence Principle (the drag coefficient and the Strouhal number, which are normalized by the velocity component perpendicular to the cylinder, are approximately independent on the yaw angle of the circular cylinder) is true over a wide range of Reynolds number. The Independence Principle (also referred to as the cosine law) is not suitable for the determination of the Strouhal number for cylinders with a yaw angle greater than 60°.Ramberg (1983)experimentally investigated the vortex shedding characteristics on finite-length yawed cylinders. The foregoing researchers further confirmed that the Independence Principle was not suitable for a cylinder at large yaw angle.

Further experimental investigations had been carried out by Shirakashi et al. (1984) , Lourenco et al. (1992) and Hayashi and Kawamura (1995) .

2.2. Numerical Investigated

2.1.2 .Numerical Simulations for Flow Past Yawed or Unyawed Bluff bodies

Moreover, numerical simulations on yawed cylinders had also been carried out Kawamura and Hayashi, (1994); Kaneko and Kawamura, (2002); Lucor and Karniadakis, (2003); Marshall, 2003. Thakur et al. (2004); Yeo and Jones, (2008). Vakil and Green, (2009); Zhao et al.,(2009). Kaneko and Kawamura (2002) used direct numerical simulation (DNS) for flow past a yawed circular cylinder at subcritical Reynolds number of 1000 and found that the Independence Principle fails for the cylinder at large yaw angles. Thakur et al. (2004) showed same vortex shedding characteristics for yawed cylinder similar to that obtained by Van Atta (1968).In addition, Vakil and Green (2009) numerical investigated yawed circular cylinders with finite aspect ratio with aspect ratios from 2 to 20in the Reynolds number range from 1 to 40. Their results showed that the Independence Principle was not accurate for yaw angle larger than 45° in such flow conditions.

Aiming at the reduction of drag and the suppression of the fluctuating lift force on cylindrical structures, most of the experimental and numerical investigations had only been carried out on cross-flow around bluff bodies of unyawed cylinders as summarized by Choi et al. (2008)

At Reynolds number 40 000, a maximum drag reduction of about 30% was obtained by Bearman and Owen (1998). Darekar and Sherwin (2001).

Numerically investigated the flow past a square cylinder with a wavy stagnation face at low Reynolds numbers. They showed that the unsteady and staggered Karman vortex wake could be suppressed to a steady and symmetric wake structure due to the waviness of the square cylinder. A maximum drag reduction of about 16% was obtained at a Reynolds number of 100 compared with the straight, non-wavy square cylinder. At high Reynolds numbers, the drag reduction increases

substantially. More recently, a special type of cylinder namely a wavy cylinder (a circular section cylinder with wavy variation of diameter along the spanwise direction) aiming at the reduction of vortex induced vibration was introduced by Lam et al. (2004).

Lam and Lin (2007, 2008, and 2009) carried out numerical simulations to study the flows around the wavy cylinders. The detailed three-dimensional wake structures behind the wavy cylinders were captured and the optimal values of spanwise wavelength X/Dm base on the control of body's drag reduction were obtained. By using the large eddy simulation (LES) method, Lam and Lin (2008) found that a wavy cylinder with spanwise wavelength X/Dm =1.9 can lead to significant drag force reduction and vibration suppression at Re = 3000. Moreover, Lam and Lin (2007, 2009) numerically investigated cross-flow past wavy cylinders with a wide range of spanwise wavelength in the low Reynolds number regime. Two optimal wavelengths for drag reduction were found at X/Dm = 2 and X/Dm = 6 for Re = 100. With a larger value of spanwise wavelength X/Dm = 6, the vortex shedding behind the wavy cylinder was greatly suppressed and the drag force was significantly reduced. Recently, Lam et al. (2010) carried out force measurements on a single wavy cylinder with wavelength ratio (X/Dm = 6) at Re from 6800 to 13,400, and performed the large eddy simulation for the same wavy cylinder at Re = 7500. The results showed that the mean drag coefficients of such wavy cylinder were evidently smaller than those of a purely circular cylinder within the same Reynolds number range. The fluctuating lift coefficients of the wavy cylinders are also smaller than that of a purely circular cylinder at the same Reynolds number. It was concluded that both the experimental and numerical results have confirmed that the wavy cylinder of X/Dm = 6 was a suitable choice for the control of cylinder vibration and drag reduction.

Previous investigations have been concentrated on the study of different types of a single unyawed wavy cylinder in cross-flow ranging from low Reynolds numbers to subcritical Reynolds numbers. What happens to the vortex shedding phenomena and force coefficients for flows at different yaw angles of a wavy cylinder remain unanswered. Such study should give further insight to the

understanding of the mechanism of force reduction by wavy cylinders at yawed conditions. Flows around yawed cylinders are quite common in engineering structures. It is hoped that this investigation will be helpful in industrial applications especially on the design of inclined cable-stayed bridges, tow cables, overhead cables, risers, etc. The present study investigates the flow around a wavy cylinder with different yaw angles. It aims at finding out whether this type of wavy cylindrical shape when used as inclined cables can suppress the body's fluctuating and reduce the drag force or not. It is anticipated that a detailed investigation could provide important information on the flow characteristics and hence be helpful to the designing of such engineering structures. By using large eddy simulation, the complex instantaneous three-dimensional (3-D) vortex structures can be captured. The vortex shedding characteristics, flow patterns and force characteristics of wavy cylinders at different yaw angles can be obtained. The relationship between wavelength, yaw angle and force reduction can be fully investigated. Such study would also provide further understanding and discovery on the physical mechanisms of flow-induced vibration suppression, drag reduction and the 3-D wake vortices interactions of the wavy cylinders at different yawed angles.

2.3.Flow Past Two Cylinders

Cylinder-like structures can be found both alone and in groups in the designs for heat exchangers, cooling systems for nuclear power plants, offshore structures, buildings, chimneys, power lines, struts, grids, screens, and cables, in both air- and water-flow. In many of these engineering applications, Karman vortex shedding is responsible for problems with flow-induced vibration and noise. A complete understanding of the fluid dynamics for the flow around a circular cylinder includes such fundamental subjects as the boundary layer, separation, the free shear layer, the wake, and the dynamics of vortices.

Less well studied and understood are the changes to the flow around a single circular cylinder which may occur when two or more circular cylinders are placed in close proximity to one another. The flow fields of multiple-cylinder configurations

involve complex interactions between the shear layers, vortices, wakes, and Karman vortex streets. The most basic multiple-cylinder configurations in cross-flow are shown in Fig. 1, where the two circular cylinders have the same diameter, D.

For the case of ‘‘infinite’’ cylinders, i.e., each cylinder’s aspect ratio (or slenderness ratio), AR=H/D (where H is the height, length, or span of the cylinder), is sufficiently high that the flow around the cylinder can be considered nominally two-dimensional, the three most important variables governing the fluid flow behaviour are (i) the spacing between the cylinders, (ii) the orientation of the cylinders in the x–y plane relative to the oncoming flow, and (iii) the Reynolds number, Re. In most studies, the Reynolds number has been defined using the uniform approach (or freestream) velocity, U, and the cylinder diameter, i.e., Re=eUD/m where r is the fluid density and m is the dynamic viscosity.

For the case of ‘‘finite’’ cylinders mounted normal to a ground plane, additional variables governing the fluid flow behaviour include (iv) the cylinder aspect ratio and (v) the properties of the boundary layer on the ground plane. The two idealized arrangements of the cylinders which have received the most study are the tandem and side-by-side configurations, shown in Fig. 1(a, b), where the geometry is described by the centre-to-centre longitudinal and transverse spacings, or pitches, L and T, respectively. In each case, the spacing between the cylinders is usually expressed in non-dimensional form, as the longitudinal or transverse pitch ratio, L/D or T/D. For the transverse and side-by-side configurations (Fig.2.1(a, b)), some authors have used the gap width, G, instead of the longitudinal and transverse spacing.

The most general arrangement of two cylinders is the staggered configuration, which is likely the arrangement most encountered in practice, since in very few cases will an oncoming flow be perfectly aligned with the cylinders, or precisely perpendicular to them. The geometry of the staggered pair of cylinders, shown in Fig. 1(c), is set by the centre-to-centre pitch, P, between the cylinders and the angle of incidence; as in the case of the tandem and side-by-side configurations, the spacing is typically expressed as a dimensionless centre-to-centre pitch ratio, P/D. Alternatively, it may be defined in a similar manner to the tandem and side-by-side

configurations, by the longitudinal and transverse spacing's, L and T, as shown in Fig. 1(c). Perhaps because of the added variable (a) used to define the geometry, however, the staggered configuration has received somewhat less research attention despite its predominance in engineering applications.

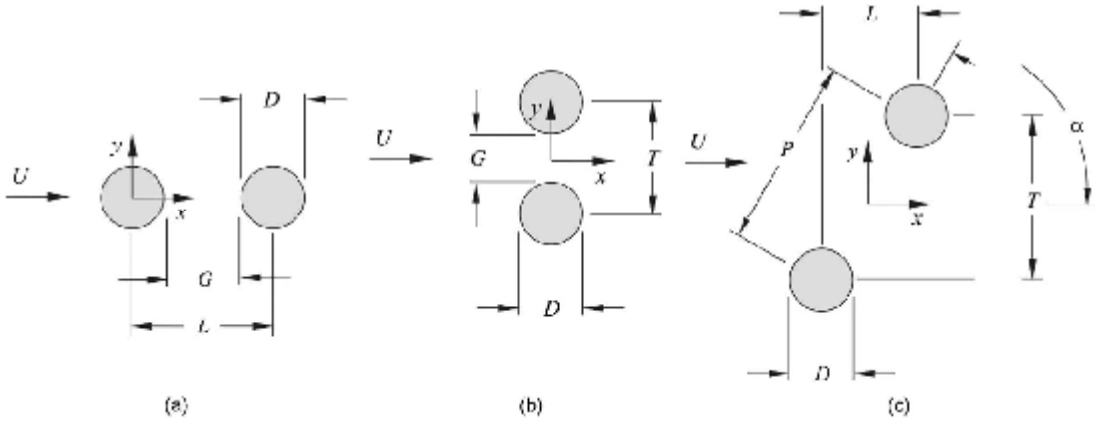

Fig. 2.1. Two circular cylinders of equal diameter in cross-flow: (a) tandem configuration; (b) side-by-side configuration; and (c) staggered configuration.

The most general arrangement of two cylinders is the staggered configuration, which is likely the arrangement most encountered in practice, since in very few cases will an oncoming flow be perfectly aligned with the cylinders, or precisely perpendicular to them. The geometry of the staggered pair of cylinders, shown in Fig. 1(c), is set by the centre-to-centre pitch, P, between the cylinders and the angle of incidence; as in the case of the tandem and side-by-side configurations, the spacing is typically expressed as a dimensionless centre-to-centre pitch ratio, P/D. Alternatively, it may be defined in a similar manner to the tandem and side-by-side configurations, by the longitudinal and transverse spacings, L and T, as shown in Fig. 1(c). Perhaps because of the added variable (a) used to define the geometry, however, the staggered configuration has received somewhat less research attention despite its predominance in engineering applications.

The fluid dynamics of multiple cylinder configurations immersed in steady cross-flow have been examined by many researchers (one of the earliest experimental studies, on two circular cylinders in tandem and side-by-side configurations, was performed by Biermann and Herrnstein (1934), who were

interested in the interference effects of airplane struts), and more than 130 such studies were collected and reviewed for this paper (many of the experimental studies are summarized in Tables 1-3). The behaviour of groups of cylinders in cross-flow has been reviewed by Zdravkovich (1977, 1987, 1993, 2003) .and Chen (1987), with the last major review article published more than 20 years ago by Ohya et al. (1989). However, within the last 10-20 years, there have been many new contributions to the understanding of the flow around multiple cylinders, and this has motivated the present review of the literature.

3. MATERIAL AND METHOD

3.1. Experimental Setup

3.1.1. Water channel

Experiments were carried out in a large-scale water channel located in the Fluid Mechanics Laboratory at Çukurova University. The model of water channel is shown in Figure 3.1. The channel has the following dimensions: a length of 8,000 mm, width of 1,000 mm, and a depth of 750 mm. The height of the water was kept constant at 600 mm during the experiments. The water channel test section is constructed of transparent Plexiglas with the thickness of 15 mm that interconnect with upstream and downstream fiberglass reservoirs. A honeycomb screen arrangement is placed at the entrance of contraction in order to regulate the flow and also drop the turbulence intensity below 2%. The contraction area ratio of the water channel is 2:1. Before the experiments, freestream velocity that can be adjusted by centrifugal pump was calibrated by PIV software. The speed of the impeller can be controlled by an ABB variable frequency drive controller unit. Thus, desired freestream velocity can be obtained in the test section. The experiments were operated at the freestream velocity that corresponds to a Reynolds number of 5,000.

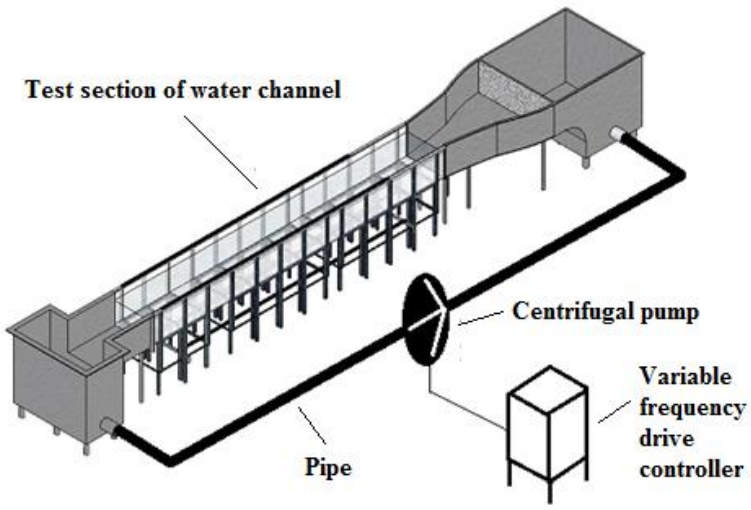

Figure 3.1. The scheme of water channel and main components

3.1.2. Particle image Velocimetry (PIV)

Particle image velocimetry technique is one of the most reliable methods for flow velocity measurement in modern fluid mechanics. It is based on the well known equation:

$$\text{Velocity} = \frac{\text{Distance}}{\text{Time Interval}} = \frac{\Delta x}{\Delta t} \tag{3.1}$$

PIV measures whole velocity fields by taking two images shortly after each other and calculating the distance individual particles travelled (Δx) within this time (Δt). From the known time difference and the measured displacement the velocity is calculated (URL-1). PIV technique basically consists of two stages; image acquisition and image evaluation (Figure 3.2).

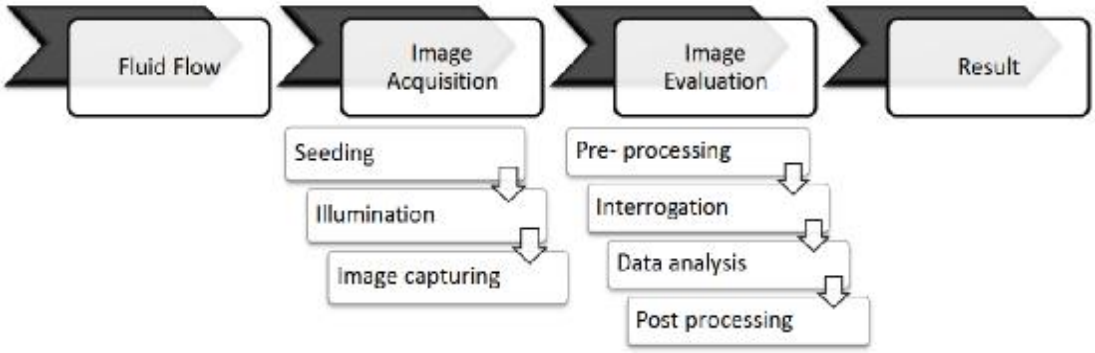

Figure 3.2. General PIV process

The first part of image acquisition is seeding the flow field by suitable seeding particles. Different types of seeding particle are used depending on the nature of the flow for PIV experiments. Seeding particles are added to the flow for tracing the velocity field by means of recording the particle images with a camera. Therefore particles must remain suspended throughout an experiment. Silver coated hollow glass spheres (S-HGS) are borosilicate glass particles with a spherical shape, a smooth surface and 10 μm in diameter, preferred for the present liquid flow applications (Fig. 3.3). The thin silver coating further increases the reflectivity.

4

Figure 3.3. Seeding particle (URL-2)

The type of seeding particle is chosen to follow the flow and in order to detect their movement an area of the flow field is illuminated by a light-sheet. The light-sheet, which is generated by a laser and a system of optical components, is not continuous, but pulsed to produce a stroboscopic effect, freezing the movement of the seeding particles. In the experiments, the New Wave Research Solo 120 XT model double-pulsed Nd:YAG laser system was used (Fig 3.4). The laser sheet is adjusted to 8 mm in thickness. The time between the light pulses i.e. repetition rate is 15 Hz.

Figure 3.4. Laser head and power supply of the Nd:YAG laser system

In order to reveal the position of the illuminated seeding particles, a CCD-camera (Charge Coupled Device) is positioned at right angles to the light-sheet, and particle positions will seen as light specks on a dark background on each camera frame. In experiments, the movement of particles was recorded by a FlowSense 2M CCD camera with a resolution of 1600 × 1200 pixels (Fig. 3.5). The camera was equipped with a Nikon AF Micro 60 f / 2.8D lens (Fig. 3.5). With the help of a

synchronizer (Fig 3.6), the camera and the pulsing light-sheet are synchronized so that particle positions at the instant of light pulse number 1 are registered on frame 1 of the camera, and particle positions from pulse number 2 are on frame 2. The camera lens images the target area onto the sensor array of a digital camera. The camera is able to capture each light pulse in separate image frames. Once a sequence of two light pulses is recorded, the images are divided into small subsections called interrogation areas (IA). The interrogation areas from each image frame, I_1 and I_2, are adaptive-correlated with each other, pixel by pixel. The correlation produces a signal peak, identifying the common particle displacement, Δx, and thus also the velocity (URL-3). DynamicStudio v3.20 software was used throughout the entire velocity measurements: from setting up the system, calibration, through the acquisition to the final data processing and presentation. Adaptive correlation method was used to process the images prior to 2D-velocity reconstruction with final interrogation area of 32 × 32 and overlap of IA with a value of 50%. A total of 7326 (99 × 74) velocity vectors were obtained for a instantaneous velocity field. Double frame mode was used for PIV operations and a total of 500 frames with 15 frame per second (fps) were obtained.

Figure 3.5. The camera and lens

Figure 3.6. The synchronizer

The number of particles in the flow is important to obtain a good signal peak in the adaptive-correlation. As a rule of thumb, 10 to 25 particles should be seen in each interrogation area. An accurate measure of the displacement, and thus also the velocity, is achieved with sub-pixel interpolation. A velocity vector map over the whole target area is obtained by repeating the adaptive-correlation for each interrogation area over the two image frames captured by the camera (Fig. 3.7).

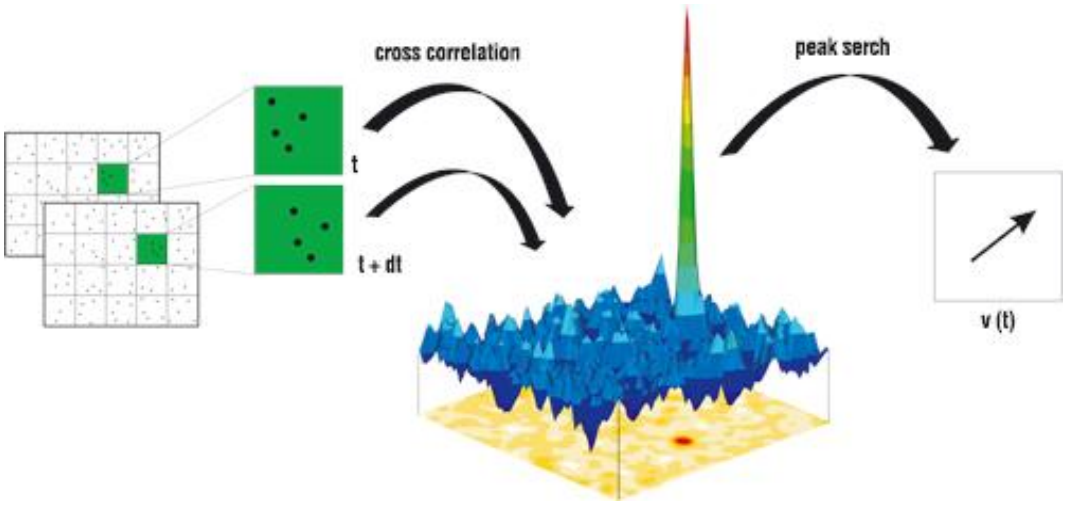

Figure 3.7. Velocity vector detection process (URL-4)

3.1.3 Angle adjustment apparatus

The yaw angle was adjusted by the apparatus given in figure below. A delrin® block with a length of 200 mm, a width of 120 mm and a thick of 30 mm was glued to the top of the another delrin® plate. The lower plate is the base of the apparatus. Then the upper block was linked with a long block that is 500 mm in length, has two

screw mount holes and seven holes with a diameter of 50 mm. The short block was fixed, however, the long block can be rotated in reference to the hinge. Screws were used to change the angle of the long block which is also equal to the yaw angle of test models. A vernier protractor with magnifying glass for precise reading of angles on apparatus was used to adjust the yaw angle. There are seven aligned holes in the long block and they were used to set the center-to-center spacing between test models.

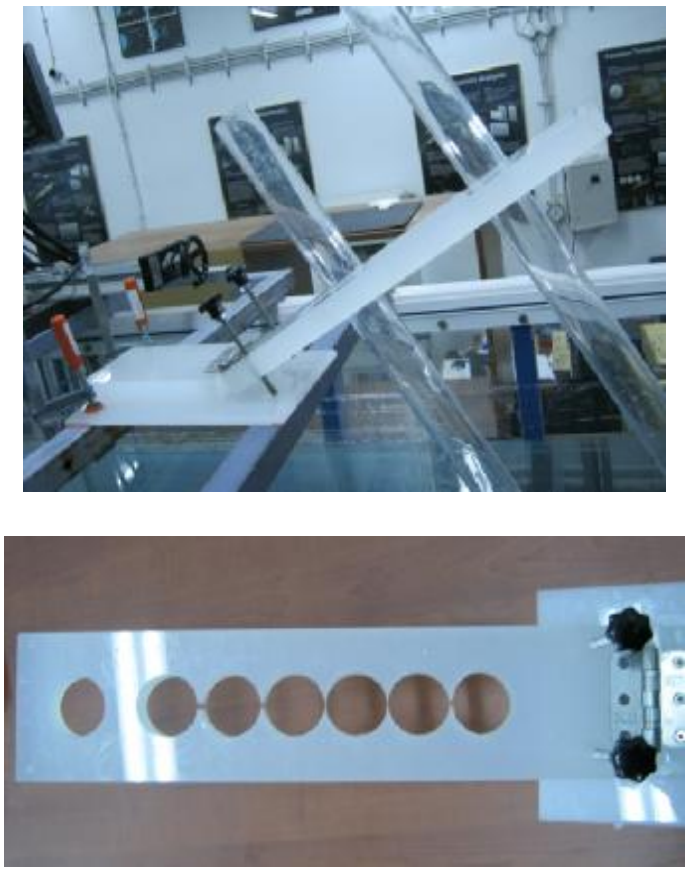

Figure 3.8. Side and top views of the apparatus

3.1.3 Test models

Two plexiglass pipes with a length of 2000 mm and with a diameter of 50 mm were used as test models. They were passed through the holes of angle adjustment apparatus and then immersed in channel with a water height of 600 mm.

The test models arranged in-tandem irrespective to the yaw angle and their immersed ends were touched the bottom of the channel during the experiments (Fig 3.9). Both centerlines of the test cylinders are coincide with the mid-plane of the test section that parallel to the side walls. The solid blockage ratio and the aspect ratio of the cylinders were, 5% and 12, respectively.

Measurements were performed in two individual planes as shown below (Fig. 3.10). The field of interest is 216 mm in length and 162 mm in height. The plan view measurement plane was 300 mm higher than and parallel to the bottom wall.

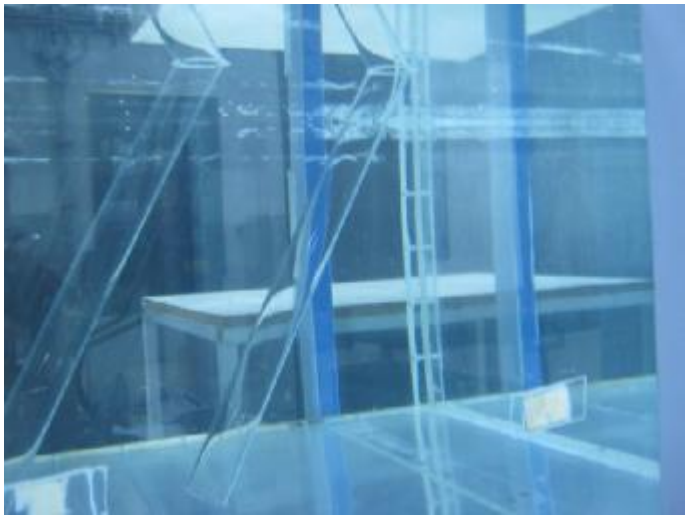

Figure 3.9. The view of immersed test models

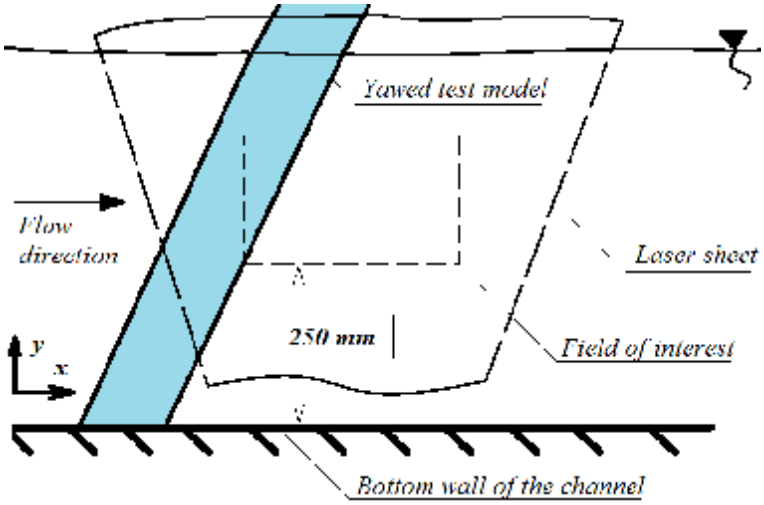

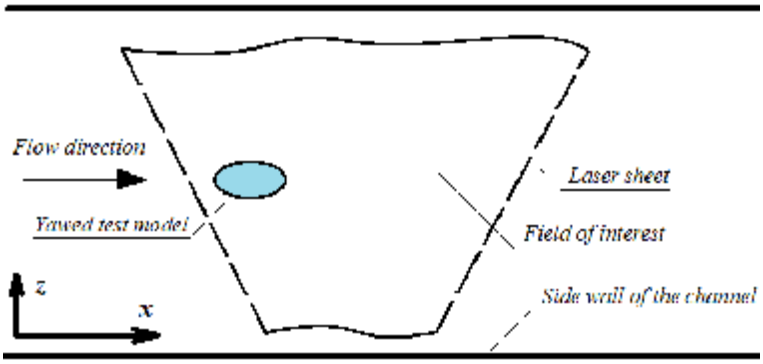

Figure 3.10. The view of immersed test models

3.2. Numerical Simulation in CFX

3.2.1. Introduction

Computational fluid dynamics (CFD) is a branch of fluid mechanics that uses numerical methods and algorithms to solve and analyze problems that involve fluid flows. Computers are used to perform the calculations required to simulate the interaction of liquids and gases with surfaces defined by boundary conditions. With high-speed supercomputers, better solutions can be achieved. Ongoing research yields software that improves the accuracy and speed of complex simulation scenarios such as transonic or turbulent flows. Initial experimental validation of such software is performed using a wind tunnel with the final validation coming in full-scale testing, e.g. flight tests.

The fundamental basis of almost all CFD problems are the Navier–Stokes equations, which define any single-phase (gas or liquid, but not both) fluid flow. These equations can be simplified by removing terms describing viscous actions to yield the Euler equations. Further simplification, by removing terms describing vorticity yields the full potential equations. Finally, for small perturbations in subsonic and supersonic flows (not transonic or hypersonic) these equations can be linearized to yield the linearized potential equations.

Historically, methods were first developed to solve the Linearized potential equations. Two-dimensional (2D) methods, using conformal transformations of the flow about a cylinder to the flow about an airfoil were developed in the 1930s.

In the twentieth century, with computers' advent and their use in complex calculations science, CFD was born and they were progressed with the development of computational power. Today, CFD is used as an accurate method for investigating and analysis of the various phenomena related with fluid flow, in industry.

3.2.2. Numerical evaluation

Flow past a cylinder has attracted the interest of many researchers in bluff body aero/hydrodynamics because, in practical applications, chimneys, lamp posts, bridge supports, offshore structures, etc., have either circular cross-section. In the present study, the fluid generally exhibit turbulent behavior due to the Reynolds number (Re = 5,000). Hence, flow was assumed fully turbulent. For the analysis of turbulent flows, the following items were considered:

1- Turbulent flows are completely unsteady. For their simulation, transient analysis should be selected.

2- Turbulent flows are three-dimensional completely .Therefore, the cylinder must be modeled in three-dimensions.

3- To enable the effects of turbulence to be predicted, a large amount of CFD research has concentrated on methods which make use of turbulence models. Advantages or disadvantages, computational cost and accuracy of results should be considered for choosing the appropriate model. In the present study, The k - ω based Shear-Stress-Transport (SST) model which is recommended for accurate boundary layer simulations was adopted.

3.2.3. Turbulence model

Turbulence consists of fluctuations in the flow field in time and space. It is a complex process, mainly because it is three dimensional, unsteady and consists of

many scales. It can have a significant effect on the characteristics of the flow. Turbulence occurs when the inertia forces in the fluid become significant compared to viscous forces, and is characterized by a high Reynolds Number.

In principle, the Navier-Stokes equations describe both laminar and turbulent flows without the need for additional information. However ,turbulent flows at realistic Reynolds numbers span a large range of turbulent length and time scales, and would generally involve length scales much smaller than the smallest finite volume mesh, which can be practically used in a numerical analysis. The Direct Numerical Simulation (DNS) of these flows would require computing power which is many orders of magnitude higher than available in the foreseeable future.

To enable the effects of turbulence to be predicted, a large amount of CFD research has concentrated on methods which make use of turbulence models. Turbulence models have been specifically developed to account for the effects of turbulence without recourse to a prohibitively fine mesh and direct numerical simulation. Most turbulence models are statistical turbulence model, as described below. The two exceptions to this in ANSYS CFX are the Large Eddy Simulation model and the Detached Eddy Simulation model.

Turbulence models are used to predict the effects of turbulence in fluid flow without resolving all scales of the smallest turbulent fluctuations. A number of models have been developed that can be used to approximate turbulence based on the Reynolds Averaged Navier-Stokes (RANS) equations. Some have very specific applications, while others can be applied to a wider class of flows with a reasonable degree of confidence. The models can be classified as either eddy-viscosity or Reynolds stress models. The following turbulence models based on the RANS equations are available in CFX and are described on the following pages.

Eddy-viscosity Models:

- Zero equation models
- Standard k− ε model
- RNG k −ε model
- Standard k− ω model
- Baseline (BSL) zonal k− ω based model. This model can only be selected

through Expert Control Parameters

- SST zonal k −ω based model
- k −ε(k-epsilon) 1E model. This model can only be selected through Expert Control Parameters
- Curvature correction for two-equation models
- Reynolds-Stress Models (RSM)
- Launder, Reece and Rodi Isotropization of Production model (LRR Reynolds Stress)
- Launder, Reece and Rodi Quasi-Isotropic model (QI Reynolds Stress)
- Speziale, Sarkar and Gatski (SSG Reynolds Stress)
- SMC-ω model (Omega Reynolds Stress)
- Baseline (BSL) Reynolds' Stress model
- Explicit Algebraic Reynolds Stress Model (EARSM)

CFX also provides the Large Eddy Simulation (LES) and Detached Eddy Simulation (DES) turbulence models.

This class of turbulence models is not based on the RANS equations. All turbulence models in CFX use advanced wall functions to model near-wall flow.

3.2.3.1.The k-epsilon Model

One of the most prominent turbulence models, the k− ε (k-epsilon) model, has been implemented in most general purpose CFD codes and is considered the industry standard model. It has proven to be stable and numerically robust and has a well established regime of predictive capability. For general purpose simulations, the k −ε model offers a good compromise in terms of accuracy and robustness.

Within CFX, the k− ε turbulence model uses the scalable wall-function approach to improve robustness and accuracy when the near-wall mesh is very fine. The scalable wall functions allow solution on arbitrarily fine near wall grids, which is a significant improvement over standard wall functions.

While standard two-equation models, such as the k-ε model, provide good predictions for many flows of engineering interest, there are applications for which these models may not be suitable. Among these are:

• Flows with boundary layer separation.

• Flows with sudden changes in the mean strain rate.

• Flows in rotating fluids.

• Flows over curved surfaces.

A Reynolds Stress model may be more appropriate for flows with sudden changes in strain rate or rotating flows, while the SST model may be more appropriate for separated flows.

3.2.3.2.The k-omega and SST Models

One of the main problems in turbulence modeling is the accurate prediction of flow separation from a smooth surface. Standard two-equation turbulence models often fail to predict the onset and the amount of flow separation under adverse pressure gradient conditions. This is an important phenomenon in many technical applications, particularly for airplane aerodynamics since the stall characteristics of a plane are controlled by the flow separation from the wing. For this reason, the aerodynamic community has developed a number of advanced turbulence models for this application. In general, turbulence models based on the ε-equation predict the onset of separation too late and under-predict the amount of separation later on. This is problematic, as this behavior gives an overly optimistic performance characteristic for an airfoil. The prediction is therefore not on the conservative side from an engineering stand-point. The models developed to solve this problem have shown a significantly more accurate prediction of separation in a number of test cases and in industrial applications. Separation prediction is important in many technical applications both for internal and external flows. Currently, the most prominent two-equation models in this area are the k −ω based models of Menter. The k− ω based Shear-Stress-Transport (SST) model was designed to give highly accurate predictions of the onset and the amount of flow separation under adverse pressure

gradients by the inclusion of transport effects into the formulation of the eddy-viscosity. This results in a major improvement in terms of flow separation predictions.

The superior performance of this model has been demonstrated in a large number of validation studies (Bardina et al).

3.2.3.3.The Reynolds Stress Model

Two-equation turbulence models (k-ε and k- ω, based models) offer good predictions of the characteristics and physics of most flows of industrial relevance. In flows where the turbulent transport or non-equilibrium effects are important, the eddy-viscosity assumption is no longer valid and results of eddy-viscosity models might be inaccurate.

Reynolds Stress (or Second Moment Closure (SMC)) models naturally include the effects of streamline curvature, sudden changes in the strain rate, secondary flows or buoyancy compared to turbulence models using the eddy-viscosity approximation. You may consider using a Reynolds Stress model in the following types of flow:

- Free shear flows with strong anisotropy, like a strong swirl component. This includes flows in rotating fluids.
- Flows with sudden changes in the mean strain rate
- Flows where the strain fields are complex, and reproduce the anisotropic nature of turbulence itself
- Flows with strong streamline curvature
- Secondary flow
- Buoyant flow

Reynolds Stress models have shown superior predictive performance compared to eddy-viscosity models in these cases. This is the major justification for Reynolds Stress models, which are based on transport equations for the individual components of the Reynolds stress tensor and the dissipation rate. These models are characterized by a higher degree of universality. The penalty for this flexibility is a

high degree of complexity in the resulting mathematical system. The increased number of transport equations leads to reduced numerical robustness, requires increased computational effort and often prevents their usage in complex flows.

Theoretically, Reynolds Stress models are more suited to complex flows, however, practice shows that they are often not superior to two-equation models. An example of this is for wall-bounded shear layers, where despite their (theoretically) higher degree of universality, Reynolds Stress models often prove inferior to two-equation models.

For wall-bounded flows try to use the SMC-BSL model. It is based on the ω-equation and automatic wall treatment. Three varieties of the Reynolds Stress Model are available which use different model constants:

• Reynolds Stress Model (LRR-IP)

• QI Reynolds Stress Model (LRR-IQ)

• SSG Reynolds Stress Model (SSG)

In general, the SSG model is more accurate than the LRR versions for most flows. This is particularly true for swirling flows. The SSG model is therefore recommended over the other models, which are there for historic reasons and because they are standard models.

Compared to the k- ε model, the Reynolds Stresses model has six additional transport equations that are solved for each timestep or outer coefficient loop in the flow solver. The source terms in the Reynolds Stress equations are also more complex than those of the k- ε model. As a result of these factors, outer loop convergence may be slower for the Reynolds Stress model than for the k- ε model.

In principle, the same timestep can be used for all turbulence model variants, but pragmatically the timestep should be reduced for the Reynolds Stress Model due to the increased complexity of its equations and due to numerical approximations made at general grid interfaces (GGI) and rotational periodic boundary conditions. If convergence is difficult, it is recommended that a k -ε or k -ω based model solution be obtained first and then a Reynolds stress model solution can be attempted from the converged two-equation solution. It is frequently observed that Reynolds Stress models produce unsteady results, where two-equation models give steady state

solutions. This can be correct from a physical standpoint, but requires the solution of the equations in transient mode.

The Reynolds Stress models may be used with isotropic or anisotropic turbulent diffusion terms in the Reynolds Stress and Epsilon transport equations. The difference is usually second order as there is often domination by the source terms and the effects of diffusion are small. An exception might be buoyant flows, which can be diffusion dominated. However, the model that uses isotropic turbulent diffusion terms is potentially more robust than the model that uses anisotropic turbulent diffusion terms.

3.2.3.4. The Large Eddy Simulation Model (LES)

The usual approach to predicting turbulent flows is to use the Reynolds Averaged Navier-Stokes equations, (RANS), which solve for time averaged quantities. However, there are some situations where the approach is not adequate,and the alternative approaches of Large Eddy Simulation (LES) or Direct Numerical Simulation (DNS) can be adopted. With these methods, time dependent equations are solved for the turbulent motion with either no approximations and all relevant scales resolved (DNS) or the equations are filtered in some way to remove very fine time and length scales (LES). These approaches require fine grids and small timesteps, particularly for wall bounded flows, as well as a large number of timesteps to generate statistically meaningful correlations for the fluctuation velocity components. However, they can give details on the structure of turbulent flows, such as pressure fluctuations and Lighthill stresses, which cannot be obtained from a RANS formulation.

Before starting an LES simulation, you should consider if it is the most appropriate solution approach. For low Reynolds numbers ($Re < 5000$) or when it is important to be able to resolve all scales (for example, for transition to turbulent flow), consider DNS if you have a large computer available. For Higher Reynolds numbers, LES might be a suitable option for cases where:

• The flow is likely to be unstable, with large scale flapping of a shear layer or

vortex shedding

- The flow is likely to be unsteady with coherent structures (cyclone, flasher)
- The flow is buoyant, with large unstable regions created by heating from below, or by lighter fluid below heavier fluid (multiphase flows in inclined pipelines)
- Conventional RANS approach are known to fail (for example due to highly anisotropic turbulence)
- A good representation of the turbulent structure is required for small-scale processes such as micro-mixing or chemical reaction
- The noise from the flow is to be calculated, and especially when the broadband contribution is significant
- Other fluctuating information is required (such as fluctuating forces, gusts of winds)
- The user can afford to wait for up to a week for results, using an 8 to 16 processor system

It should be noted that for wall bounded flows, so called ‘streaky structures’ develop in the near wall region. These ‘streaky structures’ must be resolved and this leads to high resolution requirements and computing times for LES of wall-bounded flows. This should be kept in mind and the user should consider the SAS (Scale-Adaptive Simulation) or DES (Detached Eddy Simulation) approach first before performing a LES for wall bounded flows.

3.2.3.5.The *k* - ω based SST model

One of the main problems in turbulence modeling is the accurate prediction of flow separation from a smooth surface. Standard two-equation turbulence models often fail to predict the onset and the amount of flow separation under adverse pressure gradient conditions. This is an important phenomenon in many technical applications, particularly for airplane aerodynamics since the stall characteristics of a plane are controlled by the flow separation from the wing. For this reason, the aerodynamic community has developed a number of advanced turbulence models for

this application. In general, turbulence models based on the ε-equation predict the onset of separation too late and under-predict the amount of separation later on. This is problematic, as this behavior gives an overly optimistic performance characteristic for an airfoil. The prediction is therefore not on the conservative side from an engineering stand-point. The models developed to solve this problem have shown a significantly more accurate prediction of separation in a number of test cases and in industrial applications. Separation prediction is important in many technical applications both for internal and external flows. Currently, the most prominent two-equation models in this area are the *k* - ω based models of Menter. The *k* - ω based Shear-Stress-Transport (SST) model was designed to give highly accurate predictions of the onset and the amount of flow separation under adverse pressure gradients by the inclusion of transport effects into the formulation of the eddy-viscosity. This results in a major improvement in terms of flow separation predictions.

One of the advantages of the *k* - ω formulation is the near wall treatment for low-Reynolds number computations. The model does not involve the complex nonlinear damping functions required for the *k* - ε model and is therefore more accurate and more robust. A low-Reynolds *k* - ε model would typically require a near wall resolution of $y^+ < 0.2$, while a low-Reynolds number *k* - ω model would require at least $y^+ < 2$. In industrial flows, even $y^+ < 2$ cannot be guaranteed in most applications and for this reason; a new near wall treatment was developed for the *k* - ω models. It allows for smooth shift from a low-Reynolds number form to a wall function formulation. The *k* - ω models assumes that the turbulence viscosity is linked to the turbulence kinetic energy and turbulent frequency via the relation:

$$\mu_t = \rho \frac{k}{\omega} \tag{3.2}$$

3.2.3.5. Modeling flow near the wall

Near a no-slip wall, there are strong gradients in the dependent variables. In addition, viscous effects on the transport processes are large. The representation of these processes within a numerical simulation raises the following problems:

• How to account for viscous effects at the wall?

• How to resolve the rapid variation of flow variables which occurs within the boundary layer region?

Experiments and mathematical analysis were shown that the near-wall region can be subdivided into two layers. In the innermost layer, the so-called viscous sublayer, the flow is almost laminar-like, and the (molecular) viscosity plays a dominant role in momentum and heat transfer. Further away from the wall, in the logarithmic layer, turbulence dominates the mixing process. Finally, there is a region between the viscous sublayer and the logarithmic layer called the buffer layer, where the effects of molecular viscosity and turbulence are of equal importance. The figure below illustrates these subdivisions of the near-wall region.

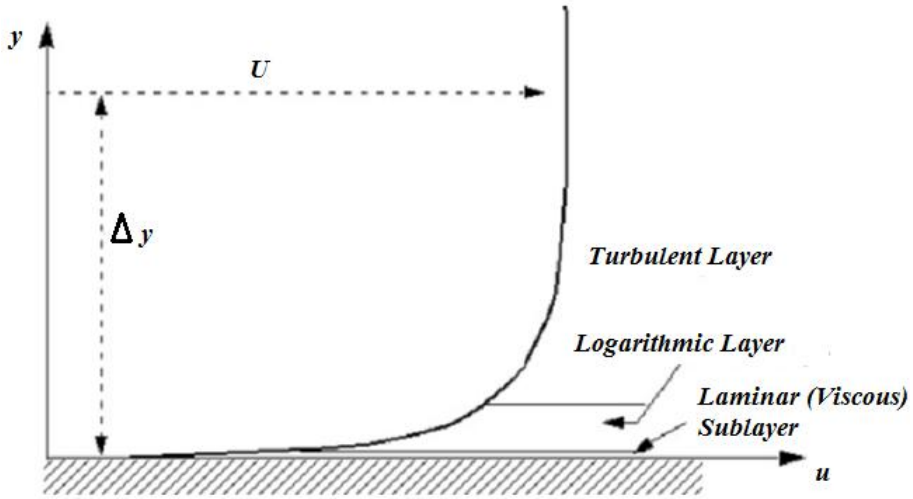

Figure 3.11. Subdivisions of the near-wall region

Assuming that the logarithmic profile reasonably approximates the velocity distribution near the wall, it provides a means to numerically compute the fluid shear stress as a function of the velocity at a given distance from the wall.

This is known as a “wall function” and the logarithmic nature gives rise to the well known “log law of the wall”. Two approaches are commonly used to model the flow in the near-wall region:

1- The wall function method uses empirical formulas that impose suitable conditions near to the wall without resolving the boundary layer, thus saving computational resources. All turbulence models in CFX are suitable for a wall function method.

The major advantages of the wall function approach is that the high gradient shear layers near walls can be modeled with relatively coarse meshes, yielding substantial savings in CPU time and storage. It also avoids the need to account for viscous effects in the turbulence model.

2- The Low-Reynolds-Number method resolves the details of the boundary layer profile by using very small mesh length scales in the direction normal to the wall (very thin inflation layers). Turbulence models based on the ω – equation, such as the SST or SMC – ω models are suitable for a low-Re method. Note that the low-Re method does not refer to the device Reynolds number, but to the turbulent Reynolds number, which is low in the viscous sublayer. This method can therefore be used even in simulations with very high device Reynolds numbers, as long as the viscous sublayer has been resolved.

The computations are extended through the viscosity-affected sublayer close to the wall. The low-Re approach requires a very fine mesh in the near-wall zone and correspondingly large number of nodes. Computer-storage and runtime requirements are higher than those of the wall-function approach and care must be taken to ensure good numerical resolution in the near-wall region to capture the rapid variation in variables. To reduce the resolution requirements, an automatic wall treatment was developed by CFX, which allows a gradual switch between wall functions and low-Reynolds number grids, without a loss in accuracy.

Wall functions are the most popular way to account for wall effects. In CFX, Scalable Wall Functions are used for all turbulence models based on the ε – equation. For k - ω based models (including the SST model), an automatic near-wall treatment method is applied.

3.2.4. Simulation of fluid flow problems

For modeling the flow around a cylinder in this project, Ansys CFX was used. In this section, summary concerning the modeling process, the initial condition and boundary conditions were presented. The following steps will be conducted.

1- Investigate the hydrodynamic forces on the cylinders.

2- Investigate the wake structure of cylinder by changing the yaw angle and center-to-center spacing ratio.

3- Investigate the instantaneous and time-averaged changes in flow characteristics.

Therefore, two types of analysis is considered i.e. quantitative analysis (hydrodynamic forces) and qualitative (the wake flow structure). Two arrangements were considered i.e. single cylinder and two cylinders in-tandem. Both categories of the simulations were performed at a Reynolds number of 5,000. Cylinders have a constant diameter of 0.05 m and with a height of 0.6 m. The computational domain was 12D in height, 8D in width and 24D in length. The test cylinder is located 4D away from the side walls and 8D downstream of the inlet. Computational domain around single cylinder is shown in the following (Figure 3.12.)

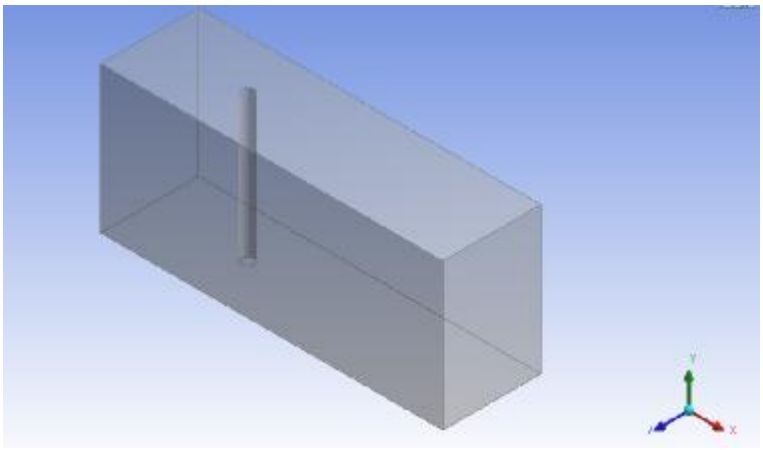

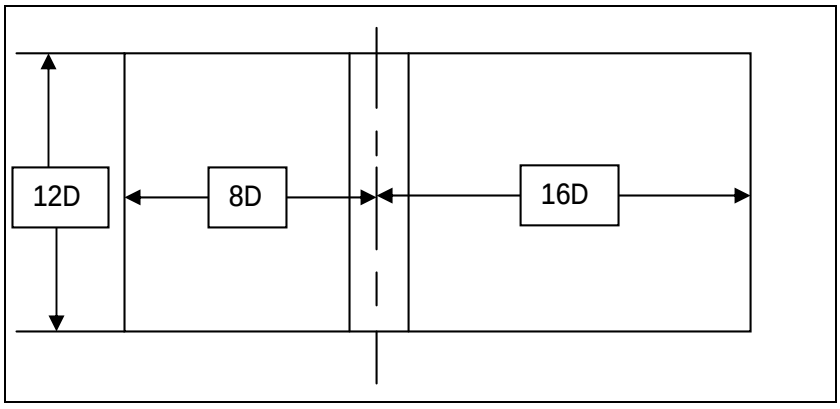

Figure 3.12. Schematic of computational domain

3.2.5. Grid generation

For each analysis carried out by CFD, quality of computational grid created on the model has a dramatic effect on the convergence, accuracy and precision of results. Especially in the present simulations, accurate prediction of the separation point's position has a significant impact in the amount of force on the cylinder. In CFD analysis were used the different methods for gridding of the flow domain.

3.2.5.1. Hybrid meshes (grids)

A hybrid mesh is a mesh that contains structured portions and unstructured portions. Note that this definition requires knowledge of how the mesh is stored (and used). There is disagreement as to the correct application of the terms "hybrid" and "mixed." The term "mixed" is usually applied to meshes that contain elements associated with structured meshes and elements associated with unstructured meshes (presumably stored in an unstructured fashion).

In the present project, hybrid meshes was used. The intense structured mesh with tetrahedral elements was applied to the surface of the cylinders. Production of this type of elements was provided by "Inflation" option in ANSYS CFX-mesh to gain more accuracy. And the other part of the flow domain comprised of unstructured meshes. Whatever elements were became smaller at the range of resolution, gridding can be adapted better on the geometry and solving will be more accurate. On the other hand, shrinking elements means to increase the number of them and smaller time step in the solution process that led a rise in the volume and computational operations, and also it makes to significant rounding error. So in terms of geometric elements may not be large enough that it does not conform to the geometry and not too small that the numerical operations are required too heavy. Hence, for optimization of girding it was essential to have full cognizance of the geometry and the physics of the problem, till to able to identify the regions of the flow with strong gradients changes and where needs for more numerical accurate and finally, the grid of around these regions was just done finer.

In the following figure, a view of created grid around the cylinder was shown. As one can see from the figure, the intense grid distribution around the cylinder started to decrease as moved away from the cylinder.

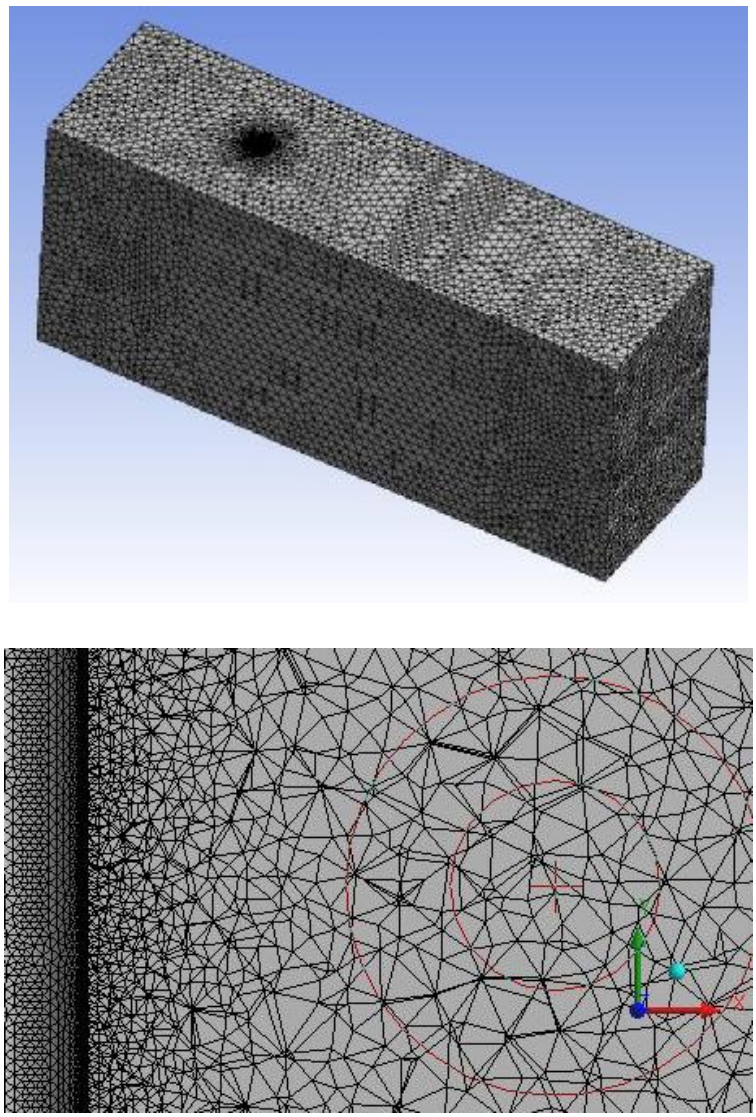

Figure 3.13. The whole flow domain with grid and zoom-in view of the grids around single cylinder

3.2.6. Boundary conditions

According to geometry of flow domain, seven boundaries were detected and appropriate boundary conditions were assigned to them. Employed boundary conditions can be classified into four categories:

- Inlet boundary conditions for upstream boundary: Fluid is entered from such boundary to solution domain. A constant velocity of 0.1 m/s was assigned.
- Outlet boundary condition for downstream boundary: Fluid is exited through the boundary from the solution domain. For this boundary due to be adequate distance and appropriate downstream boundary from cylinder, static pressure was used as a boundary condition. A constant static pressure of 0 Pa was assigned.
- No slip wall boundary condition: The velocity of the fluid at the wall boundary is set to zero. This boundary condition was assigned to the side surfaces and the surface of the cylinder.
- Free slip wall boundary condition: In this case, the velocity component parallel to the wall has a finite value (which is computed), but the velocity normal to the wall, and the wall shear stress, are both set to zero. This boundary condition was applied to the top and bottom walls. When this boundary condition was assigned to a surface, no boundary layer will be formed on the mentioned surface.

3.2.7. Transient solution and determining the time step

Generally, flow analysis is divided to two categories: Steady state and Transient. In the Steady state, analysis is eliminated the time effect, and varying amounts are independent of time. But in the in transient analysis, the changes of parameters are considered with the time and also in the equations. In the study, transient analysis is required to simulate the turbulent flow accurately.

Determination of appropriate time step is very crucial in terms of getting accurate data about the concerning flow parameters. Strouhal number is approximately equal to 0.2 in the range of $300 \leq Re \leq 10^5$(Figure 3.14). Thus, the vortex shedding frequency (f_S) can be calculated from the formula below.

$$S_{t=}f_{s*}D/U \qquad (3.3.)$$

By using the above formula, the vortex shedding frequency was determined as 0.4 Hz. The vortex shedding period (T) that is equal to 1/ f_S can be calculated too.

It was determined as 2.5 s. The vortex shedding period was divided to 166, so that, time step side was determined as 0.015 s.

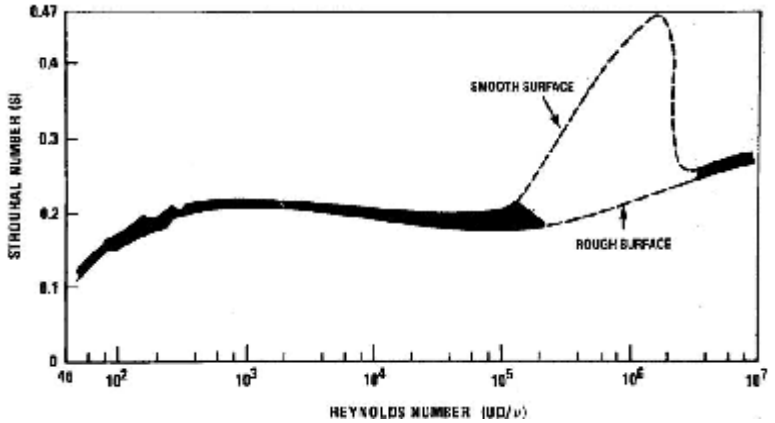

Figure 3.14. Strouhal number changes with Reynolds number for a fixed cylinder

3.2.8. Linear equation solution

ANSYS CFX uses a Multigrid (MG) accelerated Incomplete Lower Upper (ILU) factorization technique for solving the discrete system of linearized equations. It is an iterative solver whereby the exact solution of the equations is approached during the course of several iterations.

3.2.9. Physical Properties of the Fluid

Simulations were carried out in isothermal conditions. The working fluid is water. The properties of the water were shown in table below.

Table 3.1. The physical properties of the working fluid

Property	Unit	Symbol	Value
Density	kg/m^3	ρ_w	997
Dynamic viscosity	kg/ms	μ_w	0.89×10^{-3}
Water temperature	°C	T	25

3.2.10. Dimensionless parameters

Laboratory and experimental works are often time-consuming and costly. Dimensional analysis is important tool for evaluate the influencing parameters on studied phenomenon. By using non-dimensional parameters which are earned from dimensional analysis, data can be connected by using of minimum possible number of graphs. By using the dimensionless numbers can be indicated the less graphs with higher quality. In the following, other dimensionless numbers were introduced which the effect of their changes were examined (Table 3.2).

Table 3.2. Dimensionless parameters and coefficients

Parameter	**Symbol**	**Equation**
Reynolds number	Re	$\frac{\rho U D}{\mu}$
Strouhal number	St	$\frac{f_s D}{U}$
Drag coefficient	C_d	$\frac{F_D}{0.5 \rho U^2 (D \times h)}$
Lift coefficient	C_l	$\frac{F_L}{0.5 \rho U^2 (D \times h)}$
Center-to-center spacing	L/D	$\frac{L}{D}$
Yaw angle	α	-

3.2.11. Grid independence tests

A high-quality grid is critical to an accurate CFD solution; a poorly resolved or low-quality grid may even lead to an incorrect solution. It is important, therefore, for users of CFD to test if their solution is grid independent. The standard method to test for grid independence is to increase the resolution (by a factor of 2 in all directions if feasible) and repeat the simulation. If the results do not change appreciably, the original grid is probably adequate. For single cylinder case, the

medium sized grid found adequate. On the other hand, the number of elements increased and reached to 6,936,400 in the case of two circular cylinders.

Table 3.3. The results of grid independence test for single cylinder

	Number of element	**Number of node**	**Time-averaged drag coefficient**
Coarse grid	2,128,156	573,190	0.80
Medium sized grid	4,234,440	936,478	1.02
Fine grid	7,144,287	1,442,254	1.03
Very fine grid	12,016,527	3,502,041	1.03

4. INTRODUCTION

This section was comprised of two subsections. The first subsection includes the comparative analysis of numerical and experimental data of the flow parameters for single circular cylinder case. The second subsection is about the two circular cylinders located in-tandem.

4.1. Single Cylinder

In this section, experimental and numerical data will be presented. It can be noted that so much result was obtained, therefore, only the some of them will be presented. In this section flow around single circular cylinder was studied with a diameter of 0.05 mm and a height of 0.6 m at a Reynolds number of 5,000. The effects of yaw angle on the wake structure and hydrodymanic coefficients of single cylinder will be presented.

4.1.1. Parameters

Analysis performed has been listed as shown in the following table.

Table 4.1. Yaw angles tested in the thesis (Single cylinder)

Experimental	0	5	10	15	20	25	30	35	40	45
Numerical	0	-	10	-	20	-	30	-	40	45

4.1.2. Validation of the numerical model

To validate the numerical model, flow past a circular cylinder for Reynolds number of 5,000 was compared with experimental data. The cylinder has zero yaw angle in the comparison.

Table 4.2. Comparison with experimental data (Single cylinder)

	Present simulation	Anderson (2010)
Time-averaged drag coefficient	1.02	0.98

As can be seen in the above table, the drag coefficient calculated has a good aggreement with the experimental value of Anderson. The difference is less than 4%. On the other hand the drag coefficient of the single cylinder almost remained unchanged ($C_d \approx 1$) for the Reynolds numbers limited from 1,000 to 10,000 (Figure 4.1). Finally, it can be said that the result is considered to be reasonable and numerical tool is suitable for the present study.

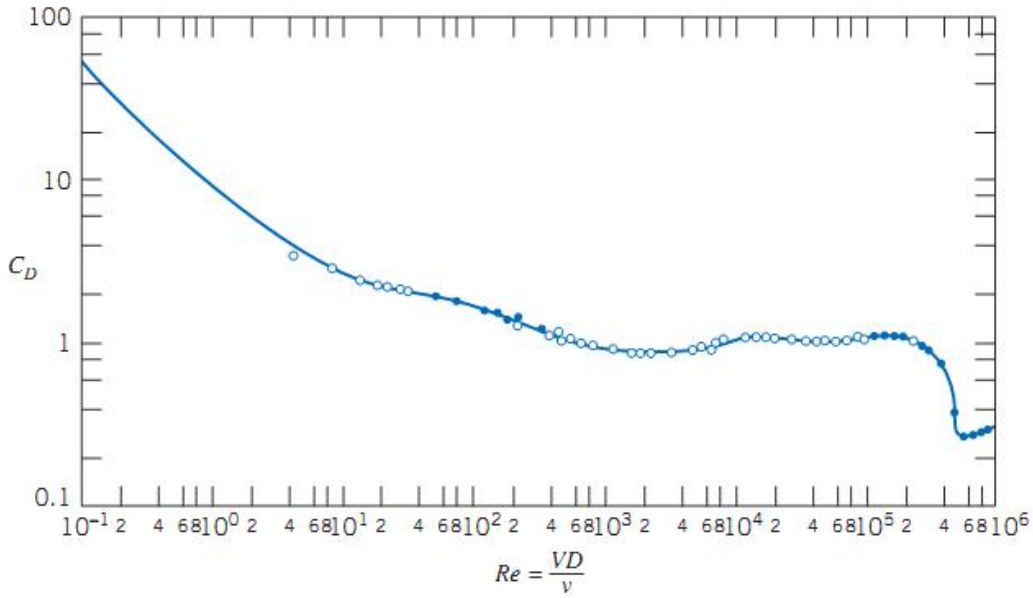

Figure 4.1. Drag coefficient for a smooth circular cylinder as a function of Reynolds Number (Schlichting, 1979)

4.1.3. Flow structure downstream of the cylinder

Figure 4.2 and 4.3 show the time averaged wake velocity field in the wake of single cylinder without yaw angle. Experimental and numerical results were given side by side in order to make a qualitative comparison. As one can see from the figure 4.2 the thickness of the wake regions are equal but the length. Moreover, the vortex cores are closer to the base of the cylinder in the numerical study. This may be arisen from the experimental a/or numerical uncertainties. The rear stagnation points were started to move further downstream slightly from the bottom to the free surface (Figure 4.3). This may be attributed to the developing boundary layer over the bottom surface of the channel.

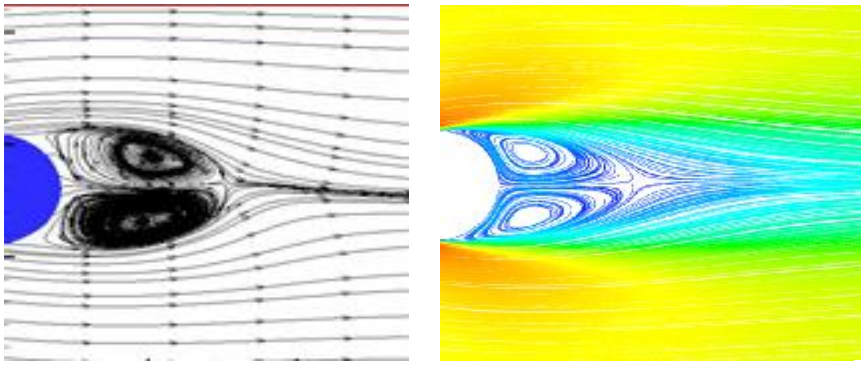

Figure 4.2. The comparison of the experimentally and numerically obtained time-averaged wake velocity fields (Plan view)

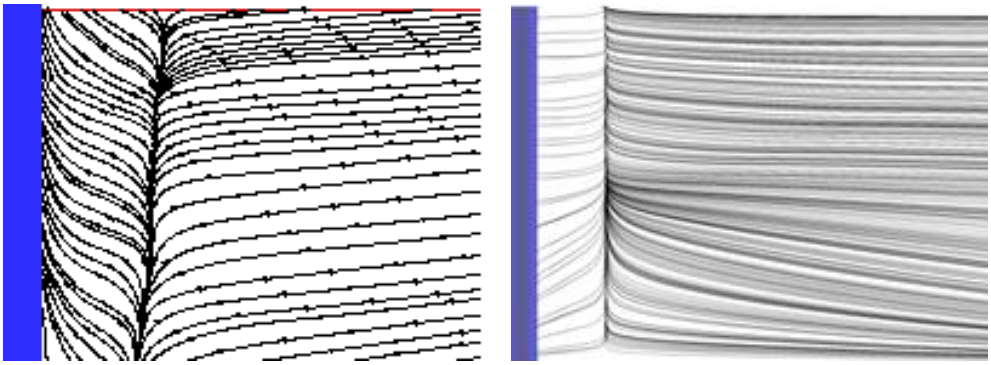

Figure 4.3. The comparison of the experimentally and numerically obtained time-averaged wake velocity fields (Side view)

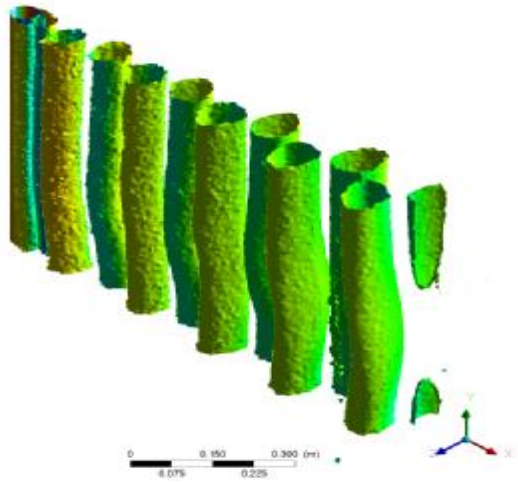

Figure 4.4. Instantaneous velocity field beyond the single cylinder (numerical results)

The Kármán vortex street can be seen clearly from the izometric view of the instantaneous wake velocity field (Figure 4.4). It is obvious that the vortex tube formed with a slight waviness.

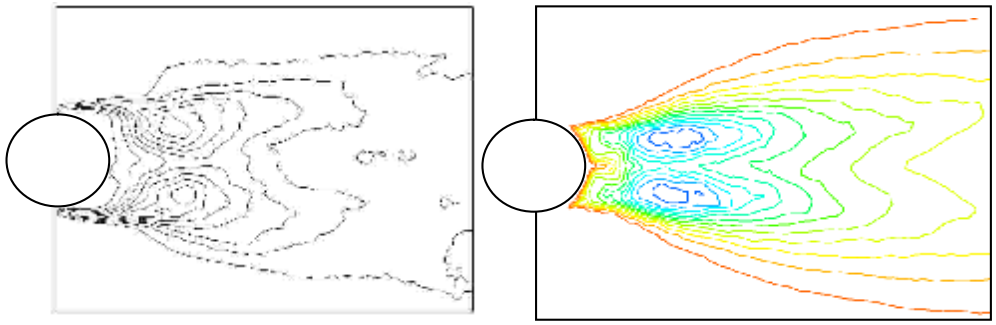

Figure 4.5. The comparison of the experimentally and numerically obtained contours of time-averaged Reynolds stress, u'u'

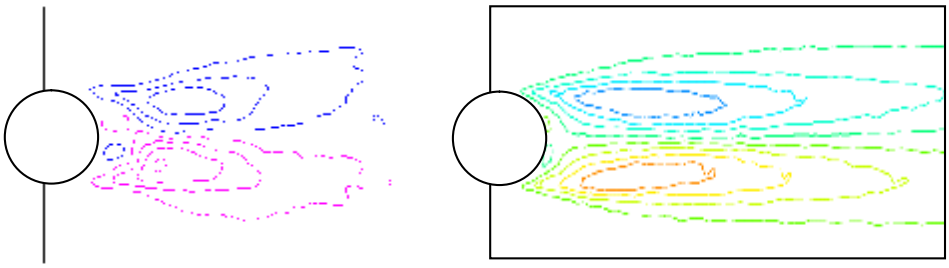

Figure 4.6. The comparison of the experimentally and numerically obtained contours of time-averaged Reynolds stress, u'v'

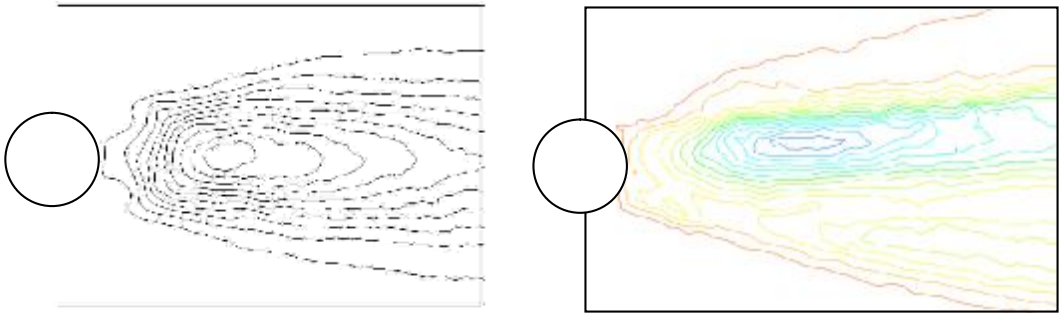

Figure 4.7. The comparison of the experimentally and numerically obtained contours of time-averaged Reynolds stress, v'v'

The distribution of the Reynolds stresses was presented in the figures above (Figure 4.5 - 4.7). As one can see, numerical results were generally in a good accordance with the experimental results.

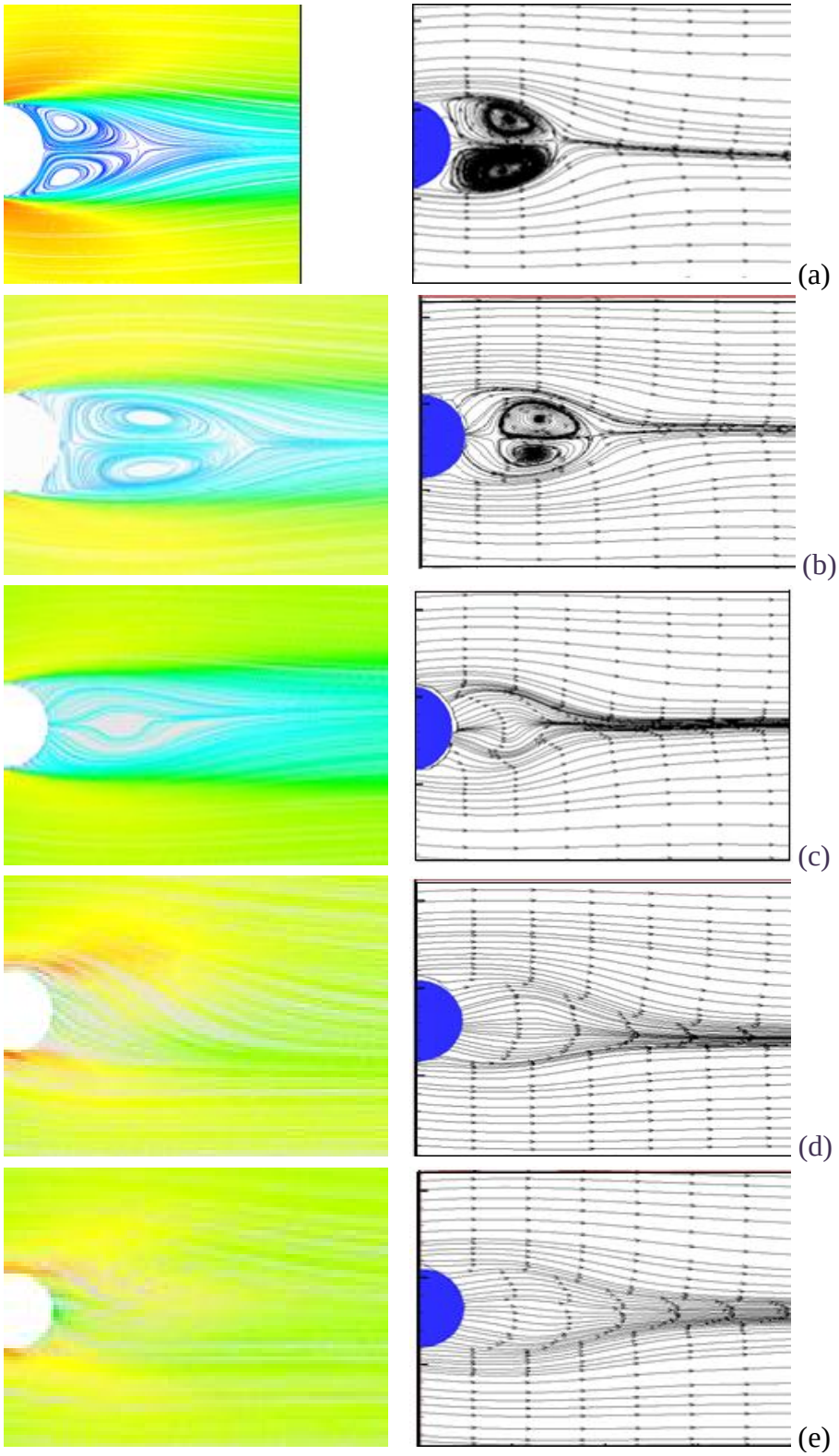

Figure 4.8. Experimentally and numerically obtained time-averaged wake velocity fields for various yaw angles (Plan view): (a) 0˚, (b) 20˚, (c) 30˚, (d) 40˚, (e) 45˚

The effects of different yaw angles on the time-averaged velocity fields beyond the cylinder were shown in figure 4.8. The results were shown comparatively. It was shown that the suppression of votrex shedding can also be predicted by numerical simulation, as yaw angle exceeded α=20˚. Furthermore, the vortex cores were moved to further downstream and another stagnation point was occurred just in front of the recirculating vortices. The movement process was also captured by the numerical simulations.

The experimentally obtained time-averaged velocity field with augmented yaw angles was presented in figure 4.9. Here, as yaw angle reached to α=25˚, the recirculating vortices in the near wake of the cylinder were disappeared. This situation may be attributed to the following: At small yaw angles, shear layers originating from the top and bottom side of the cylinder curled towards the base region due to the pressure difference and then rolled into the vortices. As incidence angle reached to α=25˚, the spanwise component of the velocity become dominant on the base surface and lowered the pressure difference (Figure 4.10.). Besides the position of the cylinder, coanda effect may also be contributed to dominance of the spanwise velocity component. As a result of these, vortex shedding was suppressed.

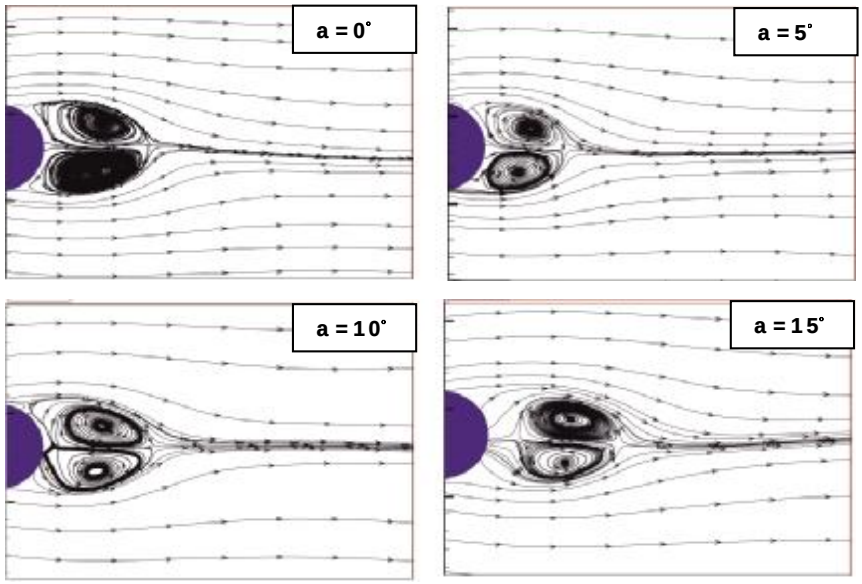

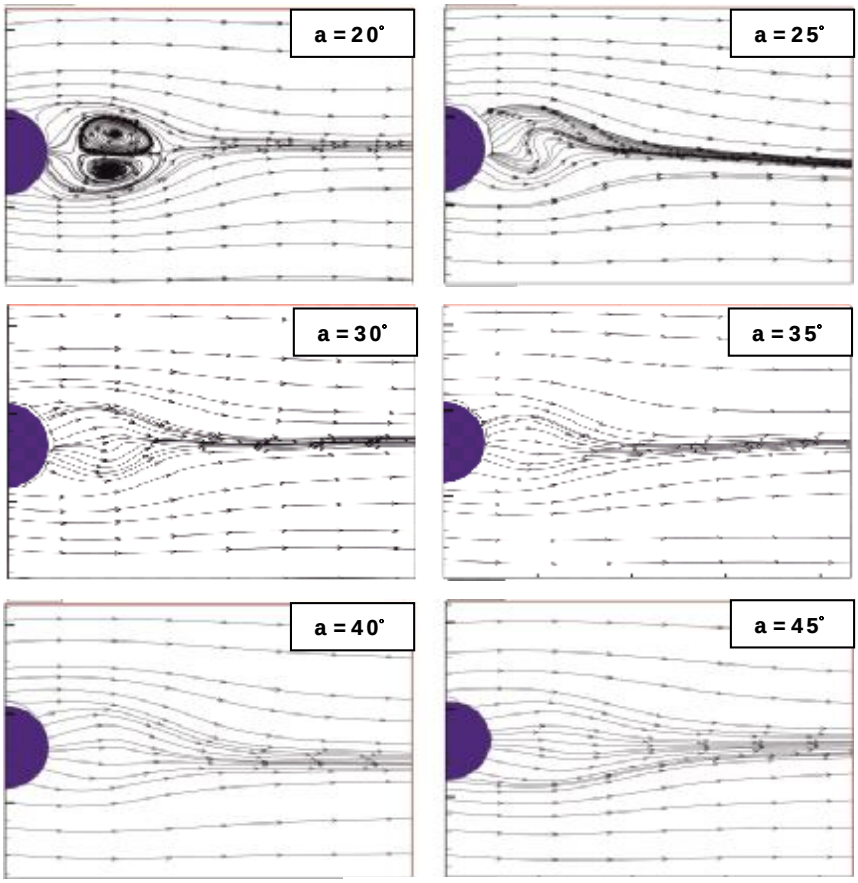

Figure 4.9. Experimentally obtained time-averaged wake velocity fields for various yaw angles (Plan view)

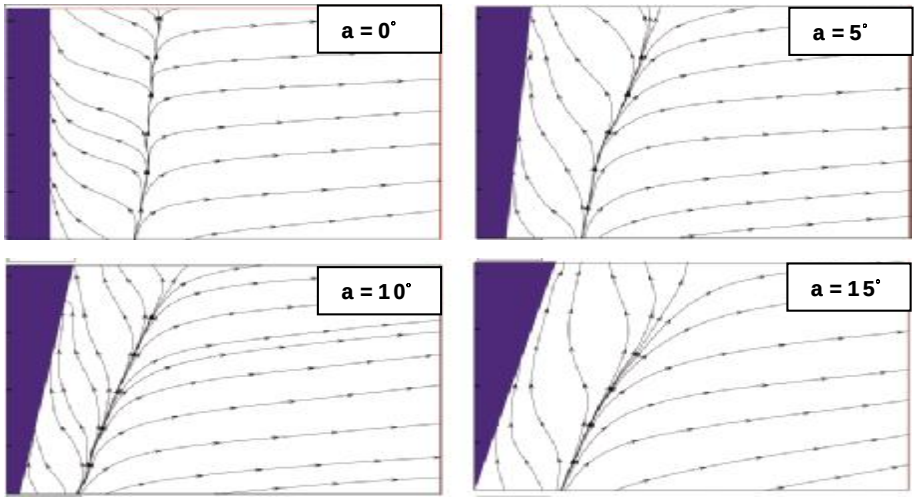

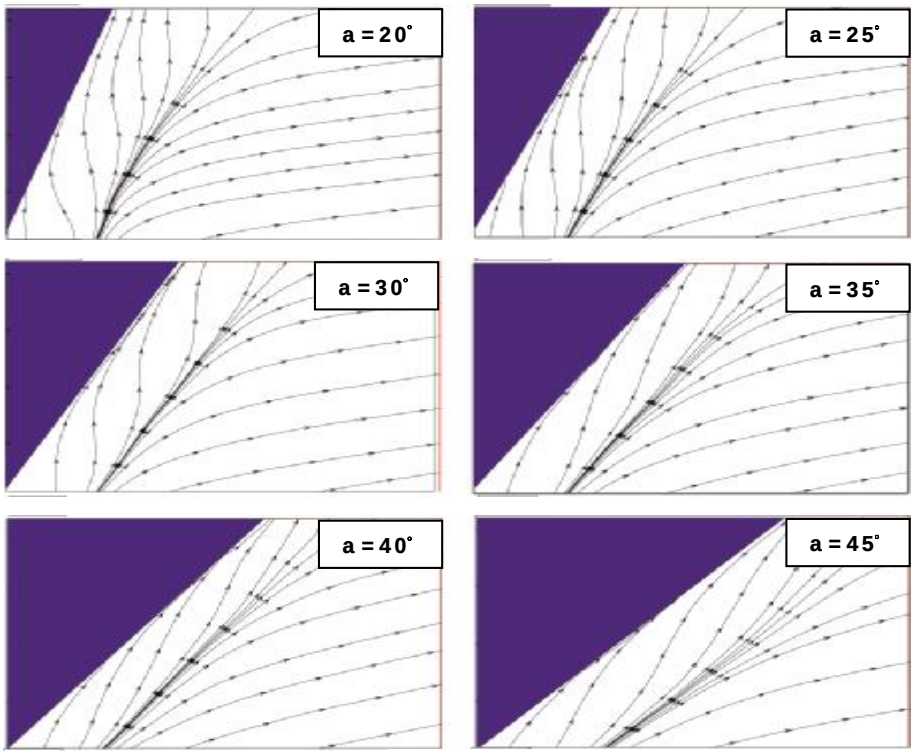

Figure 4.10. Experimentally obtained time-averaged wake velocity fields for various yaw angles (Side view)

In the numerical simulations, instantaneous three-dimensional (3D) velocity distribution beyond the cylinder revealed that as yaw angle increased, suppression of the vortex shedding started from bottom to top along the spanwise of the cylinder.

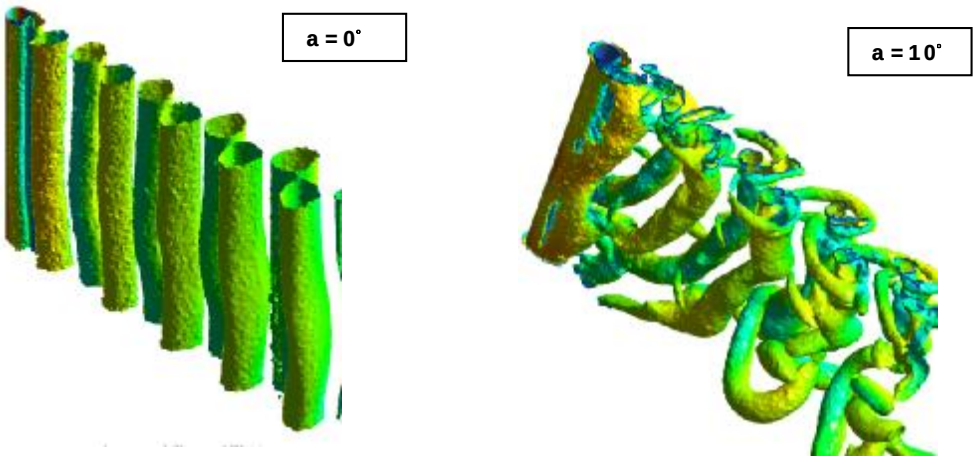

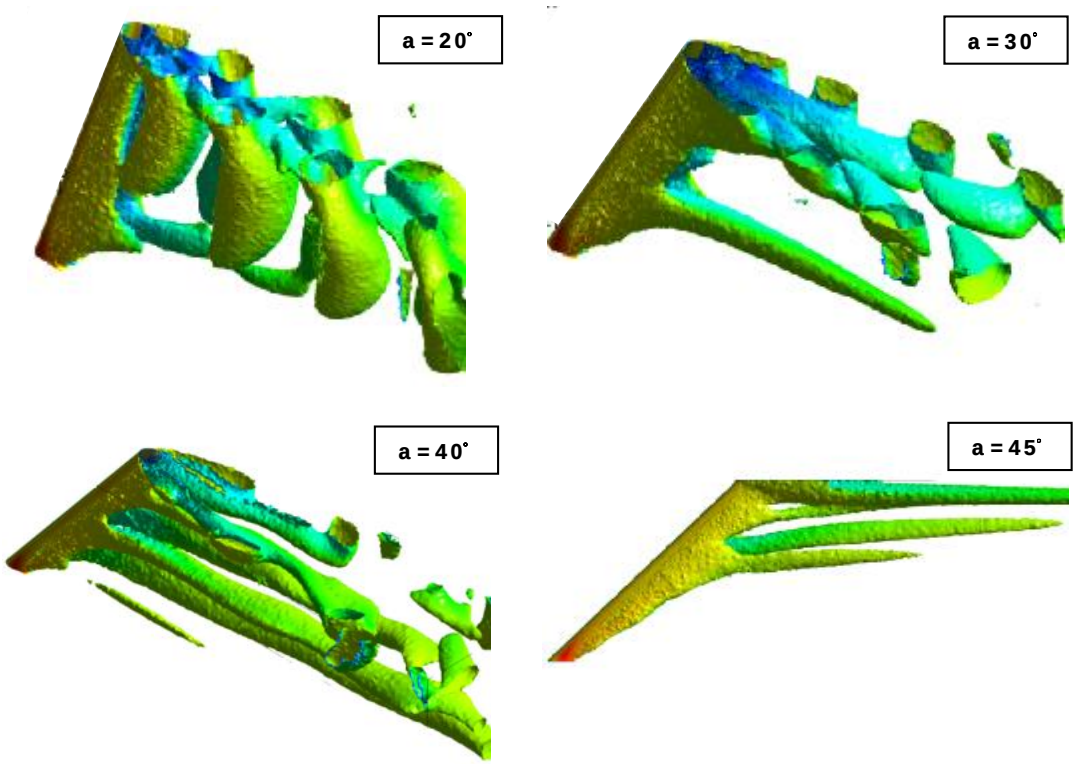

Figure 4.11. Instantaneous velocity field beyond the single cylinder for various yaw angles (numerical results)

4.1.4. Drag coefficient

The changes in drag as a function of yaw angle were plotted in figure 4.12. As can be seen from the figure, drag coefficient almost decreased proportionally with increased yaw angle. The drag coefficient were reduced to half at yaw angle of α=40˚.

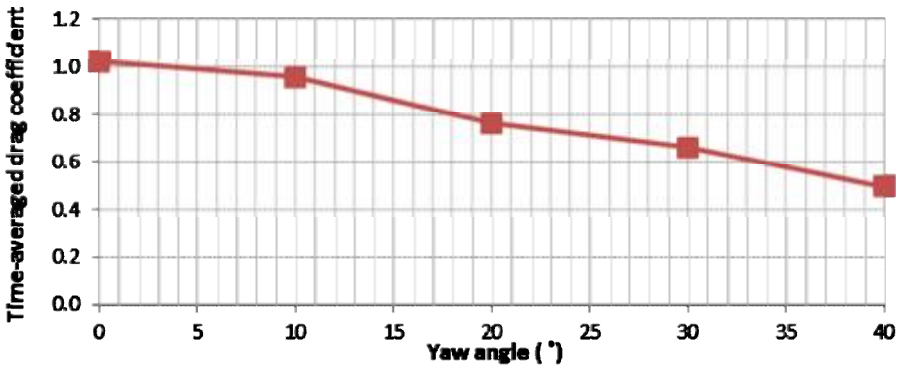

Figure 4.12. Time – averaged drag coefficient of the cylinder for various yaw angles

4.1.5. Fluctuating lift coefficient

One of the other effective parameters was lift coefficient on the flow. Due to the occurrence of the vortex shedding phenomenon in behind the cylinder, the force in the perpendicular direction had a natural oscillatory in the flow. The frequency of these oscillations was same of vortex shedding frequency (Strouhal number).

Lift coefficient variation on time for an angle of 10˚ was displayed in the following graph figure 4.13. Changes of amounts of (RMS) lift coefficient was shown then increases the yaw angle of the cylinder in the following diagram (Figure 4.14).

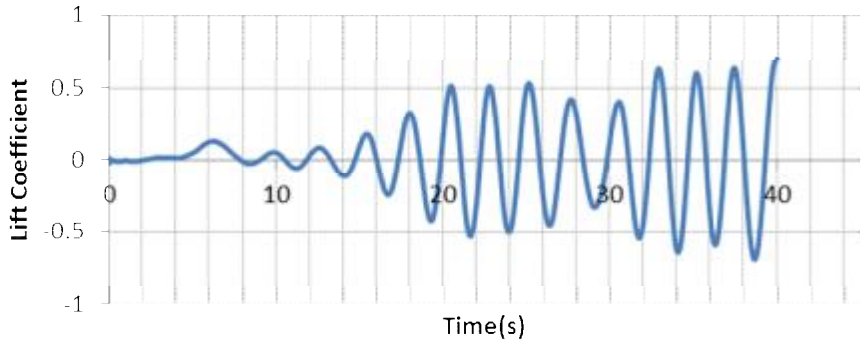

Figure 4.13. Lift coefficient variation on time for angle of 10˚ (numerical)

Figure 4.14. Root-mean-square (RMS) value of the lift coefficient of the cylinder for various yaw angles

As can be seen, the amounts of lift coefficient declined at angle of α=20˚ due to structural changes of wake (wake of three-dimensional shapes). As can be seen with increasing yaw angle of cylinder, the changes was observed in the wake structure of single cylinder. And the normal process of vortex shedding was observed at angles

from 0˚ to 20˚. Therefore, Kármán vortex street formation was changed and it was not observed any more. It was anticipated which, the changes of wake structure had a large effect on cross force coefficient (Lift coefficient) on the cylinder particularly. By using the results of numerical simulations, numerical quantities can be compared with lift coefficients based on the time for various angles. It was shown in the diagram below (Figure 4.15).

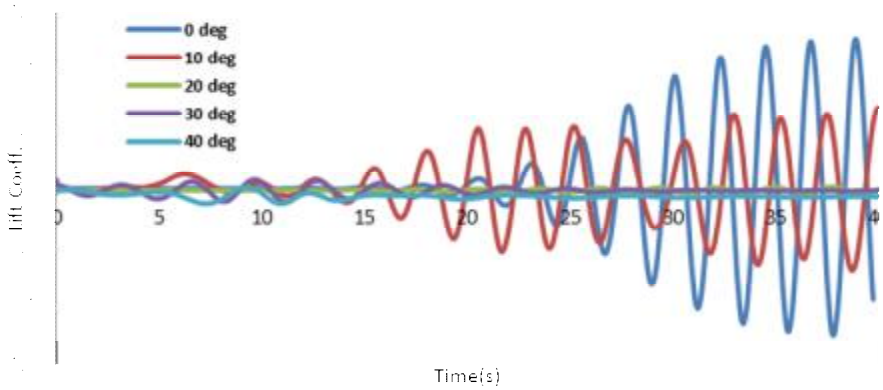

Figure 4.15. Lift coefficient variation over time for different yaw angles 0˚, 10˚, 20˚, 30˚ and 40˚ (numerical results)

According to figure 4.15, it can be seen that lift fluctuationst was decreased by increasing yaw angle of cylinder. This reduction was more significant for angles which were greater than 20˚. It was predicted that the changes of wake structure and disappearance of Kármán street have been made a reducing of lift force on cylinder at yaw angles which were greater than 20˚. If the frequency values of incoming lift force on the cylinder will be investigated and will be compared with increasing angle of cylinder it can be obtained more details. So for reaching to this aim, it was shown FFT (fast Fourier transform) chart of the incoming force on the cylinder for different angles in the following diagram.

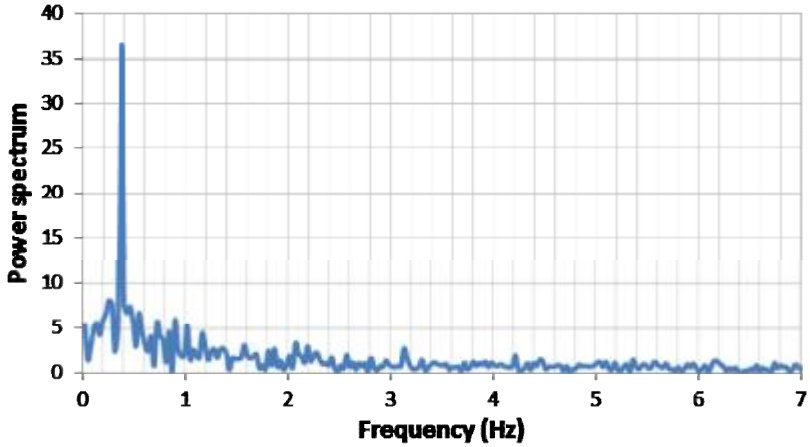

Figure 4.16. FFT and frequency analysis of a cylinder lift force at zero degrees (the experimental results)

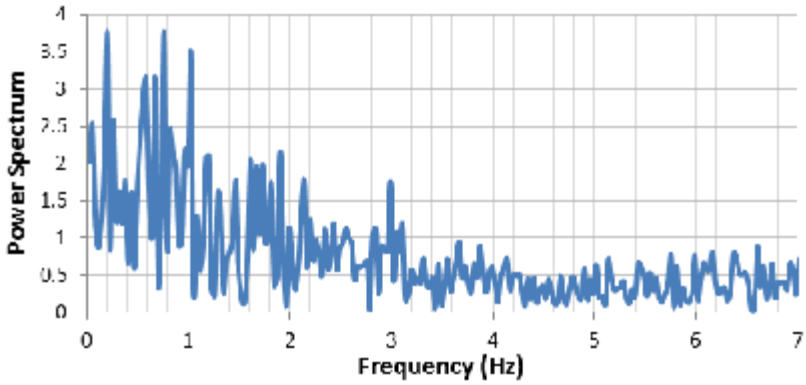

(a)

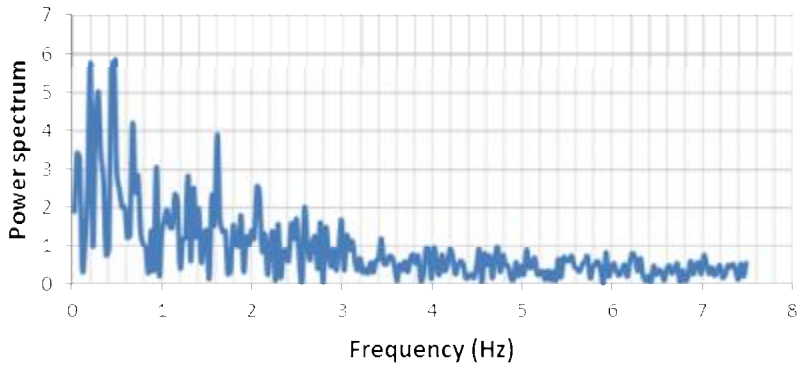

(b)

Figure 4.17. FFT and frequency analysis of a cylinder lift force at 25 and 40˚ (the experimental results) (a, b)

According to the graphs, can be observed only one dominant peak point was observed at angle of zero degrees. The frequency of vortex shedding was same with Kármán Street. Amount of Strouhal number was equal to 0.2 at zero degree. This

number also was equal to 0.192 at yaw angels of 5˚ and10˚. Thus, as which the wake structure was shown at figure 4.10, vortex shedding process were continued from the behind of cylinder until α=15˚, approximately. But Karman street was not observed after α=20˚ of cylinder. And a wake which was a set of previous vertex was replacing by shear layer which was intermittently separated from several distance of cylinder's wall. These separated shear layers from different parts of cylinder were irregularly, imported a lift force on cylinder by different frequencies. This subject was clearly observed in the fft chart.

4.1.6. Correlation for stream line‘s slop behind of single cylinder in side view plan

Another remarkable note which can be investigated in relative with increasing yaw angle was changed of stream lines' slop in the downstream. To investigate this process, angle of tangent line on stream line was calculated at all angles' positions for single cylinder The results of process angles' variation for tangent line of stream line was shown with increasing of yaw angle of the cylinder in the following diagram.

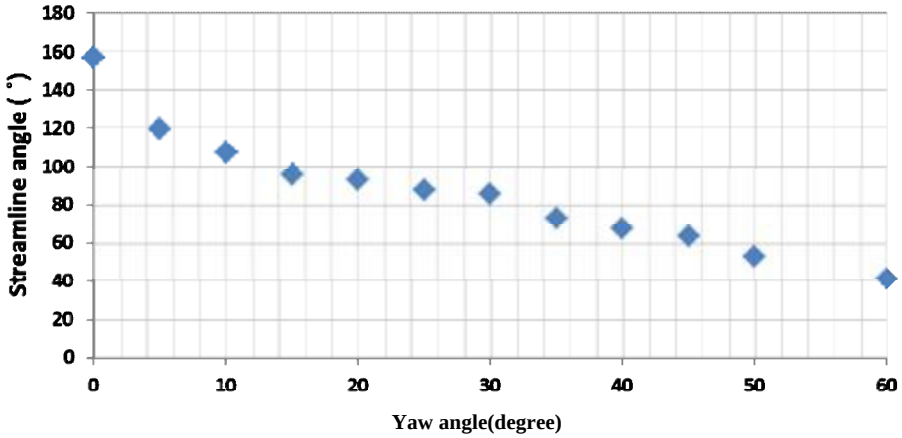

Figure 4.18. Changes of tangent line's angel of streamlines for 0˚ to 60˚ in side view

As can be seen, the slope of the tangent line of stream lines was increased with increasing of cylinder’s yaw angle. It means that the tangent lines’ angels were decreased. According to studying the pressure contours at the downstream for

different angles (Figure 4.19), can be explained that a reason for occurring this phenomenon was this fact which, the slop of the vectors and stream line to upper side changes due to the created difference pressure at the end of the cylinder with increasing the angle of cylinder.

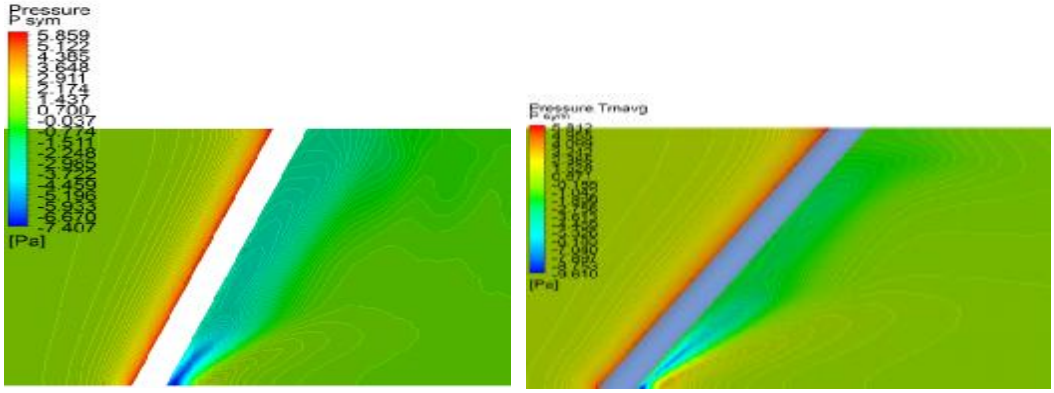

Figure 4.19. Pressure contours at α=20˚ and α=30˚, respectively (numerical results)

So that, the amount and direction of velocity which components stream lines-varies. With studying the mentioned changes can be extracted a correlation for changes of slope of stream line in the behind of cylinder in relative with angle of cylinder. This relationship was shown in figure below.

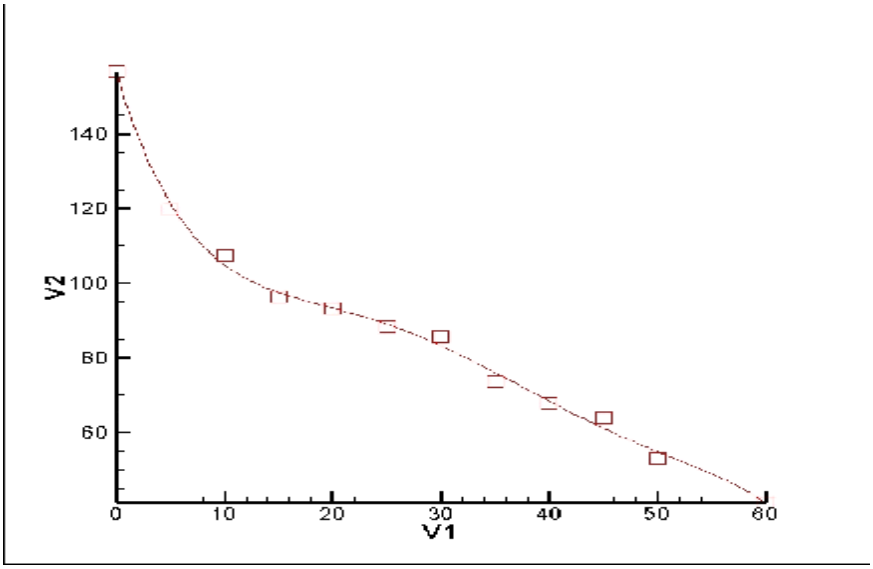

Figure 4.20. The relationship between stream lines ‘slope with increasing yaw angle in single cylinder

Table 4.3. The calculated correlation for the slope of tangent line of single cylinder

$y = A + Bx + Cx^2 + Dx^3 + Ex^4 + Fx^5$	
A= 1.563E+002	B= -9.614E+000
C= 6.206E-001	D= -2.019E-002
E= 2.987E-004	F= 1.649E-006

.

4.2. Two Cylinders In-tandem

In this section, experimental and numerical results were provided on the structure of flow around two yawed circular cylinders in tandem. The effects of the distance from center to center of cylinders and yaw angle were investigated. The experimental system and the measurement instruments as well as the process of conducting experiments were similar to the experiments carried out for the single cylinder described in the previous chapters.

4.2.1. Numerical simulations

According to the numerical results presented in the previous part, SST turbulence model successfully predicts the flow structure around single cylinder, consequently, the SST turbulence model and same numerical set up was used for simulating the flow around two cylinders in tandem. The used grid for the numerical analysis was shown figure 4.21. The grid had 6,936,400 elements and 1,744,211 nodes. For all analyzes carried out, the same dimensions of grid's resolution was used.

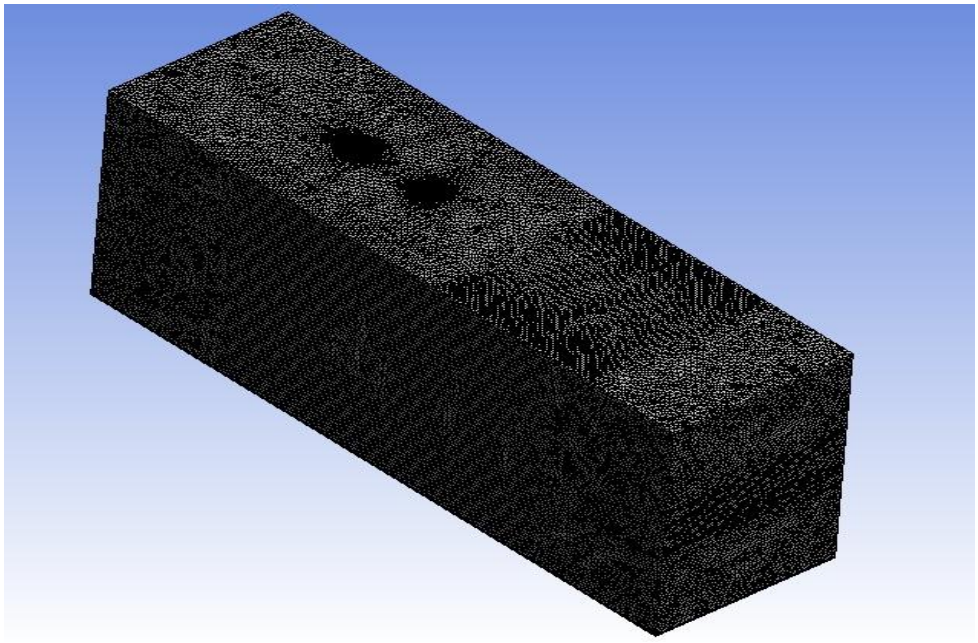

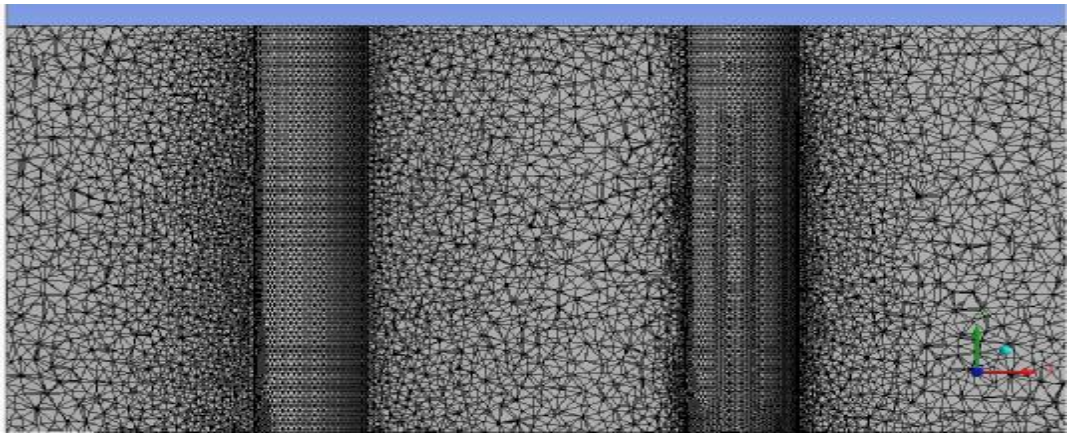

Figure 4.21. The used grid for the numerical analysis for two cylinders in tandem

The number of parameters investigated can be showed at the PIV experiments and the numerical simulations for two cylinders in the table 4.4. In the present study, the effect of two parameters was investigated on the wake structure of the flow around two cylinders and also the force coefficients on the streamwise (drag) and on the cross-stream (lift). As can be seen, many analyzes were carried out (more than 90 of numerical runs and experimental analysis have been done) was unprecedented at its same researches. Due to the large number of data, only the excerpts of results were exposure and also, a greater emphasis was been on some outcomes, which include major changes in comparison with other results.

Table 4.4. Yaw angles and center-to-center spacing ratios tested in the numerical simulation (two cylinder)

L/D	Yaw angles (˚)				
1	0	15	20	25	30
1.5	0	15	20	25	30
2	0	15	20	25	30
2.5	0	15	20	25	30
3	0	15	20	25	30
3.5	0	15	20	25	30
4	0	15	20	25	30
4.5	0	15	20	25	30
5	0	15	20	25	30

1- The effect of yaw angle of two cylinders: In these experiments, the effect

of yaw angle was investigated for both cylinders which their yaw angle changes simultaneously and equally then the vertical flow direction at yaw angle of 0 ˚– 15˚ – 20˚ – 25˚ and 30 degree.

2- The effect of the distance between the cylinders**:** For this purpose, non -dimensional number was defined as the gap ratio which was the distance between centers of the cylinders on the cylinder diameter (L/D).

In the following these factors will be explained in detail.

First of all, the streamline structure can be studied in horizontal and vertical plan and their changes according to the parameters can be understood. The structure of streamlines and wake has significant effects on the numerical values of drag and lift coefficients of cylinders. In the following, the relevant results were presented. It is noteworthy that, the numerical and experimental studies were used as complement each other for further investigations. For example, the streamlines variations and Reynolds stress changes were obtained from PIV experiments' outcomes and three-dimensional wake structure, the coefficients values of the aerodynamics forces, pressure distribution and turbulent quantities have been obtained from the numerical analysis.

Therefore, the exception of the special cases which comparison was done between the results, the main aim of studying other results was to discover the cause of the mentioned phenomena. For proving this agreement in the following figures were shown for the comparison of experimental and numerical results at different gap ratios for zero degree.

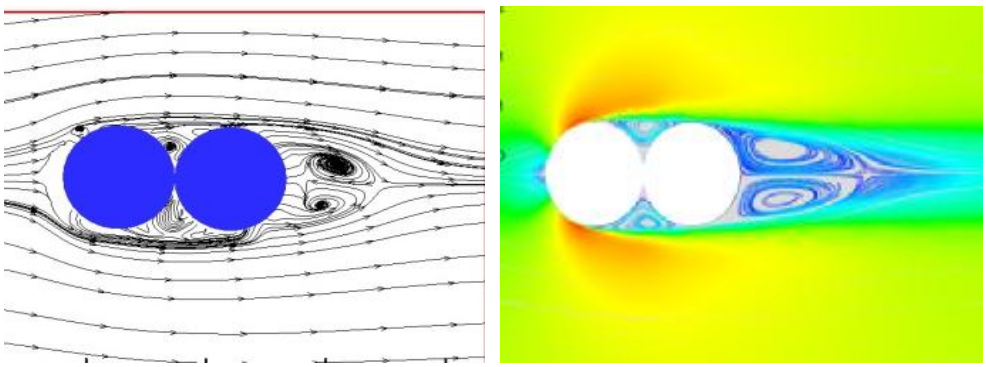

Figure 4.22. Comparison of experimental (left) and numerical (right) results at 0˚ and L/D = 1

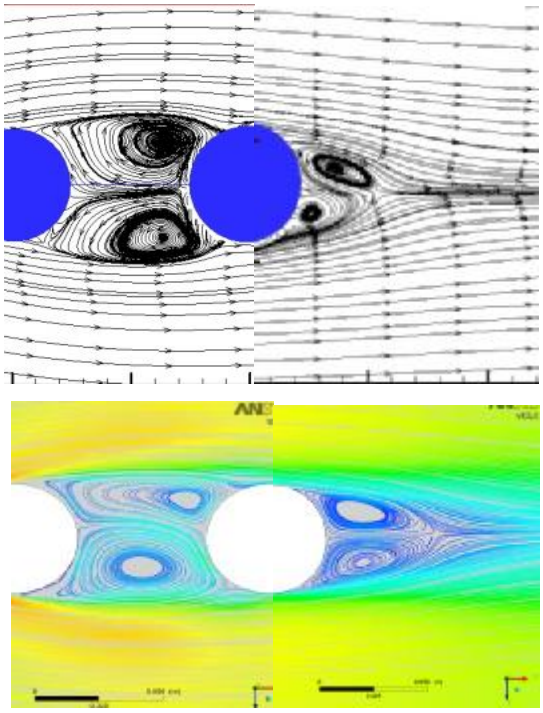

Figure 4.23. Comparison of experimental (above) and numerical (below) results at 0˚ and L/D = 2

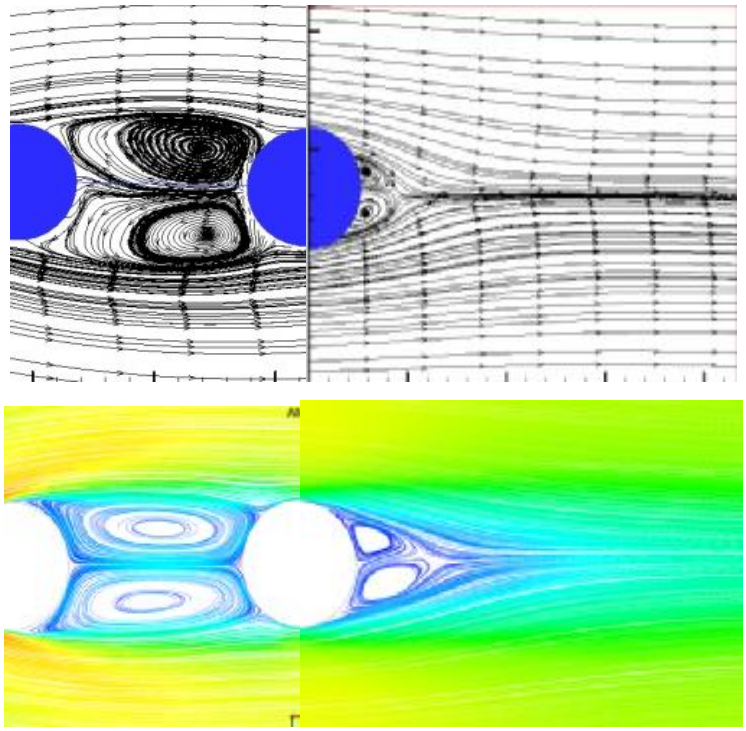

Figure 4.24. Comparison of experimental (above) and numerical (below) results at 0˚ and L/D = 3

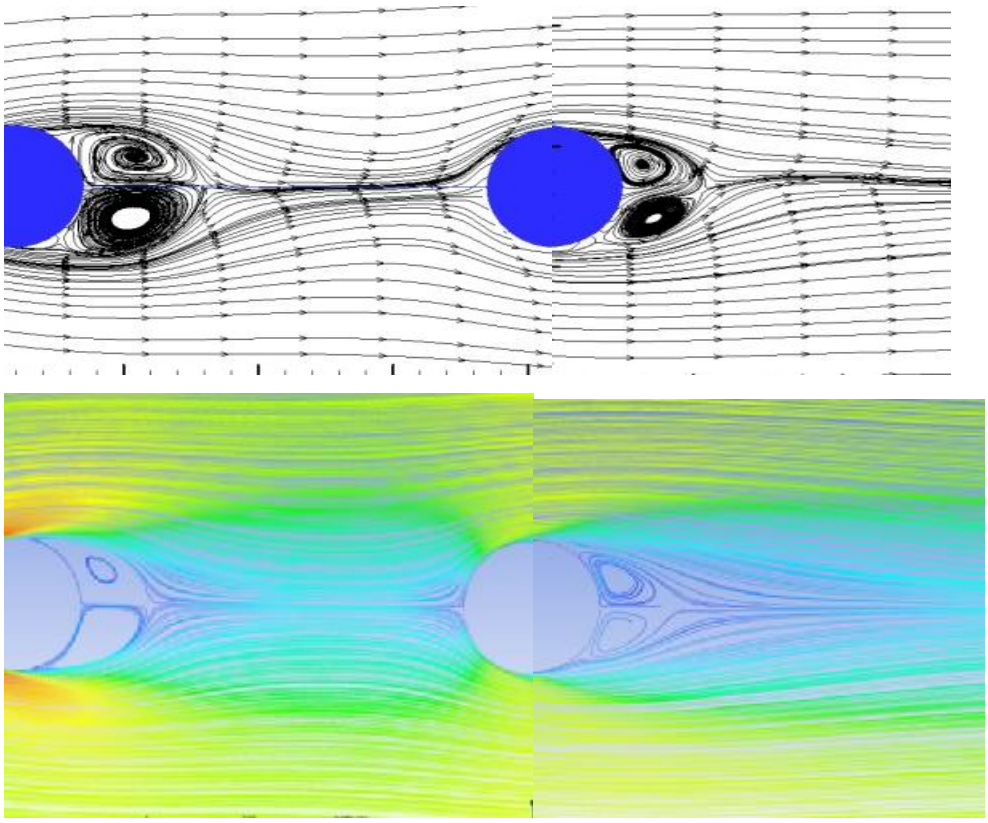

Figure 4.25. Comparison of experimental (above) and numerical (below) results at 0˚ and L/D = 4

As was observed, there was a good agreement between numerical and experimental results. Since the flow structure observed at L/D=4 is similar to that observed at L/D=5, the streamline topology for L/D=5 case were not included into the thesis.

4.2.2. The effects of gap ratio on the cylinders without yaw angle

4.2.2.1. Time-averaged streamlines

The streamline topologies for various gap ratios between tandem cylinders were given in the following figures.

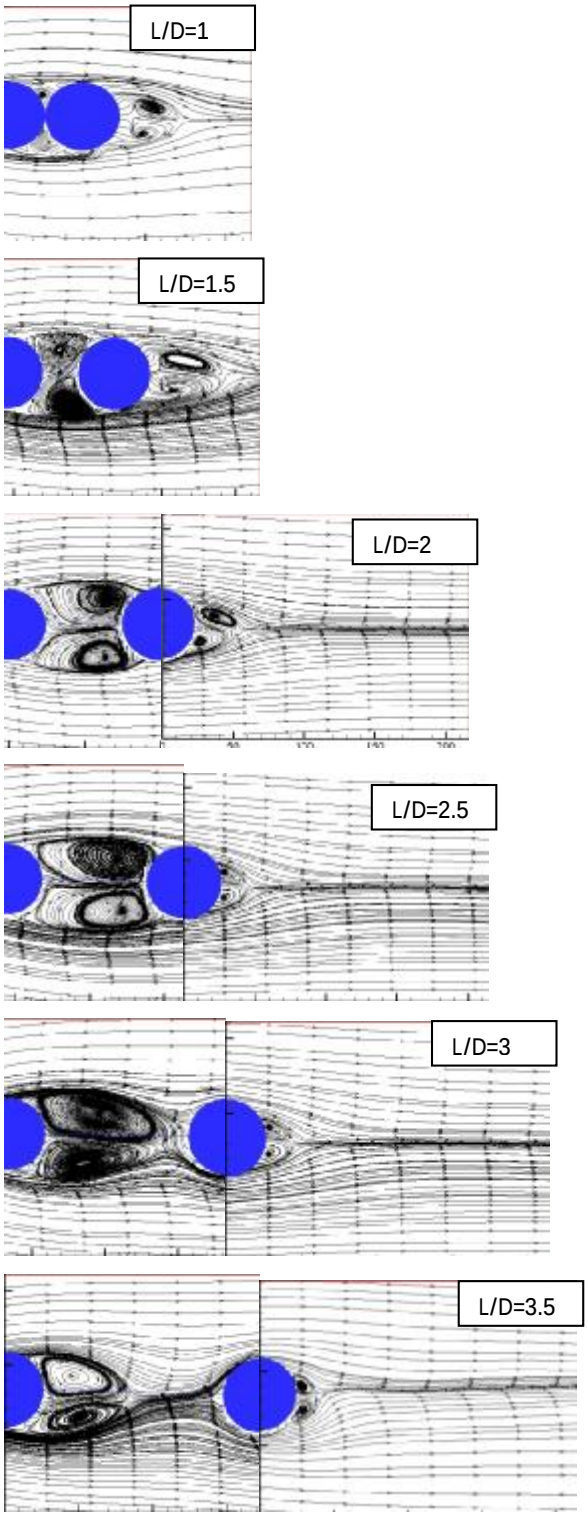
L/D=1
L/D=1.5
L/D=2
L/D=2.5
L/D=3
L/D=3.5

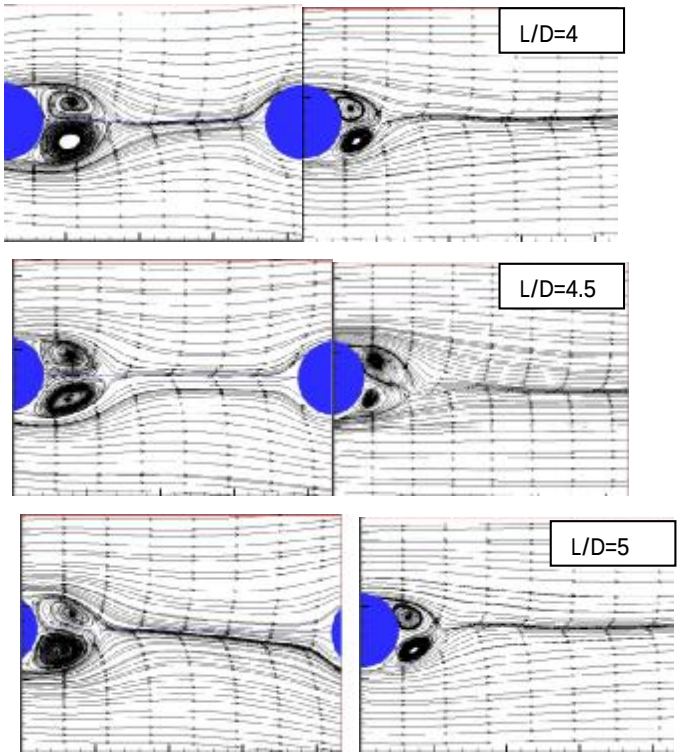

Figure 4.26. Streamline topology between two cylinders in tandem with configuration from L/D=1 to 5

As can be seen, for the ratio of L/D=1, only two small vortices were observed in both the top and bottom of the tangent region. The vortex was slightly formed larger dimension at downstream cylinder.

Some vortex was formed at pitch ratio of L/D=1.5 with far awing cylinders from each other in between the cylinders. The vortices were grown and were become larger slowly by increasing spacing between the two cylinders of each other.

However, dimension of the vortex was decreased in behind of downstream cylinder until pitch ratio of L/D=3. One of the other important points were the distance from the center vortex of first cylinder was increased until pitch ratio L/D=3. But after this, a decrease was observed at distance of vortex centers from the upstream cylinder.

By approaching vortex centers to upstream cylinder, streamlines were converged sooner and also the length of recirculation region was increased between two cylinders. After the value of L/D=3, the dimension of vortex increased in the

downstream cylinder with increasing spacing between the cylinders which leaded to effect on the amount of force on the cylinder.

4.2.2.2. Time-averaged vorticity patterns

Time averaged vorticity patterns for tandem arrangement for various gap ratios were seen in figure 4.27 below.

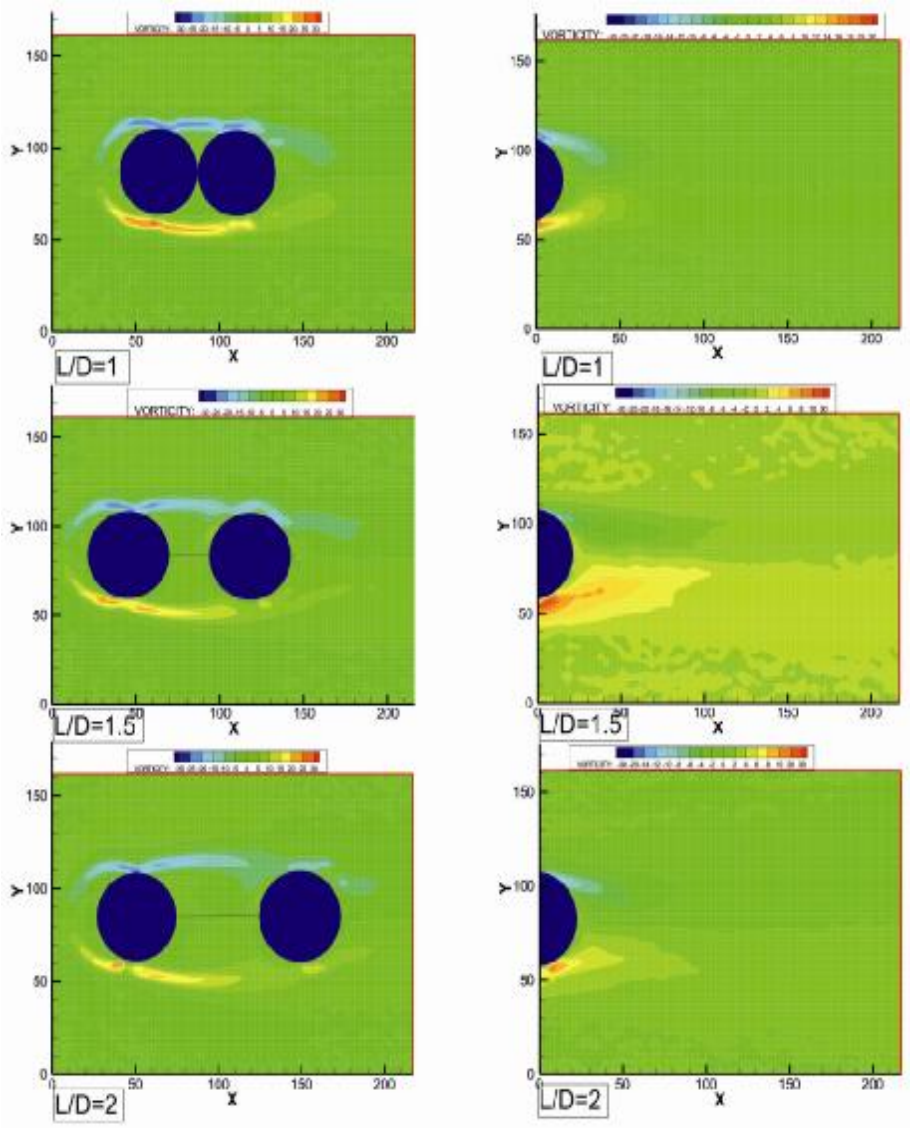

Figure 4.27. Time averaged vorticity contours for 0˚ from L/D=1 to L/D=2 (Experimental)

As can be seen from Figure 4.27, the shear layer jointed together at both cylinders in small center-to-center gap ratios (L/D=1-1.5). By increasing gap ratio, separate shear layers occur for both cylinders. This phenomena occurred while length of the shear layer in the upstream cylinders was increased and became larger until gap ratio equal to L/D=3. But then shear layers became smaller in the shoulders of upstream cylinder gradually.

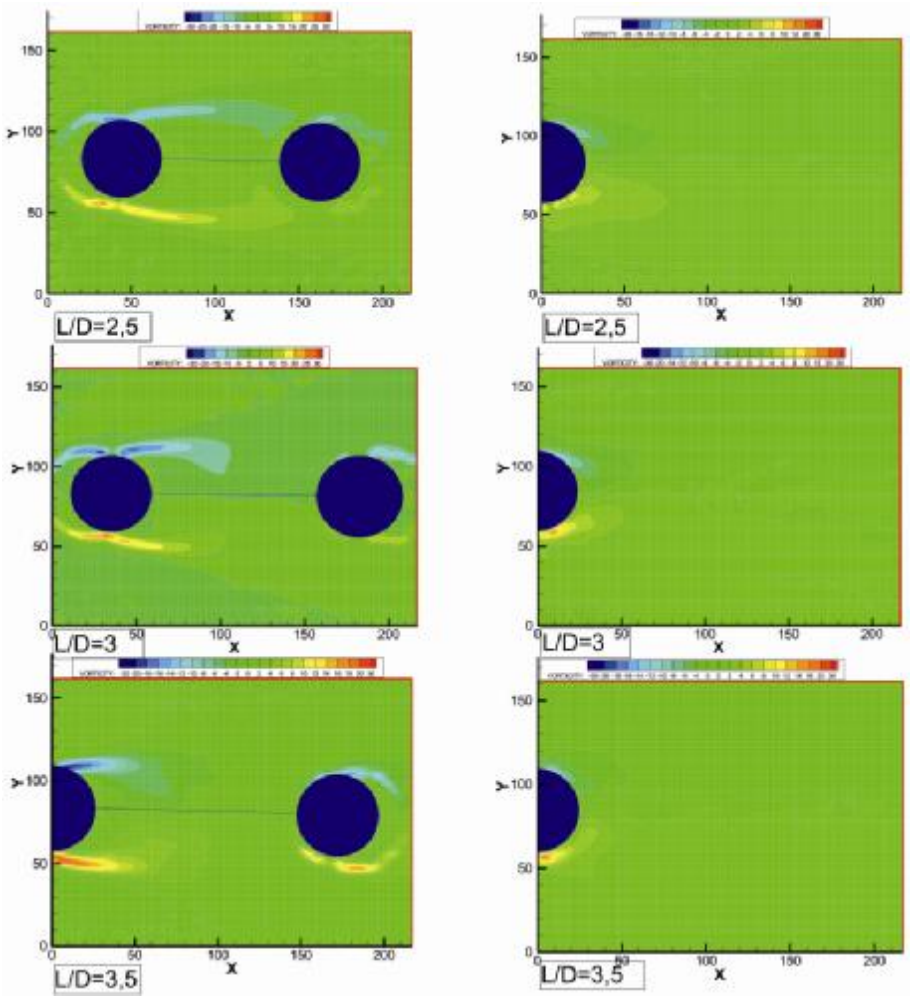

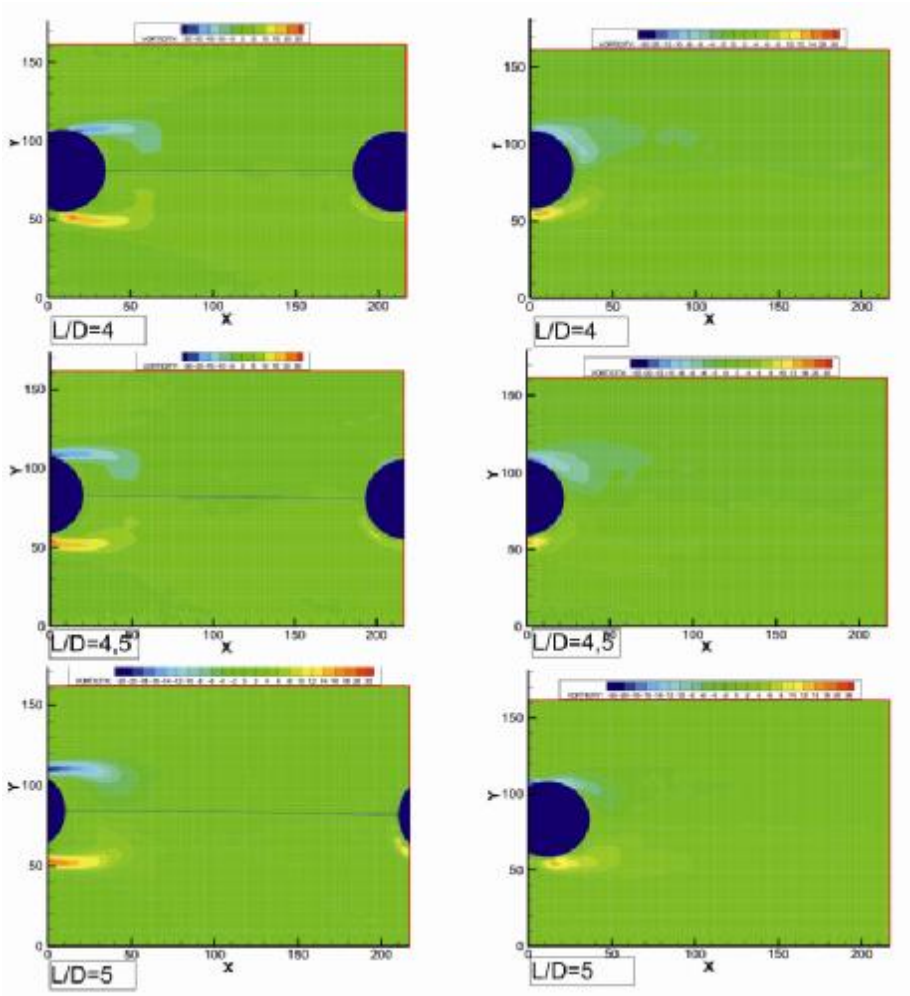

Figure 4.28. Time averaged vorticity contours at 0˚ from L/D=2.5 to L/D=5

4.2.2.3. Vortex formation

The process of vortex formation was shown for gap ratio of L/D=1.5 to investigate the wake formation and development of vortices at different instances in the figure below.

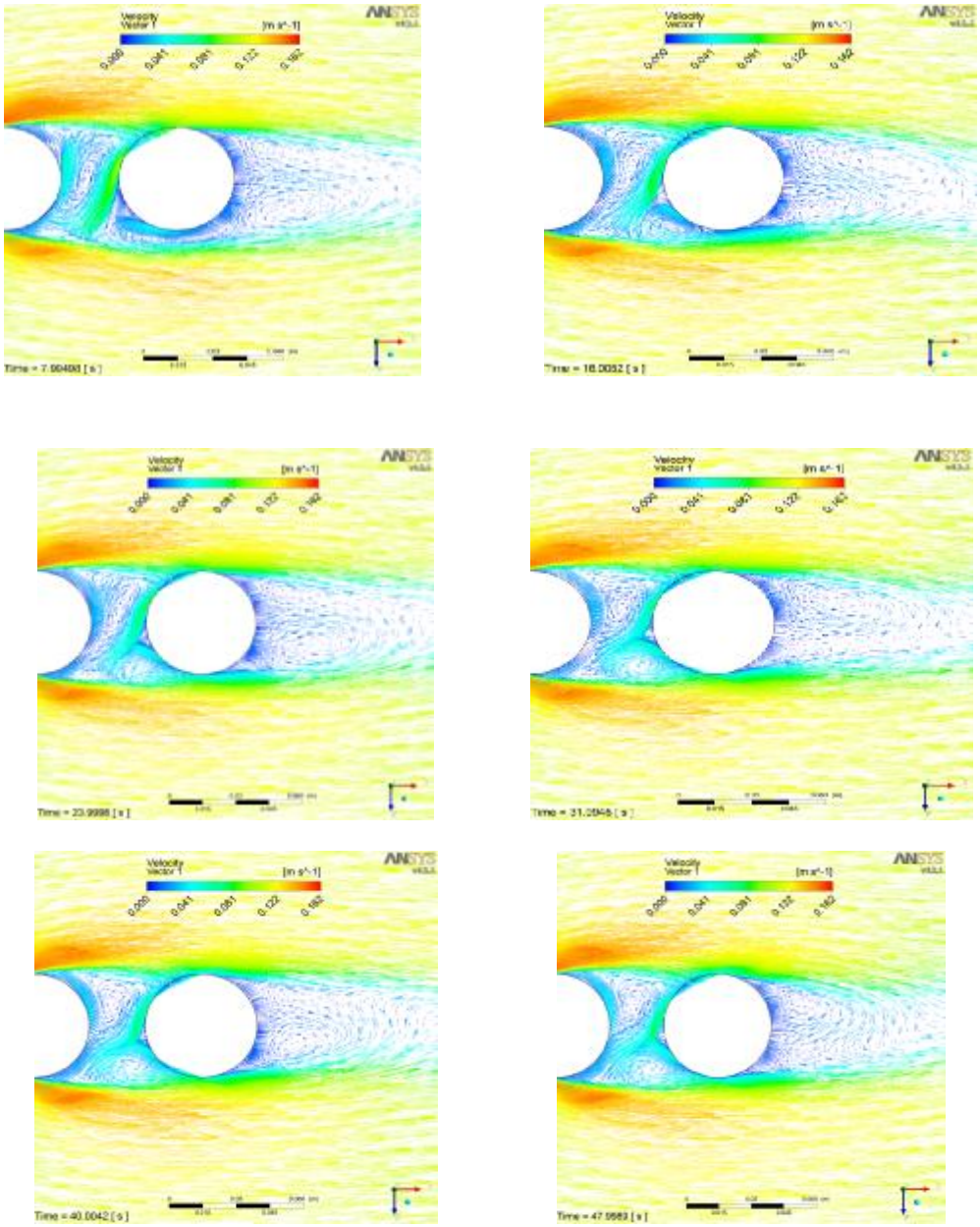

Figure 4.29. Instantaneous velocity vector field around the cylinder at L/D=1.5 in the initial times

According to figure 4.29, only one vortex was observed between two cylinders in the initial times (about 7 to 9 second), also two pairs of vortex were observed in the downstream which had a large elongation in the flow direction and their center distance were high from downstream cylinder. The vortex structure

which was seen in the experimental results, were partly asymmetric, also the dimension of up vortex was larger than the down vortex.

As time progresses (about 16 to 23 seconds), another vortex formation was observed in the spacing between the two cylinders which started to grow from lowest point of the downstream cylinder. Over time, these vortices moved slightly upward and toward the first cylinders simultaneously. As shown in the PIV experimental results, saddle point of two vortices between two cylinders moved backward and became closer to upstream cylinder. Another significant point is that dimension changes of two vortices downstream continued to time, that vortices remained asymmetric during of deformities presses.

4.2.2.4. Time-averaged drag coefficient

As was mentioned before, wake structure and vortex formation have more influences on aerodynamics force to cylinders. In the following figure 4.30, drag and lift coefficients changes was shown for both cylinders with increasing spacing ratio between them at angle of zero degree.

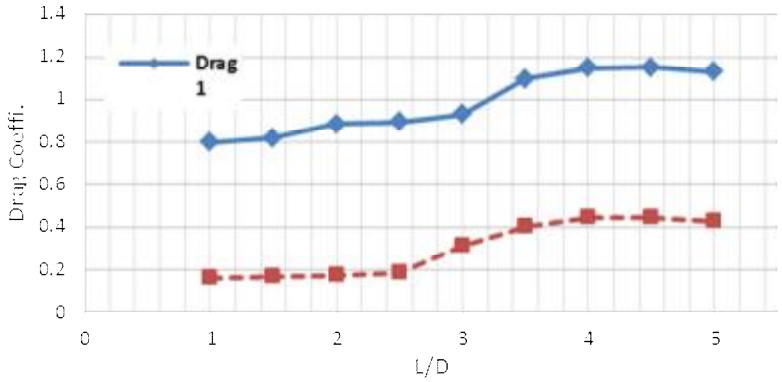

Figure 4.30. Drag coefficient variations with angle of zero degree to spacing ratios between cylinders

As can be seen, in the all gap ratios, upstream cylinder's drag coefficient was greater than downstream one since the wake structure of upstream cylinder had an important influence on the downstream cylinder. As process was observed, drag coefficient in both cylinders was generally increased with increasing gap ratio. For downstream cylinder, cause of the drag coefficient increase induced a decrease of

upstream wake effect on downstream because the vortices were closer to upstream in the between distance with growing spacing ratio. Due to increase fluid momentum after ratio of L/D=3, drag coefficient increased. For further investigation in this issue, stream wise velocity contours were exposure.

With visualization of velocity component's variation, average streamwise velocity increased was concluded in between the cylinders with increasing spacing ratio. So that it climbed up from 100 mm/s at ratio of L/D=2.5 to about 350 mm/s at ratio of L/D=5. These increases of velocity made to increase flow momentum in this range. The cause of the wide range of momentum variation could be concluded due to pressure distribution between two cylinders.

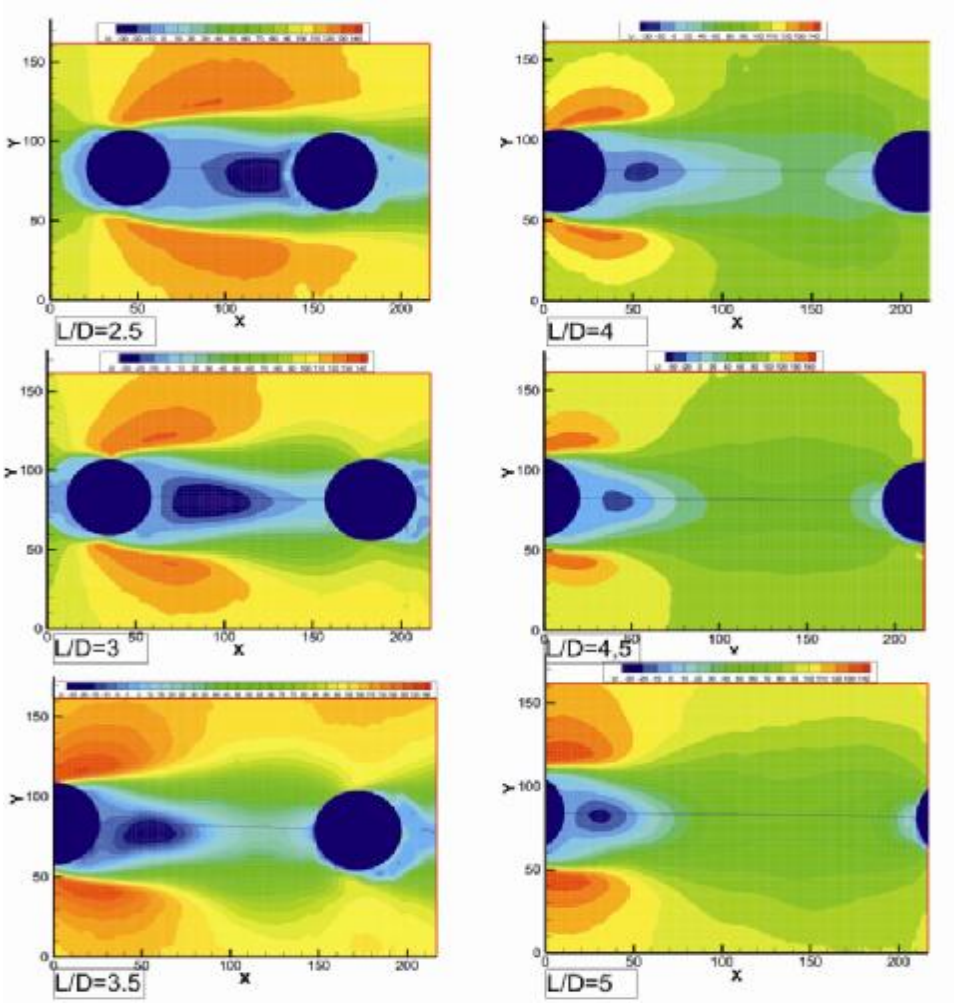

Figure 4.31. Streamwise velocity (u) from L/D=2.5 to L/D=5

Therefore, when gap ratio was too small, the high effect of stagnation point's pressure induced downstream cause to reduce the flow velocity in this range. Increasing the spacing between the cylinders led to get away stagnation point of the second cylinder, consequently fluid velocity increased in this range. This subject can be investigated by studying the pressure distribution between two cylinders (Figure 4.32).

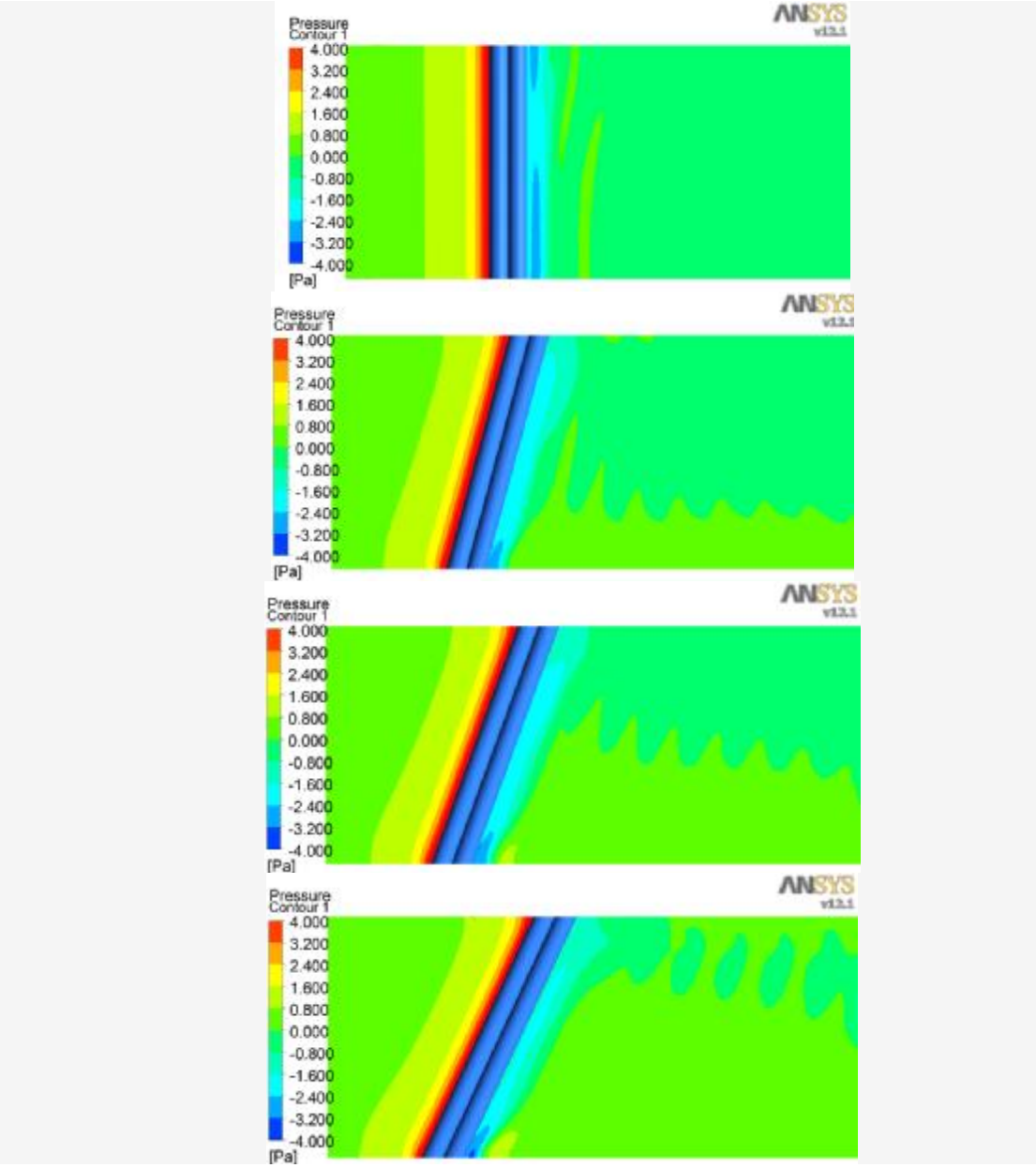

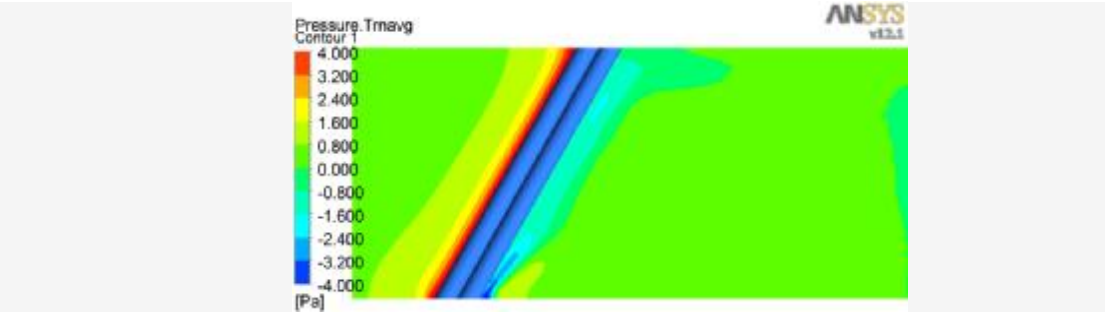

Figure 4.32. Pressure contours of two cylinders at L/D=1 for various yaw angles

4.2.2.5. Turbulent Kinetic Energy (TKE)

Another important parameter is the variation of turbulent kinetic energy in the flow field. Generally TKE can be considered kinetic energy per mass which was transferred by eddy in a turbulent flow. In general, there was the highest pressure region at upstream (stagnation point) and the lowest pressure region was at downstream which this region was the main part of the formation and eddy production. TKE energy was taken of mean flow for production of eddy, and therefore the maximum amount of TKE was observed in this region. With getting away from this region and by bopping eddy with mean flow, the energy decreased and dissipation eddy began. After that, an increase of TKE was observed due to eddy formation and eddy production in downstream.

TKE can be calculated using two-dimensional approximation (Lee and Lee 2008)

$$\bar{w}^2 \approx \frac{1}{2}(\bar{u}^2 + \bar{v}^2), \quad k = \frac{1}{2}\rho(\bar{u}^2 + \bar{v}^2 + \bar{w}^2) \approx \frac{3}{4}\rho(\bar{u}^2 + \bar{v}^2),$$

TKE variation was shown in the following figure. As can be seen from Figure 4.33, with increasing gap ratio between the cylinders, a composed bubble shape region deformed and gradually became two bean-shaped structures in the downstream region.

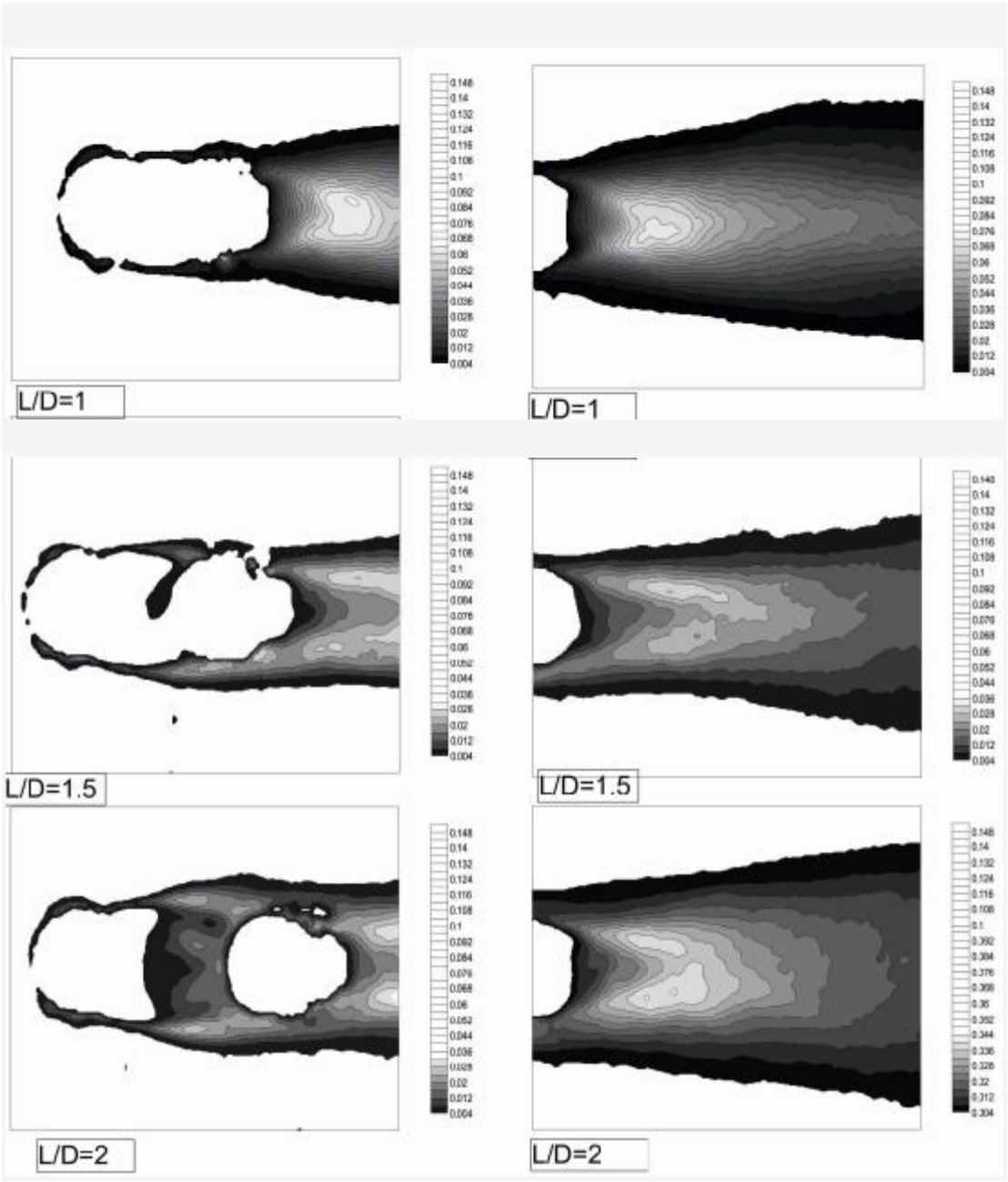
L/D=1
L/D=1
L/D=1.5
L/D=1.5
L/D=2
L/D=2

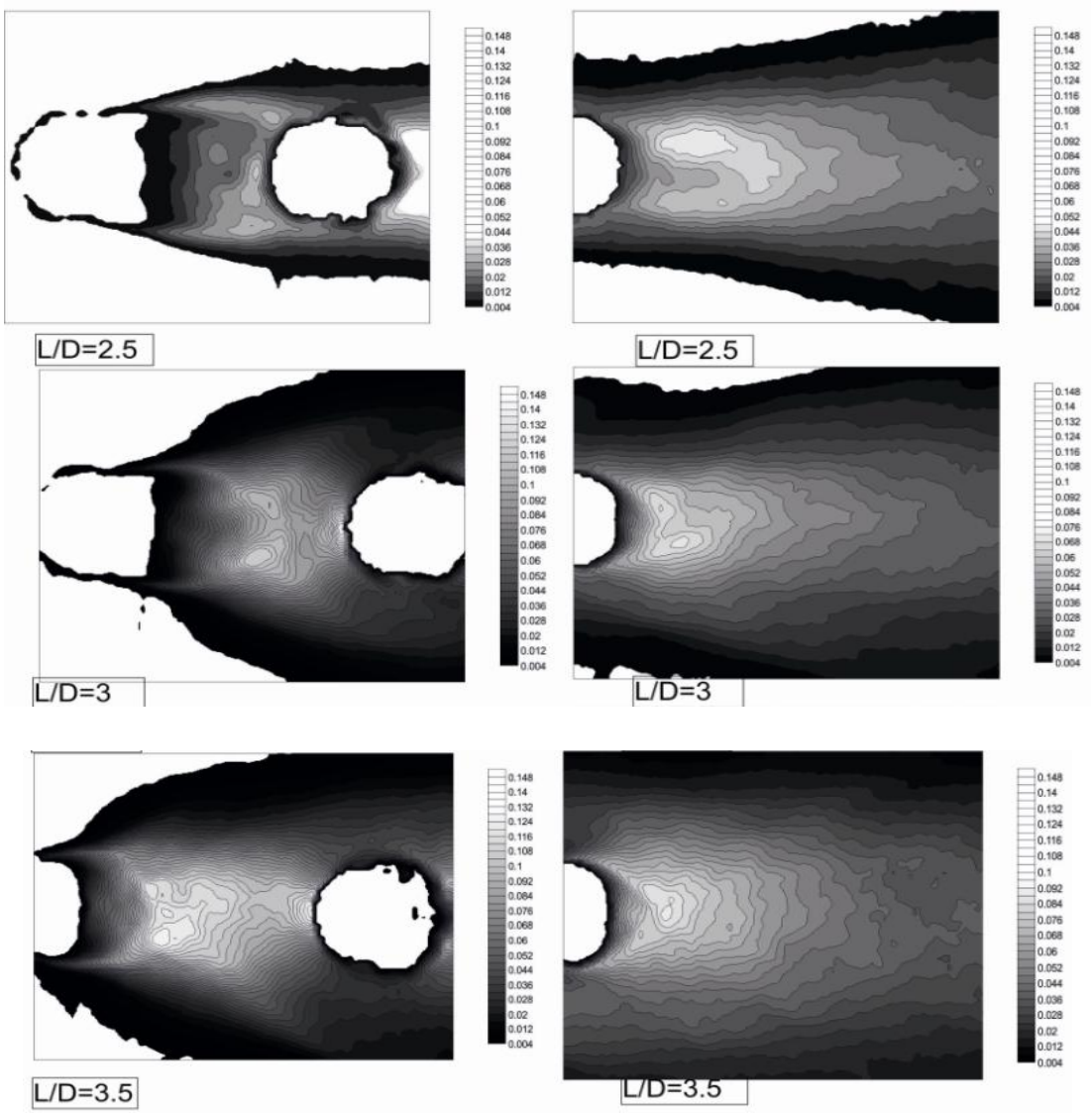
0.148
0.14
0.132
0.124
0.116
0.108
0.1
0.092
0.084
0.076
0.068
0.06
0.052
0.044
0.036
0.028
0.02
0.012
0.004
L/D=2.5
L/D=2.5
L/D=3
L/D=3
L/D=3.5
L/D=3.5

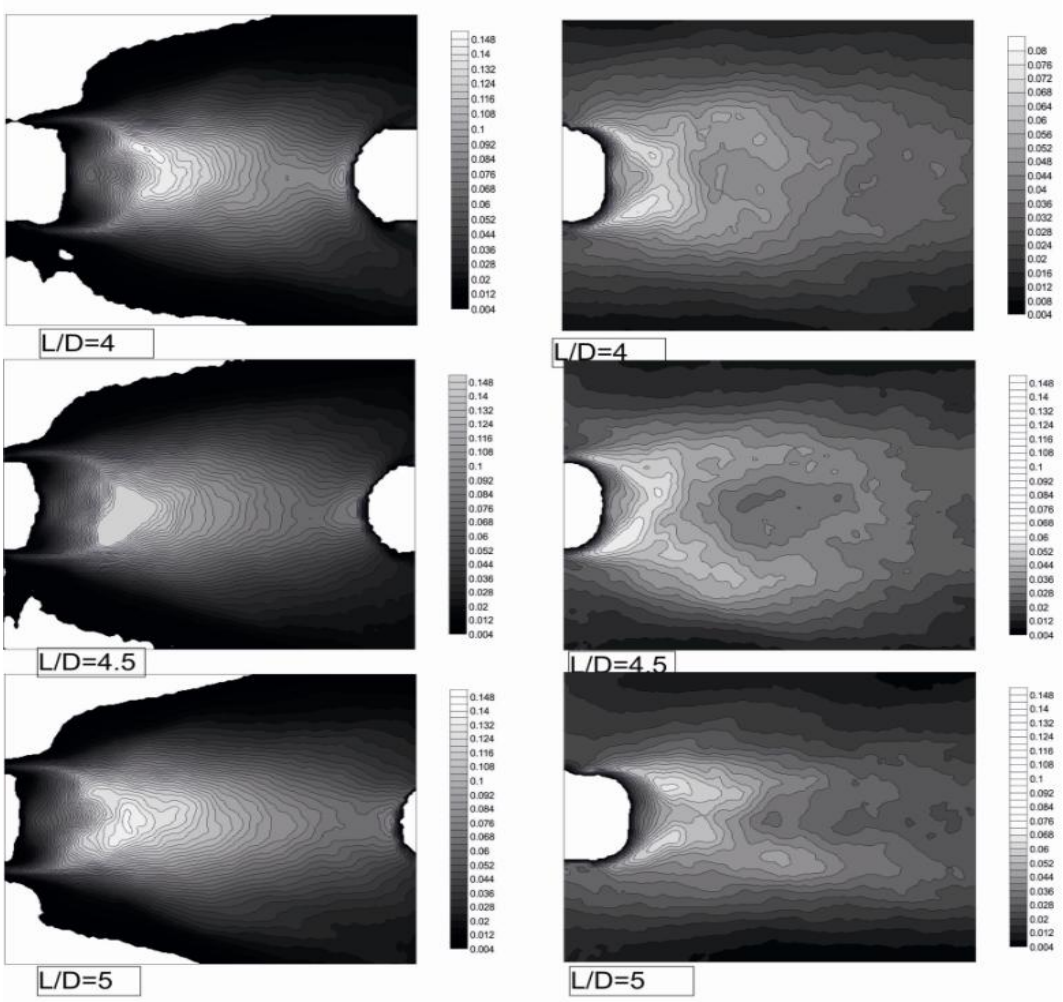

Figure 4.33. TKE contours of two cylinders in tandem for various spacing ratios at α=0˚

As can be seen, with increasing spacing between center to center of cylinders, TKE quantity was increased at the behind of both cylinders. But its upstream amount was increased much higher than in the downstream amount. This issue indicates that vortex interaction of two vortices was greater in the between region of two cylinders. So, the maximum TKE reached from 0.068 amount at spacing ratio of L/D=1 to 0.084 amount at spacing ratio of L/D=5 in downstream. While the maximum value of TKE at upstream reached from 0.028 in L/D=2 to 0.132 value at spacing ratio of L/D=5.

4.2.2.6. Reynolds stresses

Reynolds stress was other quantities of the flow domain which was studied frequently. In the figure 4.36, the effects of the spacing ratios between two cylinders were implied at zero degree on the Reynolds stress.

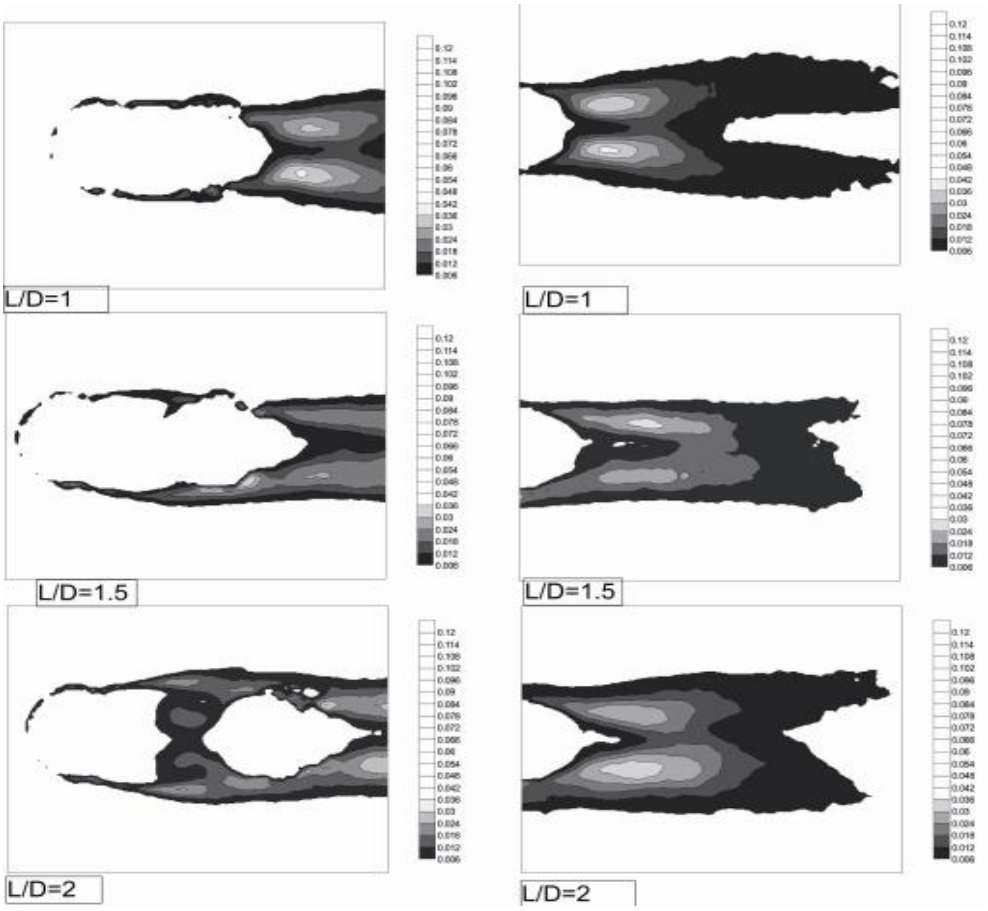

Figure 4.34. Reynolds stress (u'u') contours up to L/D=2

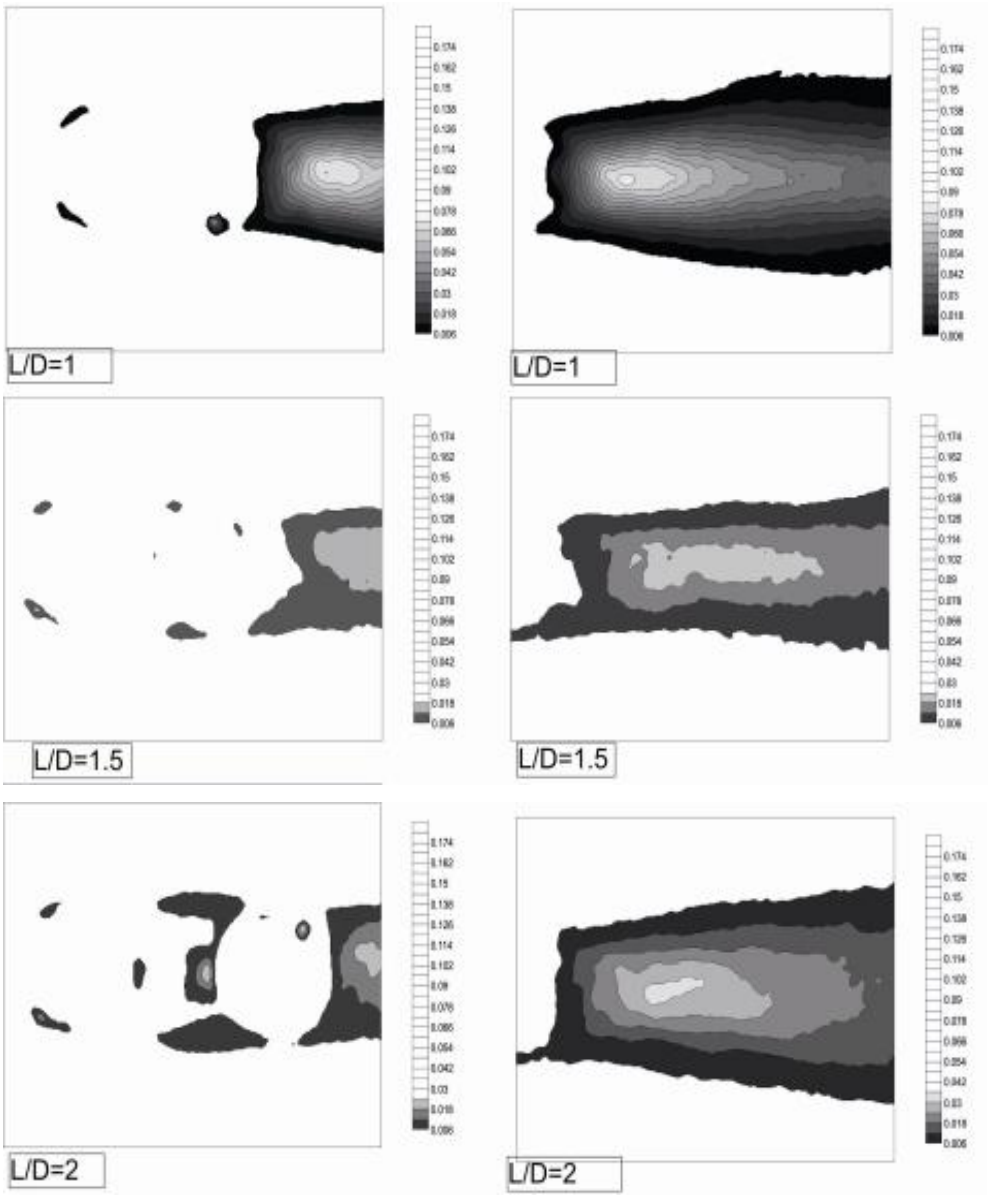

Figure 4.35. Reynolds stress (v'v') contours up to L/D=2

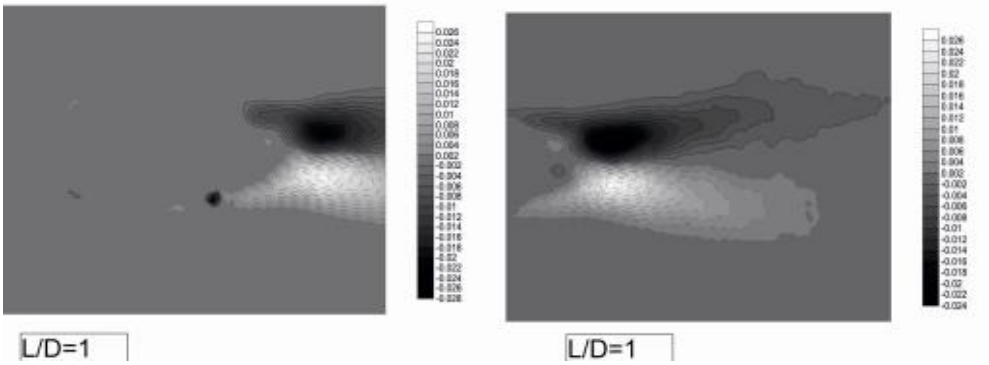

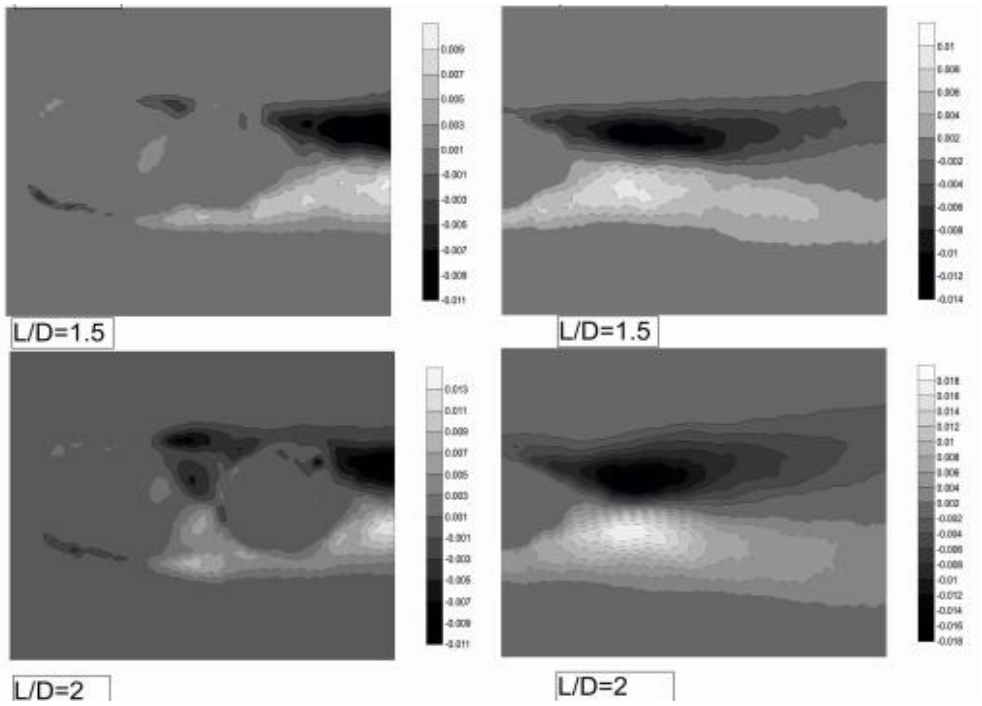

Figure 4.36. Reynolds stress (u'v') contours up to L/D=2

As previously observed, two symmetrical structures according to center line were observed from the contours of u'u' and u'v' in the range of L/D = 1, 1.5 and 2 which increased with the increment of the distance between their centers. And their further elongations were seen along the center line.

The important point is which with increment L/D ratio between cylinders, u'u' quantity increased at the end point of the first cylinder. Such that maximum value at ratio of L/D=1 increased from 0.036 to 0.102 at L/D=5 ratio. At L/D=2 ratio, the bubble-shaped structure was being formed in the middle of the cylinder. According to figure 4.47, a region was observed with a maximum valve of Reynolds stress at v'v' 'contours that was located on center line. Also, these results by Cantwell & Coles and Mittal & Balachandar are predicted (Cantwell and Cole, 1983), (Mittal and Balachander 1865, 1995).

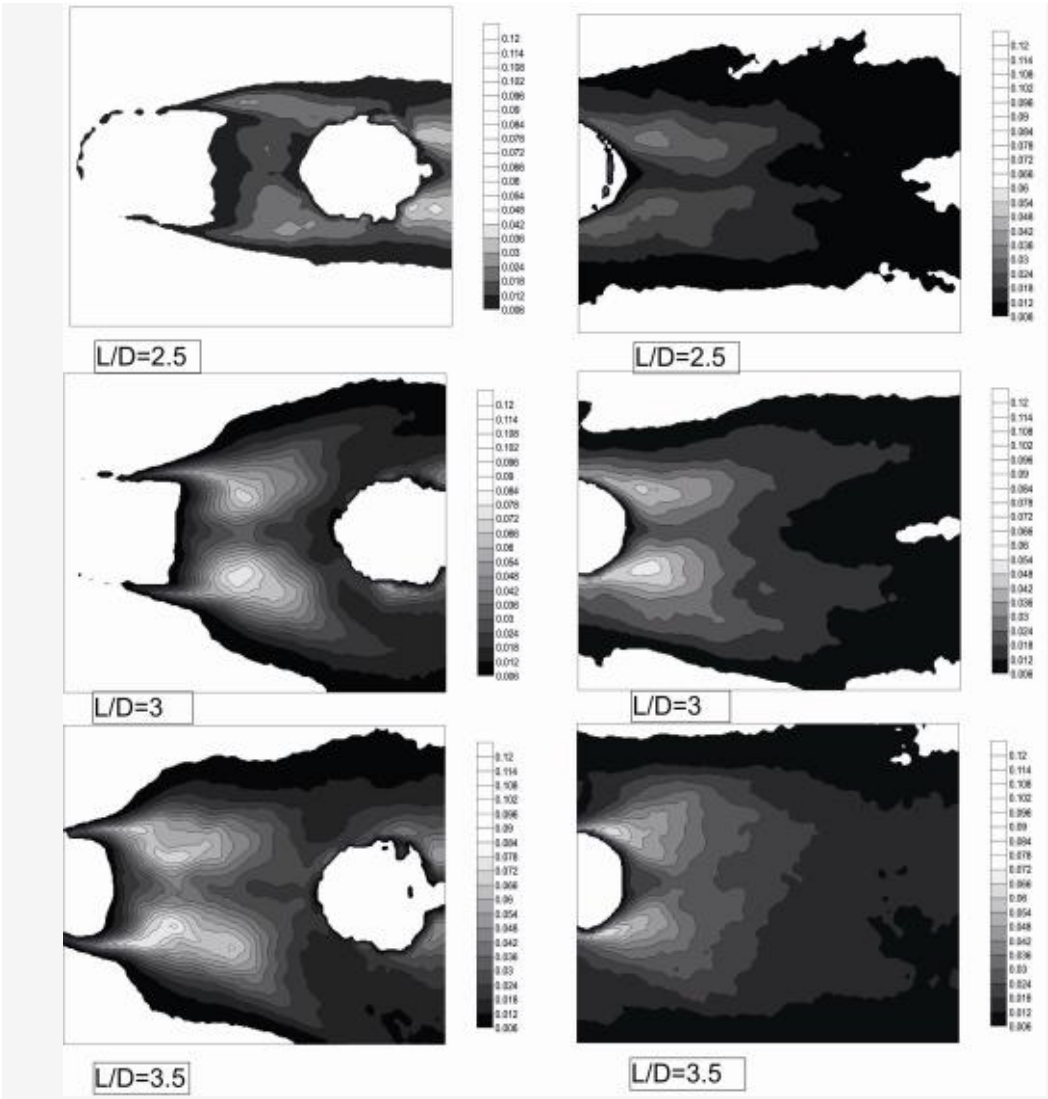

Figure 4.37. Reynolds stress (u'u') contours from L/D=2 to 3.5

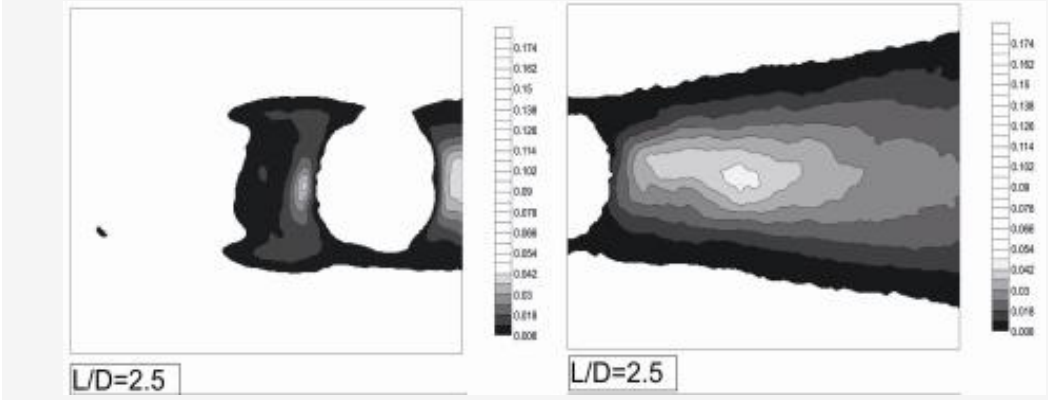

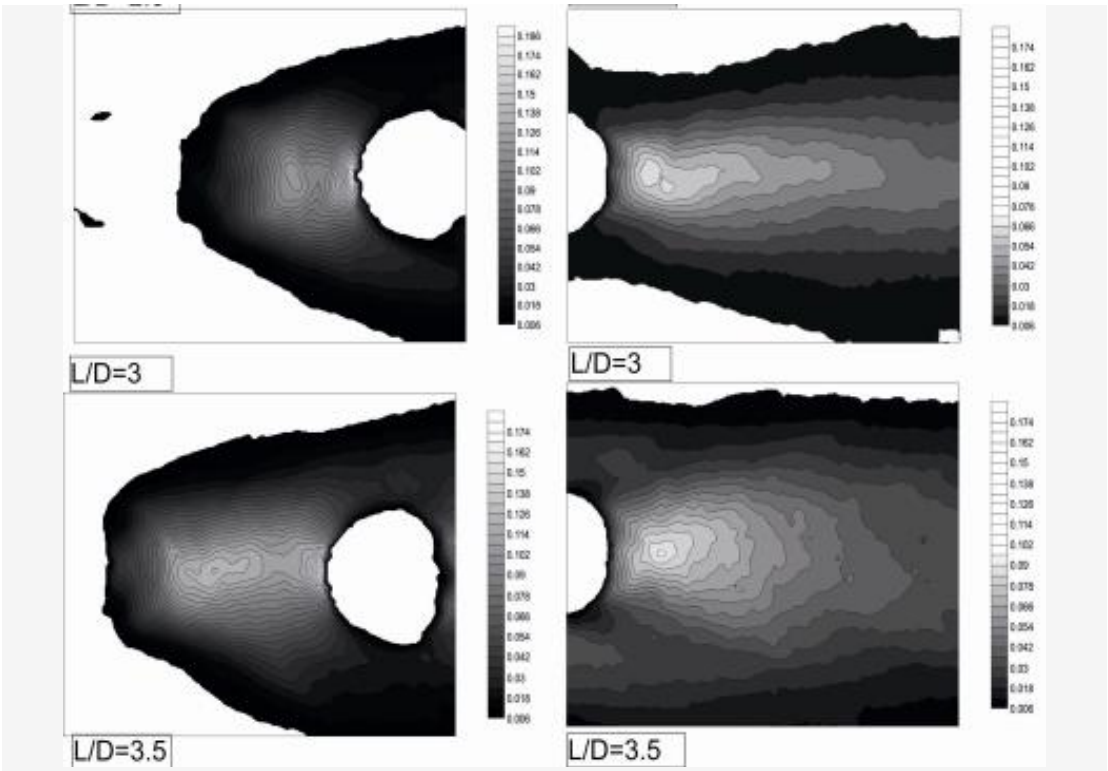

Figure 4.38. Reynolds stress (v'v') contours from L/D=2 to 3.5

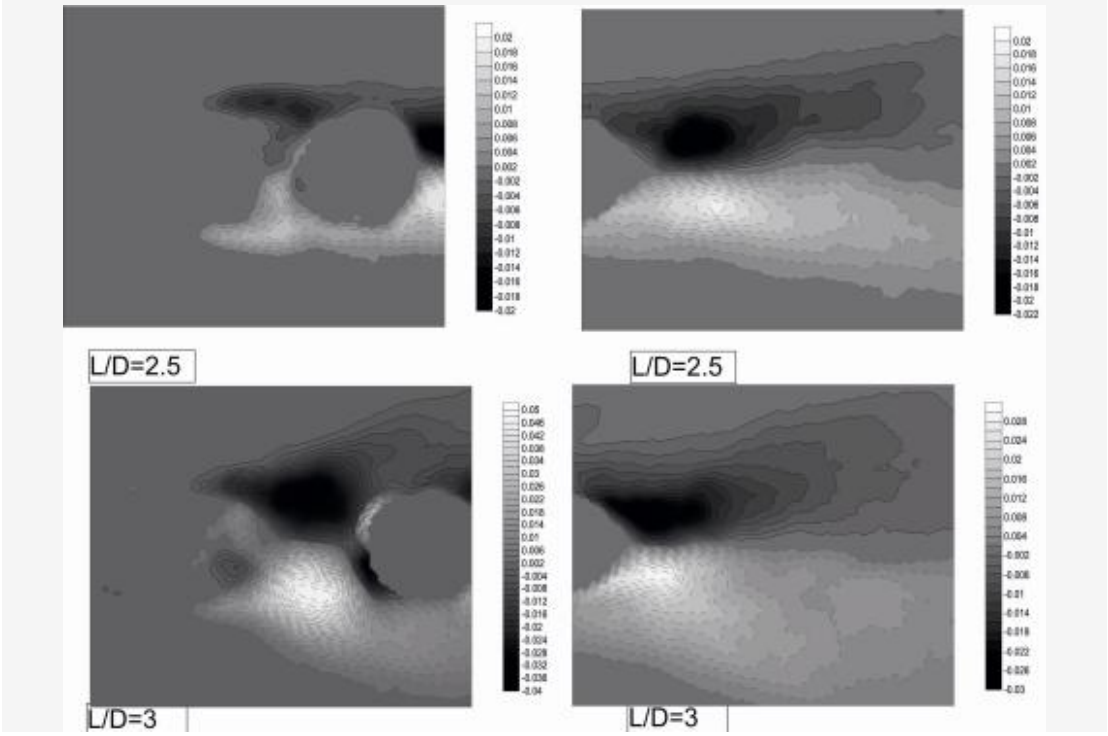

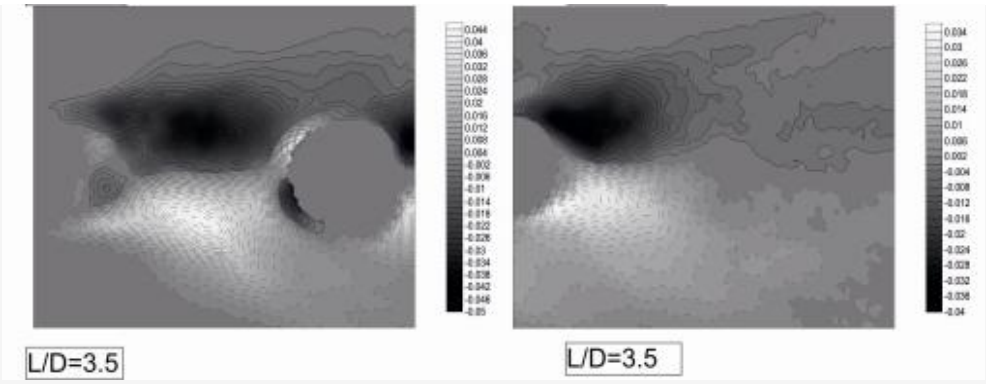

Figure 4.39. Reynolds stress (u'v') contours from L/D=2 to 3.5

With increasing L/D between two cylinders, the highest value of v'v' contour was formed at the downstream location of second cylinder. It is noticeable that with increasing the distance between the cylinders or increasing ratio of L/D, the region of maximum transverse Reynolds stress was getting closer to the cylinder behind the second cylinder. In addition, another considerable point is that with increasing L/D ratio, maximum value of v'v' was decreased at L/D=1 from amount 0.78 to 0.048 at L/D=2 ratio, and then it gradually increased with increasing L/D, finally it reached to 0.102. The value at L/D=2 from 0.054 was started to increase, with a consistent ratio until about 0.174 at L/D=5 ratio in the behind of first cylinder or region between two cylinders.

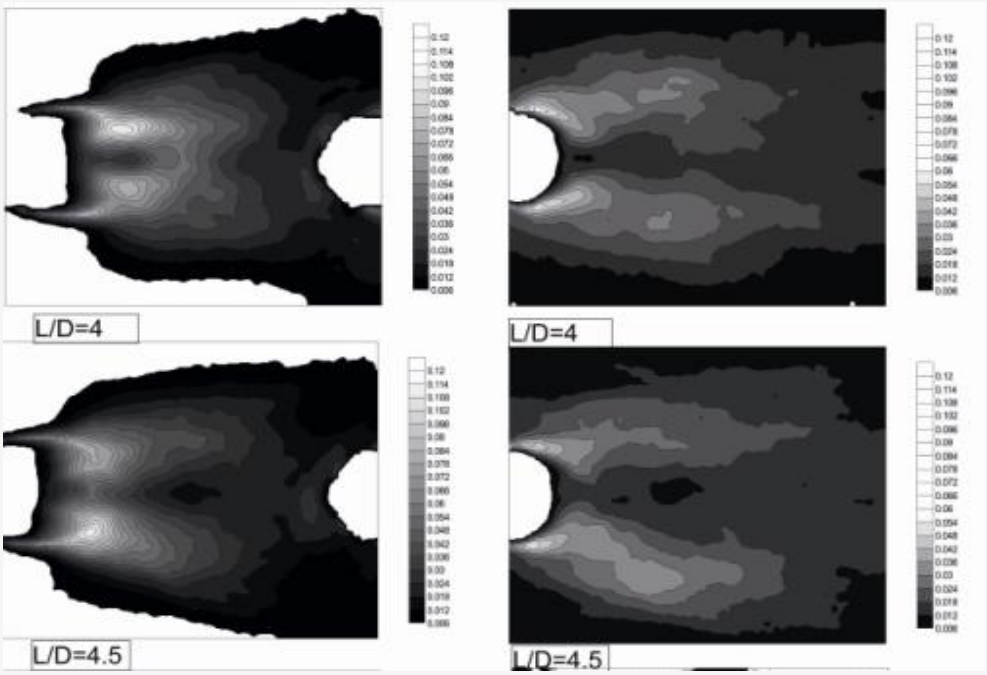

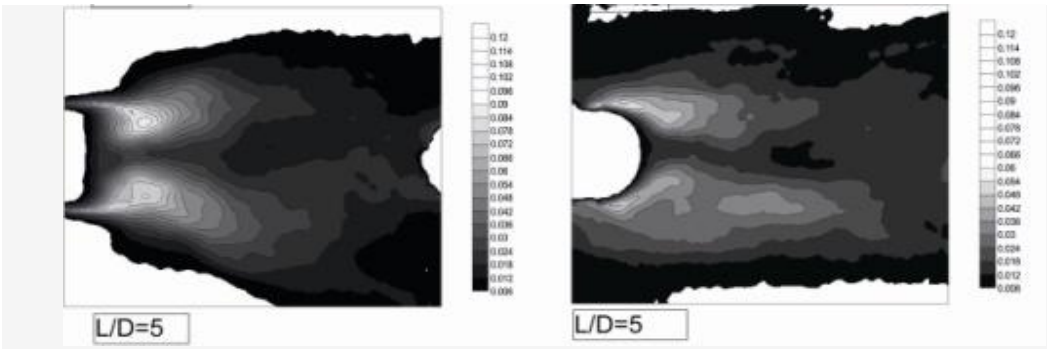

Figure 4.40. Reynolds stress (u'u') contours from L/D=4 to 5

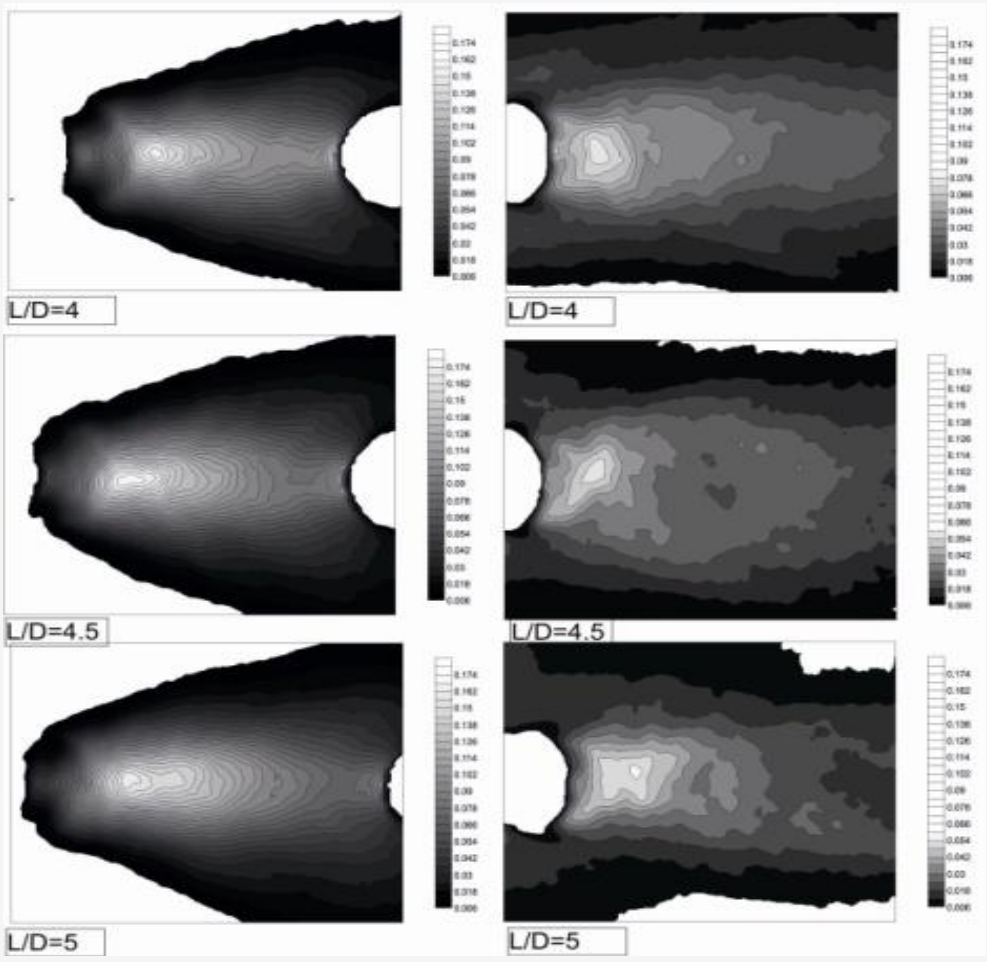

Figure 4.41. Reynolds stress (v'v') contours from L/D=4 to 5

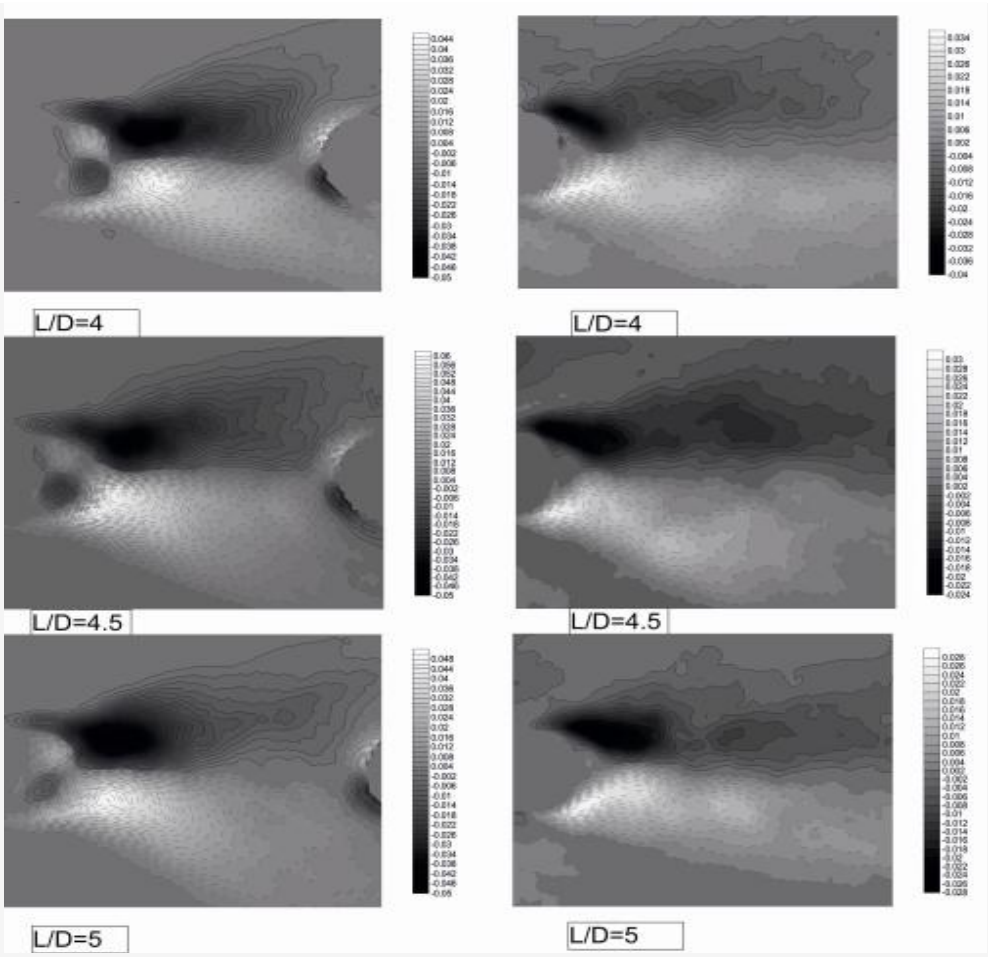

Figure 4.42. Reynolds stress (u'u') contours from L/D=4 to 5

4. 2.2.7. Vortex shedding

Three-dimensional wake structure of cylinders and effect of L/D ratio on the cylinder wake was shown in the following figures.

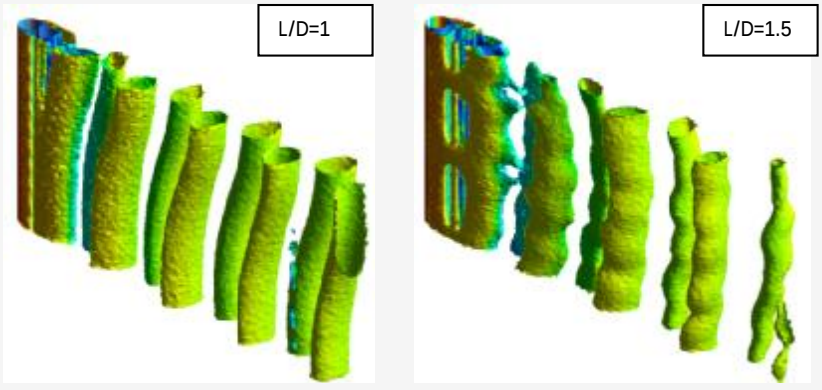

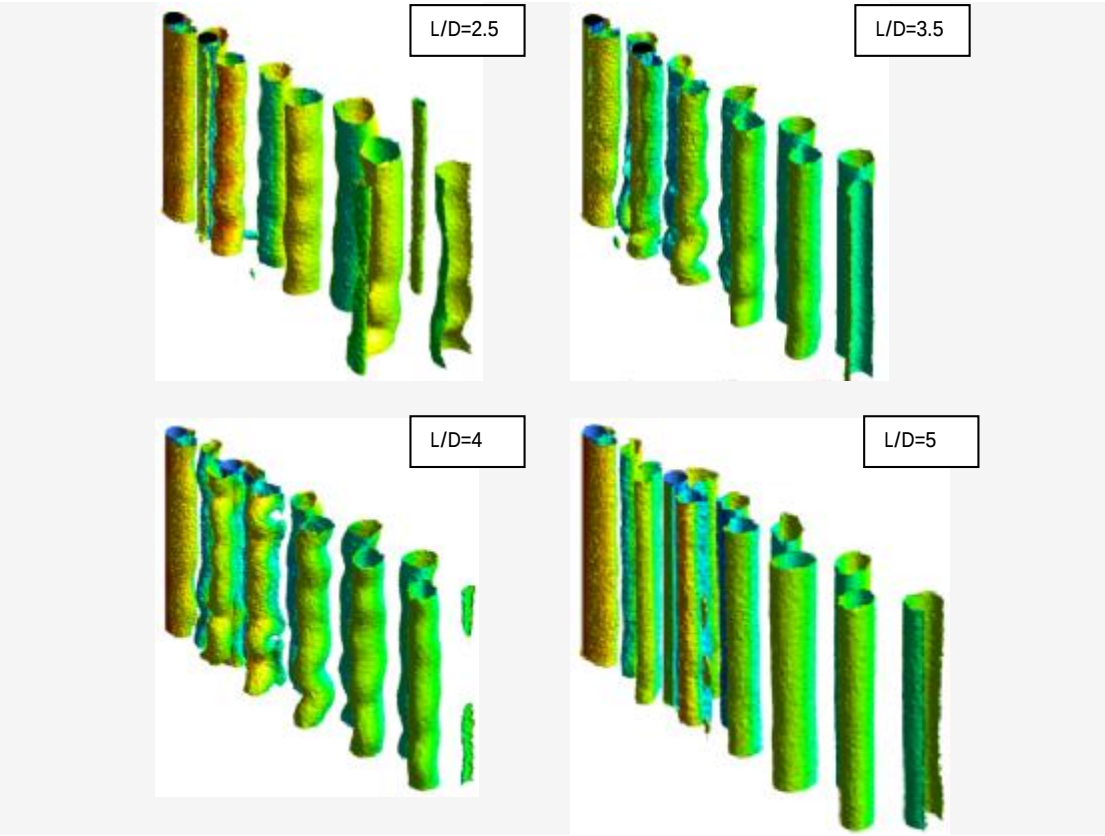

Figure 4.43. Instantaneous velocity field beyond the cylinders for various gap ratios (numerical results)

For the detection of wake structure, swirling strength was used at level of 0.01. In general, with regardless of some minor differences, it can be said that, wake structures behind of cylinders in tandem were very similar to the single cylinder's wake structure. But, the existing differences can be investigated in the following. In fact, three different types of wake structures behavior were identified in this study as:

The first type of behavior at L/D=1 in this study, the two tandem cylinders behavior like a single bluff-body. Only, vortex structure separation has more curvature then single cylinder's rule vortex curved, especially when it was get far from cylinder.

For second type is from L/D=1.5 to 4, the effect of exiting downstream cylinder was clearly noticeable. Vortex structures separation lose its regular cylindrical shape in the bottom part of channel, especially. Finally, they were formed

like a wavy shape. Of course, these structures lost with getting away from the cylinder. And the vortices were become to their previous cylindrical regular shape.

Fainally ,with reaching to L/D=5, the wake structure became so similar to the wake structure around the single cylinder. The following figure was shown the flow around single circular cylinder.

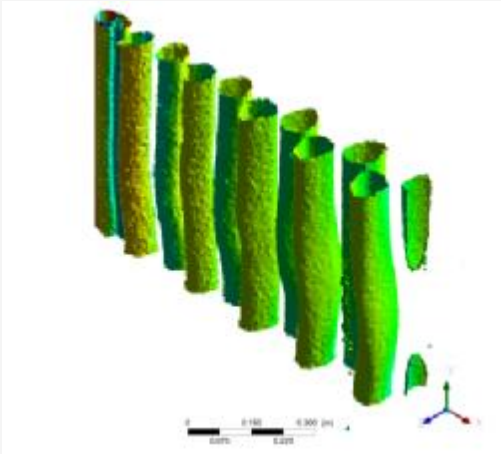

Figure 4.44. Wake structure of the single circular cylinder at α= 0˚ and Re=5000

4.2.3. The effects of yaw angle on the cylinders

In this section, the effects of angle variations will be investigated relative for both cylinders on the streamline at the different ratios of L/D in flow direction. It should be mentioned that angle of both cylinder changed equally and simultaneously. The effects of angle variations of the cylinders were carried out for angles of 0˚, 15˚, 20˚, 25˚ and 30˚ and also the ratio of gap of L/D=1, 1.5, 2, 2.5, 3, 3.5, 4, 4.5 and 5 as PIV experiments and numerical computations. Due to the high number of results, some of the results were implied. So, due to special variations observed, the results were implied for ratio of spacing between cylinders at L/D=1 and L/D=4 at angles from 0˚ to 30˚. And finally, outcomes obtained of 15˚ were investigated for completing discussion and for having a good comparison between the effect of L/D ratio and angle changes for all the ratio of spacing.

In the previous section was studied about the effect of spacing ratio's variations of between the cylinders at the angle of zero degree, and it was observed

that parameters of the flow domain were close to behavior of flow around single cylinder with increasing spacing ratio of cylinders.

4.2.3.1. Spacing ratio of L/D=1

4. 2.3.1.(1). Time-averaged streamlines

To investigate the effect of yaw angle variation, first of all, the angle variations were investigated for ratios of small distances at L/D=1. In the figure 4.39, the streamline topology was displayed for different yaw angles at L/D=1 case. Due to the limitations of measurements, only the streamlines beyond the downstream cylinder were studied.

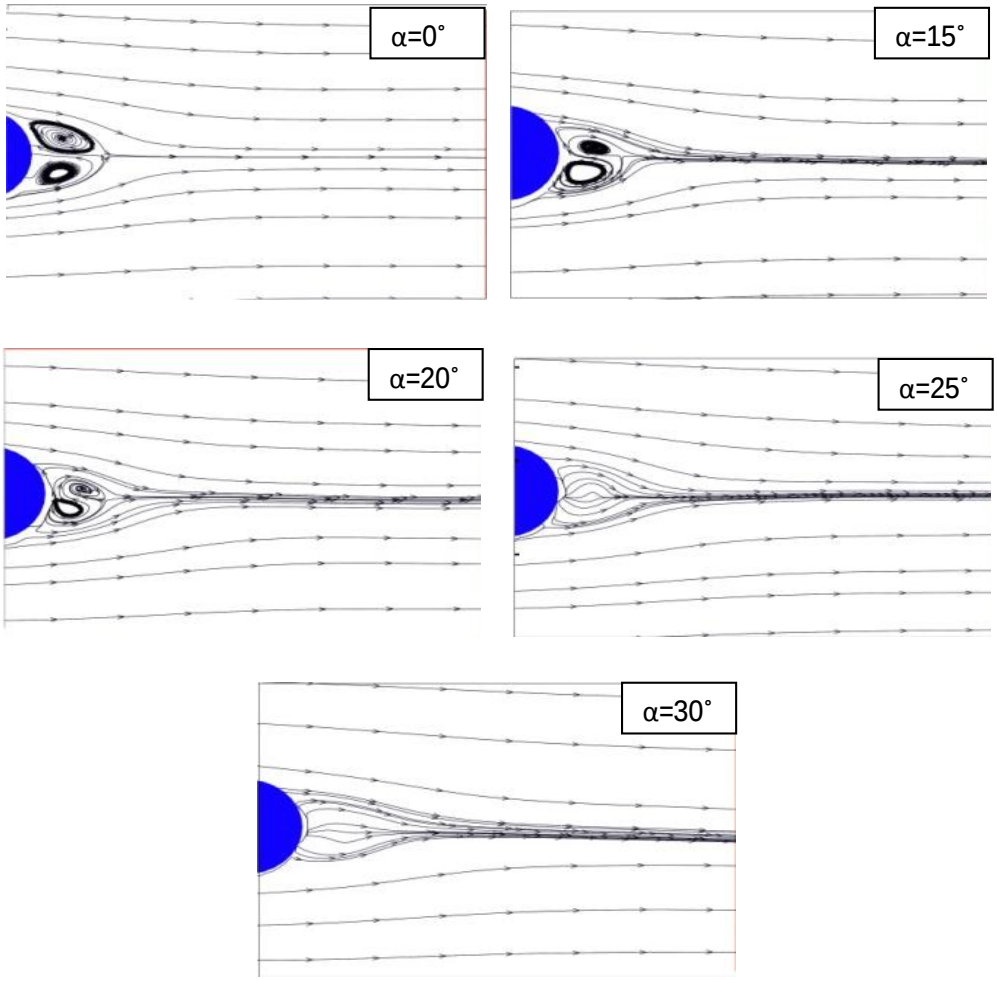

Figure 4.45. Streamlines in the wake of downstream cylinder for various yaw angles

At gap ratio of L/D=1, a bluff body was observed due to be tangent cylinders with together and then it could be considered which the geometry was changed. Especially, it occurred due to excite cavity where cylinder was connect completely. So, it is important the evaluation and comparison outcomes of this section with the results of the flow around a single cylinder. At zero degree, there was a pair vortex which also was observed at single cylinder but with a difference of the vortex dimension whose was smaller dramatically and also, length of the reattachment region became smaller in behind the vortex. At the angle of 15˚ in the behind single cylinder was seen two similar vortices with larger dimension and opposite directions.

The distance between their centers were far from cylinder's axis then yaw angle of zero degree, while streamlines around the two cylinders were revealed two smaller vortex at 15˚ for L/D=1, the distance between centers of vortices from cylinder's axis was much closer then single cylinder case. In the single cylinder, Kármán Street was formed at zero degree whose was slowly disappeared with increasing angle cylinder so vortex pairs were not observed at 25˚ in behind of single cylinder. Although the transition process of wake was occurred after the 25˚ for two cylinders in tandem, dimension of two cylinders' vortex were much smaller than the single cylinder. As initially mentioned, this phenomenon was induced upstream cylinder undoubtedly.

4.2.3.1.(2). Vortex shedding

The three-dimensional structure wake of side view of behind of downstream cylinder was shown for angles from 0˚ to 30˚, at pitch spacing ratio of L/D=1.
Results were carried out with numerical analysis in the figure 4.45.

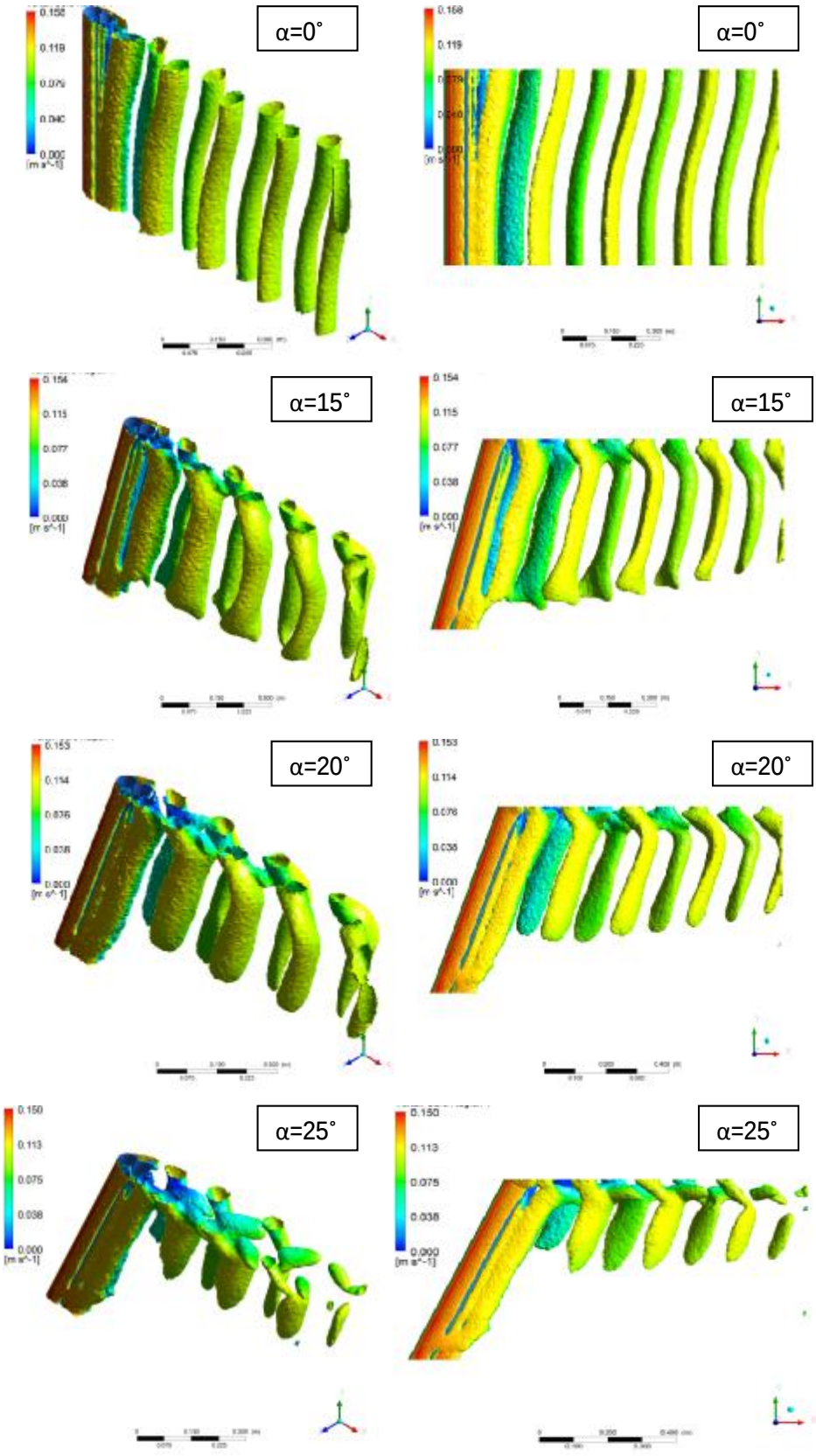
α=0°
α=0°
α=15°
α=15°
α=20°
α=20°
α=25°
α=25°

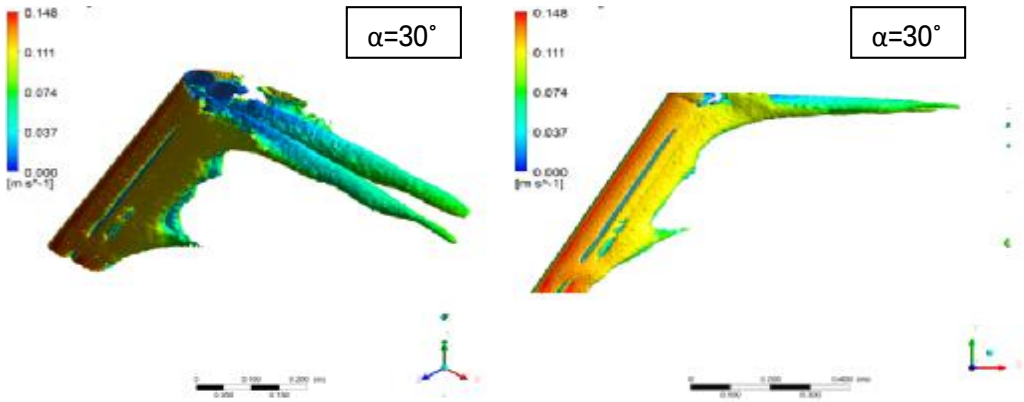

Figure 4.46. The three-dimensional structure wake of side view in behind of the downstream cylinder for angles from 0˚ to 30˚ at L/D=1

According to the figure above, it can be observed that vortex was formed around the downstream cylinder alternating and symmetrically at zero degree. As was mentioned in the previous section for single cylinder, vortex rules were became as mild curvature at top of cylinder, undoubtedly it was created due to existence of minimal pressure difference at cavity region between two cylinders.

With increasing yaw angle of cylinders from 0˚ to until 15˚; vortex direction was changed in the opposite direction of yaw angle of cylinders (un-clockwise), which it was happened as first cavity event. Simultaneously, length of the vortex decreased very regular and steady with forwarding vortex along to channel. Again, in the angle 20˚ with its developing in channel, length of the vortex was become smaller than the previous state, and also upper curvature of the vortex was increased. So, vortex became short and curved to like “V” shape in the end of the tunnel.

At 25˚, length of vortex became much shorter, so that it could not even reach in the middle of the channel's high. So according to it, it is quite natural and reasonably which streamlines at angle of 25˚ did not indicate any vortex at horizontal symmetry plane.

It should be mentioned, although the streamlines was not indicted Vortex shedding phenomenon in the middle plane, however, vortex shedding process continued at upper than this plane (Figure 4.45). With increasing angle of cylinder and reaching the angle of 30˚, the wake of cylinders was completely changed. And

two vortex shedding were created on both top sides of the downstream cylinder which were started to occur instead of previous vortex shedding disappeared.

4.2.3.1.(3). Time-averaged drag coefficient

This phenomenon anticipated that the variation of the wake structure may have a significant effect on the drag coefficient of the cylinder; to investigate this issue, drag coefficient for both cylinders was compared with drag coefficient of single cylinder and each other too, in figure 4.46.

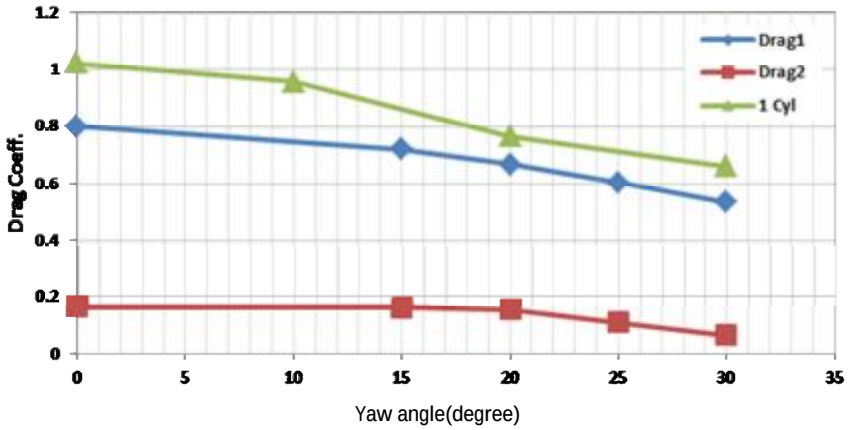

Figure 4.47. Drag coefficient of upstream, downstream and single cylinders

According to figure, drag coefficient decreased with increasing yaw angle of the cylinders consistently, with becoming shorter length vortex. Finally, it was reached to minimum value at 30˚. Generally, with comparing drag coefficient for both cylinders at all yaw angles with single cylinder it was smaller than drag coefficient of single cylinders. The main cause for this phenomenon, as was mentioned at the L/D=1, because of the tangent cylinder was created a bluff body basically. This new body due to have different geometrical structure in compared of a cylinder will have different wake structure and the different of separation point position. Therefore, the drag coefficients will be different.

4.2.3.2. Spacing ratio of L/D=2

4.2.3.2.(1). Time-averaged streamlines

Streamlines was indicated in the downstream cylinder at L/D=2 in figure 4.47. As can be seen, same trend of previous case (L/D=1) was occurred at streamlines L/D=2 in middle symmetry plane.

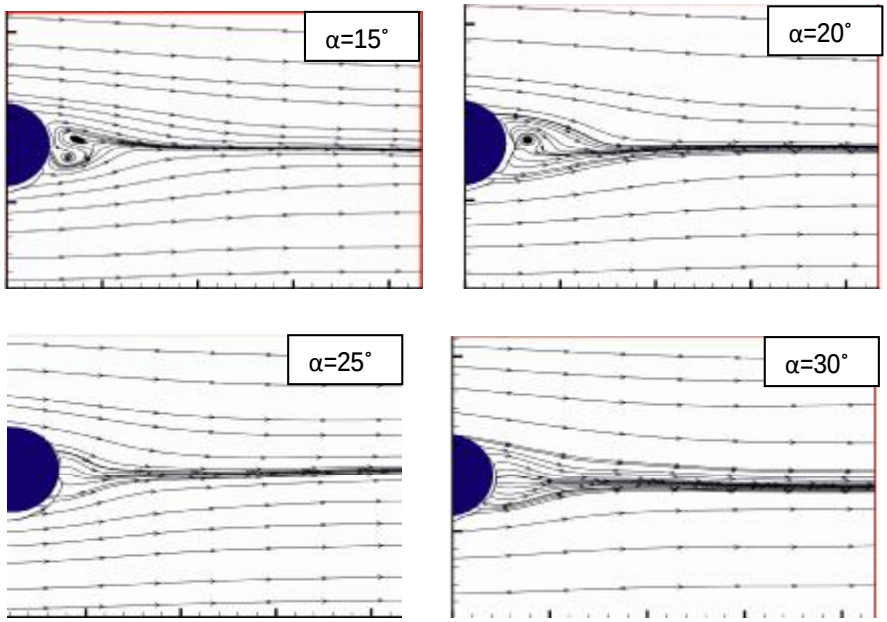

Figure 4.48. Streamlines in the downstream cylinder from yaw angle of 15˚ to 30 ˚

Streamlines was indicated in the downstream cylinder at L/D=2 in Figures 4.47. As can be seen, same trend of previous case (L/D=1) was occurred at streamlines L/D=2 in middle symmetry plane. In this spacing ratio between two cylinder, dimension of vortices are smaller than L/D=1. Undoubtedly this phenomenon was due to existence of upstream cylinder which made influences on wake dimensions.

4.2.3.2.(2). Turbulent kinetic energy

It was indicated in TKE contours (Figure 4.48). Fundamentally, the cause of being larger amount of TKE is induced eddy production behind the downstream cylinder in this range. The following figures can be observed, TKE with increasing yaw angle of cylinder was reduced and after 25˚, the contour had no maximum TKE. Therefore, after this angle was stopped eddy generation in the region.

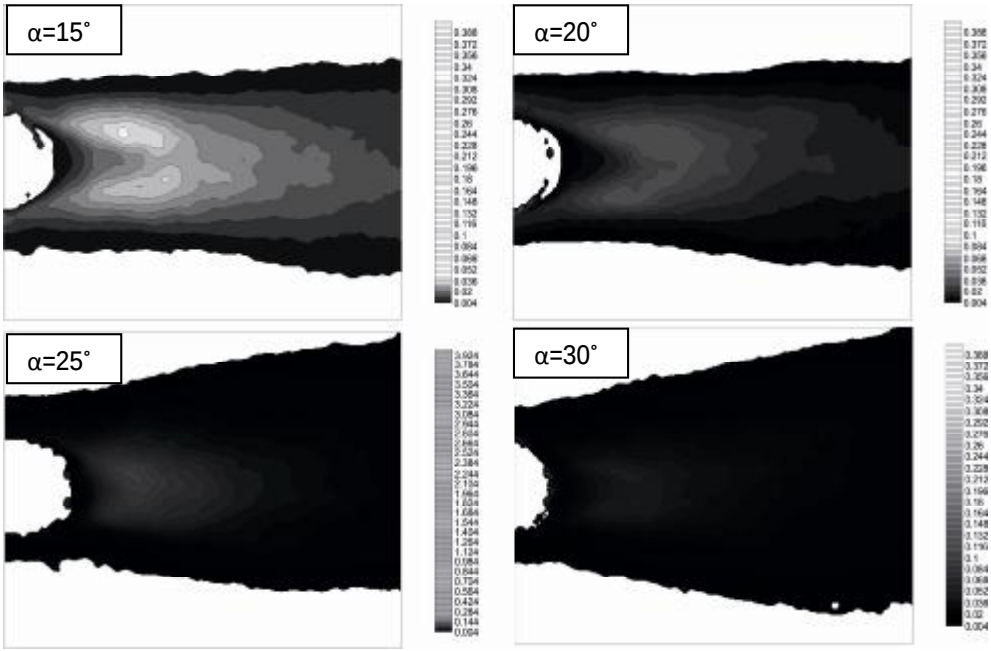

Figure 4.49. Changes in TKE with increasing yaw angle at L/D=2

4.2.3.2.(3). Time-averaged drag coefficient

In figure 4.44, drag coefficient variations was illustrated for both cylinder to increase yaw angle in L/D=2. In this ratio, drag coefficient of the upstream cylinder was very close to drag coefficient of single cylinder in greater angle of 20˚. The reduction in drag coefficient was observed in both cylinders with increasing angle of the cylinder.

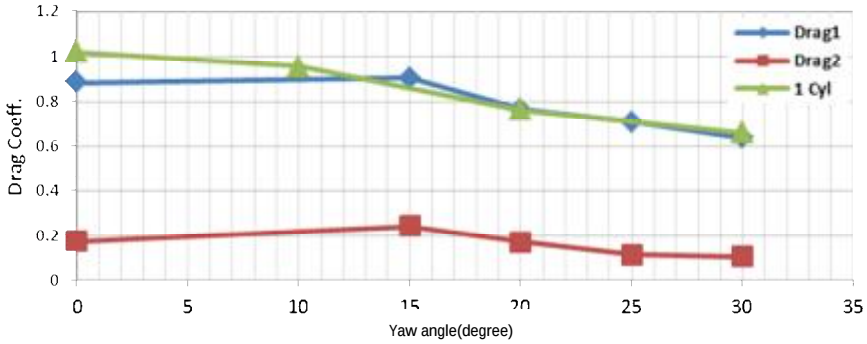

Figure 4.50. Changes of drag coefficient with increasing yaw angle at L/D=2

4.2.3.3. Spacing ratio of L/D=4

In this section, to have better study, the effect of changing yaw angle of the cylinders on basic flow parameters was presented in spacing ratio of L/D=4.

4.2.3.3.(1). Time-averaged streamlines

By comparing streamlines structure were indicated at the downstream cylinder in the figure 4.50. And also, streamlines of single cylinder and also for the ratios of L/D=1 and L/D=2 was observed a significant difference.

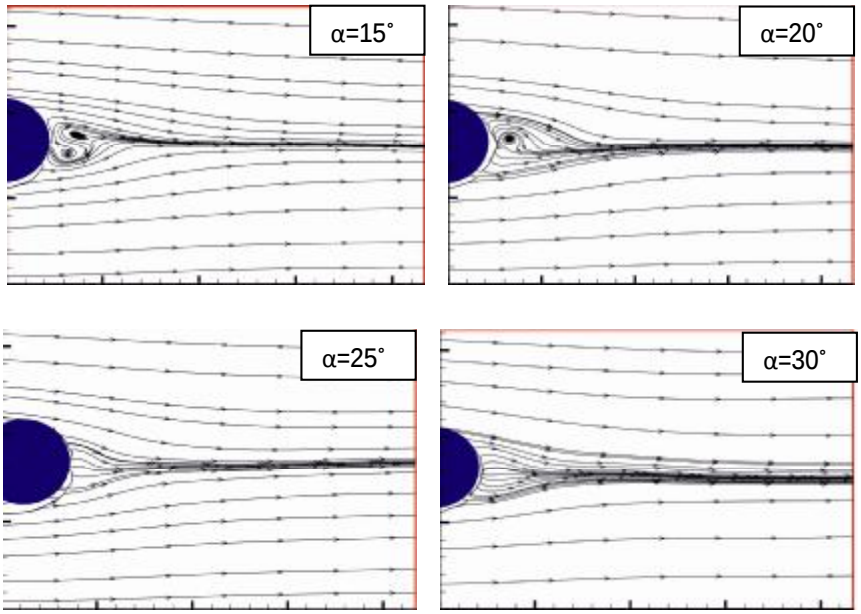

Figure 4.51. Streamlines of behind downstream cylinder from 15˚ to 30˚

The vortex pair that were observed in wake of single-cylinder and ratio of L/D=1 and L/D=2, suddenly disappeared at angle of 25˚. Also position of the separation point was moved, and it was predicted before, which this issue will have the effects on drag coefficient.

According to the mentioned analysis of single cylinder, which vectors of streamlines existed from bottom to top of channel in various yaw angles (Figure 4.10), it was seen the effects of these upward streamlines was increased at L/D=4, in compared to other values of L/D.

As that the effect of L/D ratios increasing was mentioned, with increasing spacing between of cylinders, the created wake in behind of upstream cylinder or between of two cylinders was similar to the wake generation in the downstream of single cylinder. So while the L/D was less than 1, 2 and 2.5, saddle point phenomena occurred just behind the downstream cylinder. But for greater ratios, it was created in upstream cylinder, furthermore of downstream cylinder. It was clearly indicated at ratio of L/D=4 in figure 4.51.

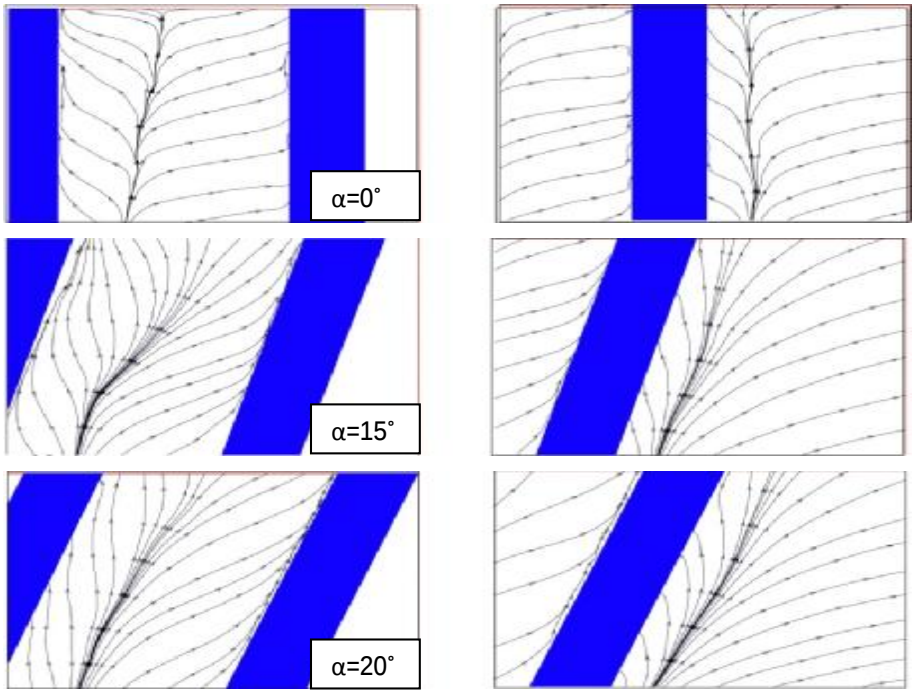

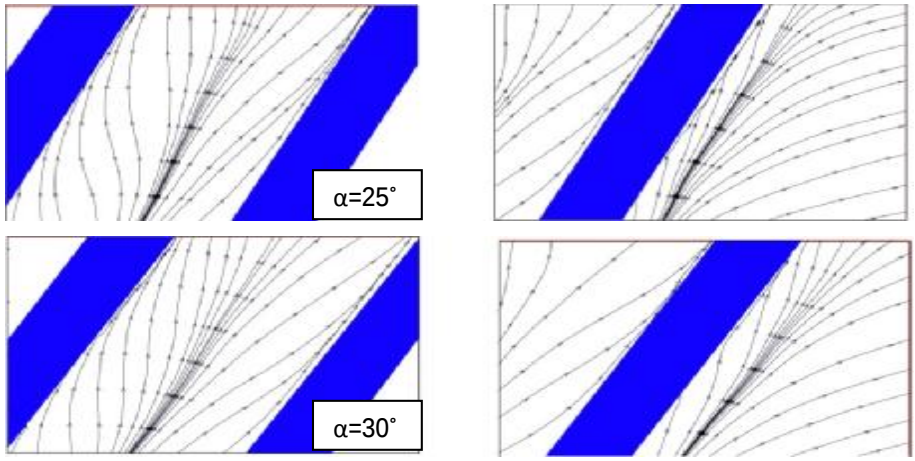

Figure 4.52. Time-averaged streamlines beyond the cylinders for various yaw angles

4.2.3.3.(2). Vortex shedding

With the investigation of three-dimensional structure on the flow, the possibility of further study will be provided for effect of increasing angles of cylinders in this spacing ratio.

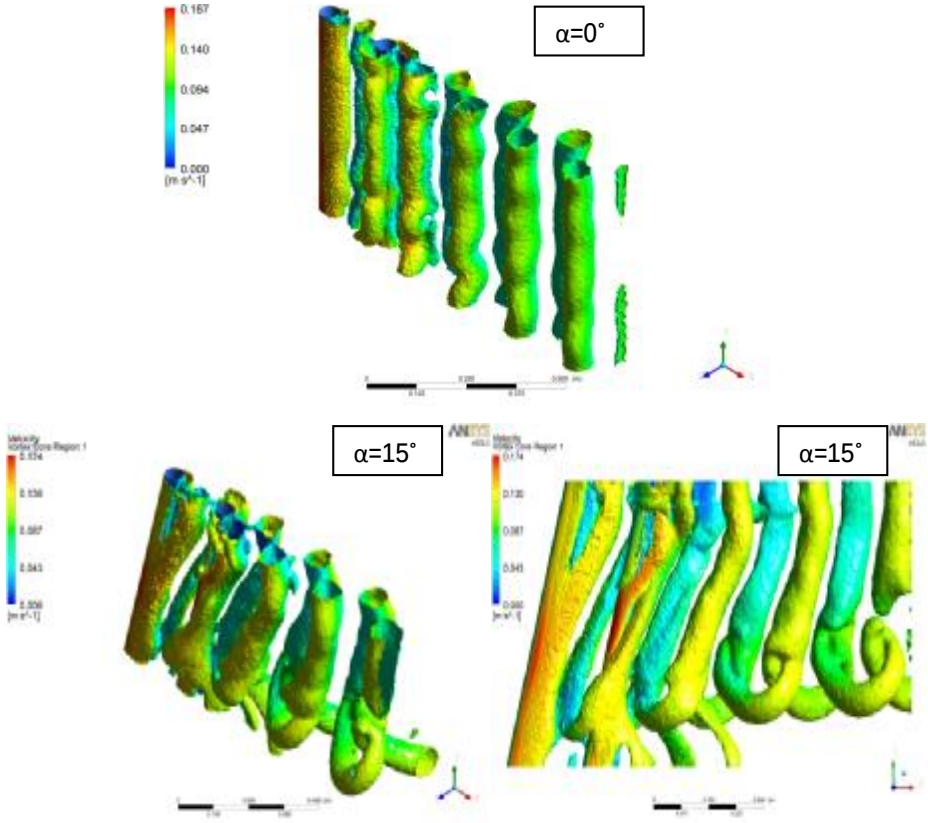

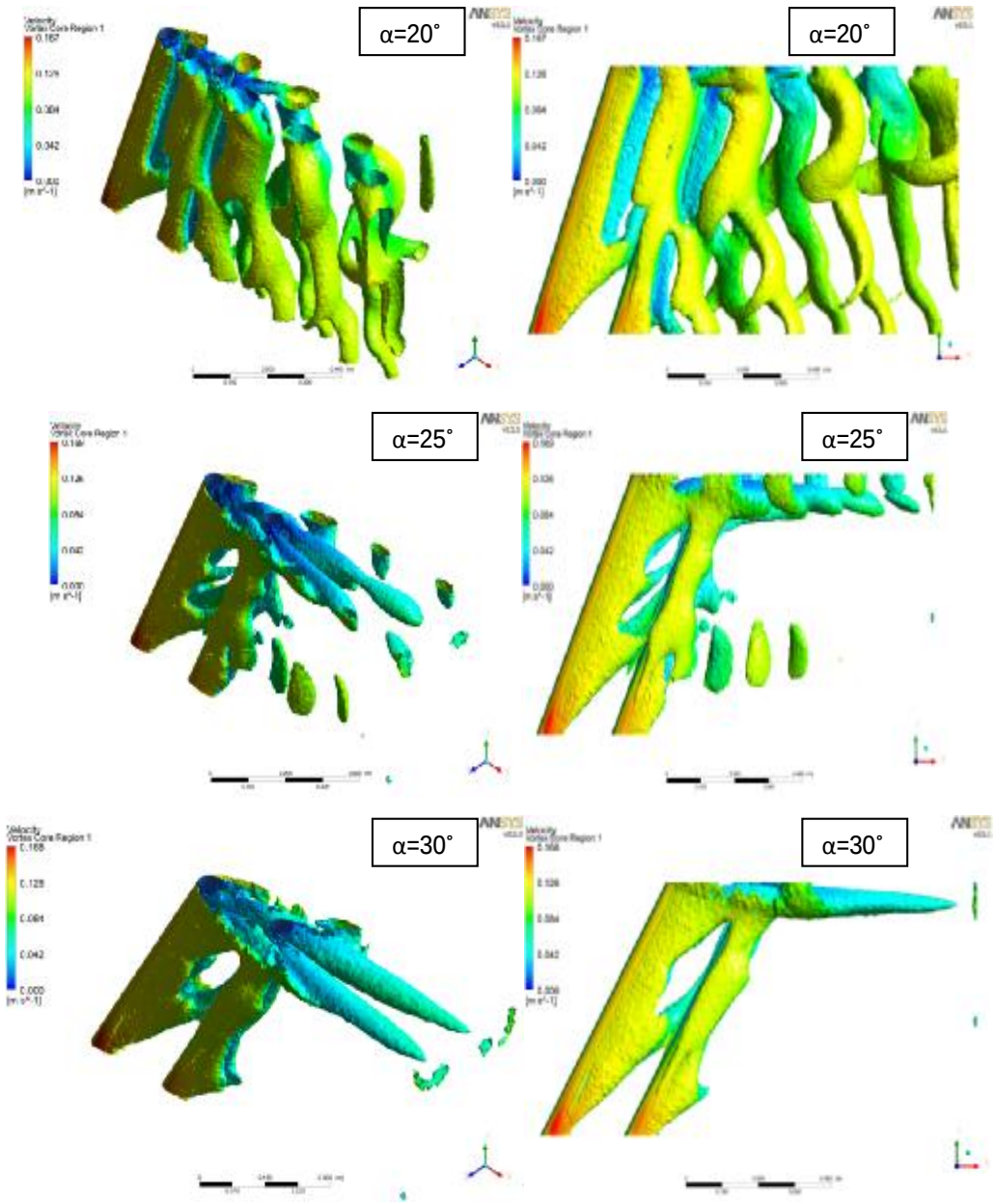

Figure 4.53. The three-dimensional structure wake of side view in behind of downstream cylinder for angles from 0˚ to 30˚

The change in the wake structure was observed for increasing yaw angle in figure 4.52. In general, the phenomenon of vortex shedding was continued until angle of 25˚ of cylinder like a state occurred of ratio of L/D=1. After that, the wake structure was similar to the previous case. So with investing on results, it can be concluded that by increasing spacing between the cylinders ,although, the wake

structures was changed partly, but it had not any effect on the yaw angle which the transition region occurred at same angle .

In the ratio of spacing between two cylinders, L/D=2, was observed that by increasing the angle of the cylinder, vortex length became shorter. Finally, the wake structure was varied. But in the ratio of L/D=4, as can be seen, this process was different.

In this gap ratio between two cylinders with increasing yaw angle of cylinders, vortices were deformed into two (multiple) branches at the end of cylinder. The first change was happened at 15˚. Vortices were started to divide into two parts from the lowest point of the cylinder and interconnected structures and such as chains were made that they continued in the following of cylinder. With increasing angle of cylinder and reaching to 30˚, another branch was created at the end of vortex that it continued in the wake of cylinder continuously.

By reaching to 25˚of cylinders, wake transition and transformation began such as previous case. And finally at 30˚ completely different flow structure was observed compared to other yaw angles. The next noteworthy point is the effect of changing the angle of the cylinder and its wake on aerodynamic forces of cylinder.

4.2.3.3.(3). Drag coefficient

In the following figure was shown changes of drag coefficient on the cylinder by changing the yaw angle of the cylinder and was compared with drag coefficient of single cylinder.

Drag coefficient for small ratios of L/D=1, 1.5 (in this range there was a new bluff body shapes) was less than the sum of drag coefficient of two cylinder.

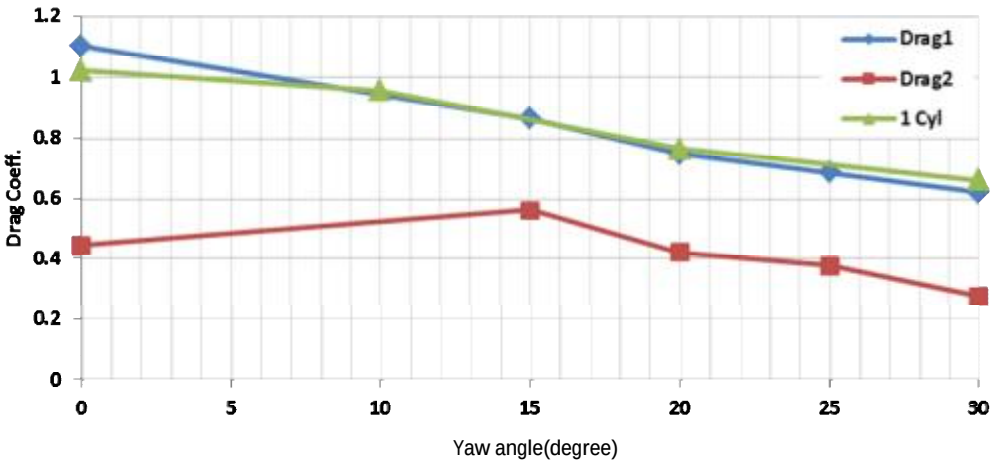

Figure 4.54. Comparison of drag coefficient with increasing angle of cylinder for single cylinder and two cylinders (numerical)

With increasing spacing between cylinders, and reaching a ratio of L/D=4, changes of drag coefficient of the upstream cylinder was very closer to behavior of drag coefficient of single cylinder. Also the process of drag reduction with increasing angle of cylinder was observed in this spacing ratio. Another point, drag coefficient of the downstream cylinder was increased in the angle of 15˚, which this phenomena was more intangible at spacing ratio of L/D=4 in comparison with previous spacing ratios.

4.2.3.3.(4). Lift coefficient

As was shown in the following figure 4.55, in the small angles fluctuations of lift coefficient started from zero regularly and increased constantly due to the phenomenon of vortex shedding formation and growth of the Karman street behind a circular cylinder, until that it was fixed to the stability of the wake structure oscillation's of domain. But for large angles, after changing the wake structure, oscillations of lift begin with high-domain and after stabilizing the wake structure, oscillations of lift was attenuated.

In range of L/D=3 ratio to L/D=3.5 ratio, a sharp increase of lift mount was observed at downstream cylinder. The inherent cause of this phenomenon can be explained with increasing dimension of the vortex in mentioned range. As was

mentioned, the size of the vortex at downstream decreased from L/D=1 to L/D=3 ratio and then their dimension increased until L/D=5 ratio.In addition maximum value of lift coefficient occurred at L/D=4.

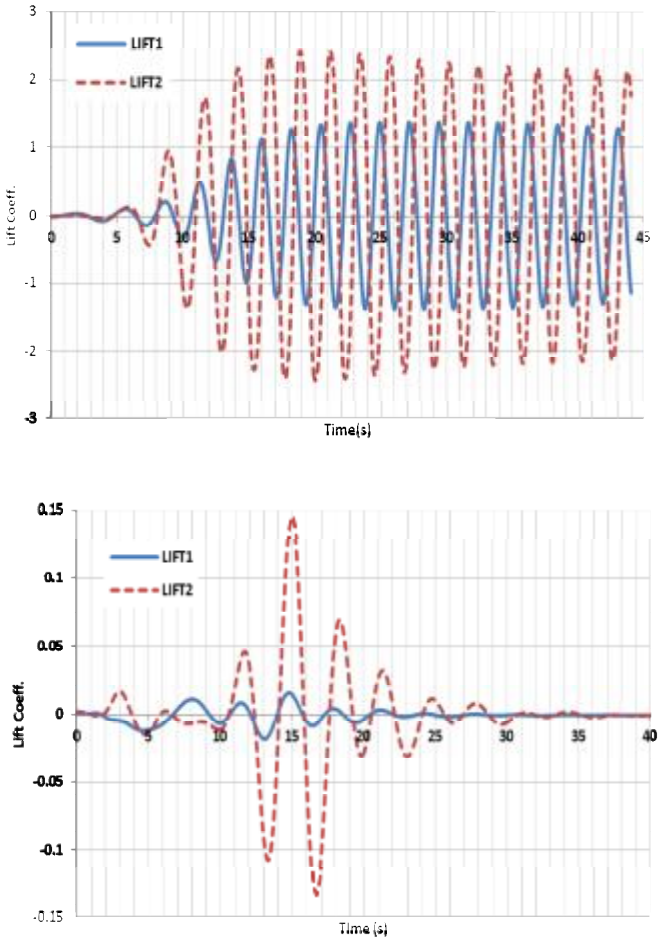

Figure 4.55. Lift coefficient – time history for angles of 15˚ and 30˚, respectively

4.2.3.4 Wake region

In the previous sections, some issues were mentioned about saddle point distance of second cylinder in the wake. In this section, a quantitative study was presented distance changes of this point depending on angle change and spacing of between two cylinders.

Finally, a function of them was recommended. In the following diagram, dimensionless distance variation of Saddle point is drown from the second cylinder on the cylinder diameter (S/D) with depending on the spacing ratio of cylinders

(L/D) for angles from 0˚ to 30˚. Thus with increasing spacing of between of cylinders until to ratio of L/D=3 spacing formation of saddle point decreases but then it increases with increase of L/D ratio.

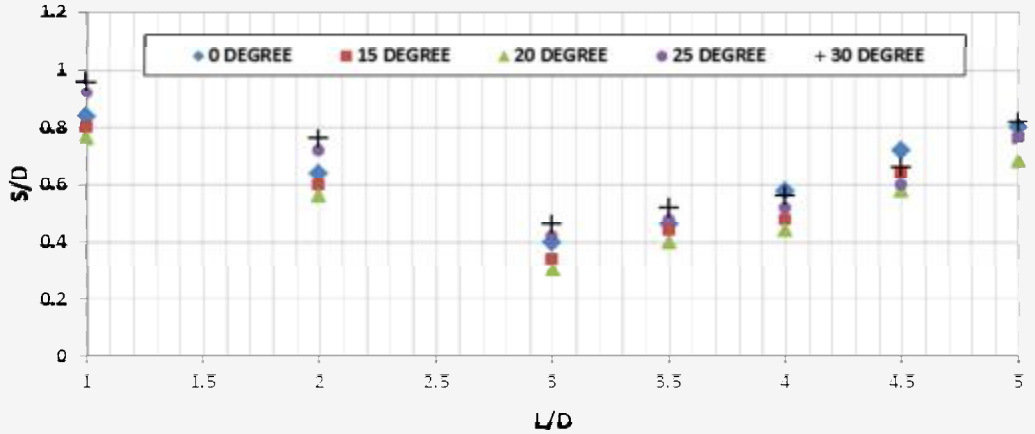

Figure 4.56. Interval changes of saddle point from the second cylinder

To calculate this distance, side views of streamlines were used (Figure 4.61), which was obtained from PIV results. It means that the distance between saddle point and second cylinder was measured at Tecplot software in side streamlines plane. As can be seen, a similar process of spacing changes (S/D) was for different angles with increasing gap ratio (L/D) in the cylinders. This result before this section was cited in investigation of the streamlines and also it was mentioned about becoming smaller of vortex behind downstream cylinder and becoming closer to the cylinder. It can be considered that the ratio of L/D=3 was transition region. This means that with increasing spacing of between two cylinders after transition point, the effect of them on to each other was reduced gradually and slowly and saddle point distance was increased.

The same case can be considered the changes of increasing angles on base of several of L/D ratio was plotted in the following chart.

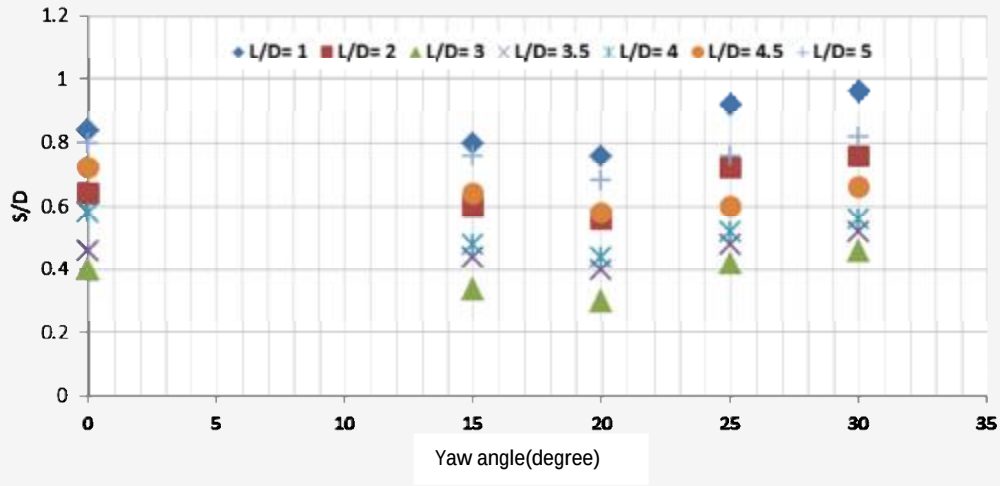

Figure 4.57. Changes of saddle point distance then to angle of second cylinder position on based L/D ratio

In this case, a reduction of the distance ratio of S/D was observed and then was seen an increasing growth of S/D ratio until angle of 30˚ at all ratio of L/D. In the presented results for the single cylinder, a diagram was presented for changes of streamlines' gradient with depending on the angle changing of the cylinder. And a correlation was provided.

4.2.3.5 Streamline gradient

In this section, the same approach of changes in the slope of streamlines was illustrated around the downstream cylinder for the ratio of various spacing between of cylinder in the figure 4.53. Process of results obtained of PIV experiments was similar to case described in single cylinder section.

By using side view of streamlines in Tecplot software, it was calculated a slop of the streamline in middle point of cylinder's high by using below equation:

$$Slope = \frac{y_2 - y_1}{x_2 - x_1}$$

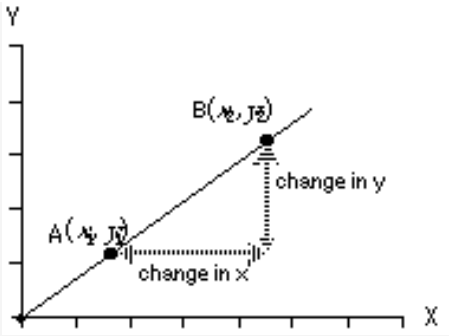

Figure 4.58. Calculation of slop between two point

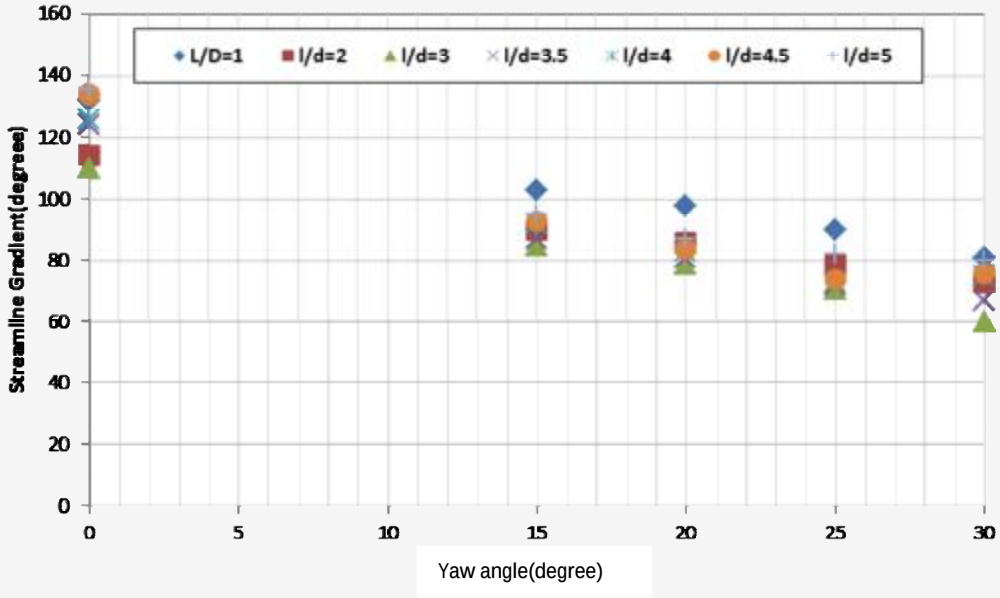

Figure 4.59. Variations of streamlines' slope with increasing the angle cylinders

4.2.3.6. Correlation between the yaw angle and streamline gradient

Also, for two cylinders was observed a reduction of streamlines' slope with angle increase of cylinders. This parameter can somewhat be independent of the number of upstream cylinder. The results for all ratios of L/D did not have so much difference with each other. The following functions were provided for data extracted.

Table 4.5. Correlation for indicating relationship between angels of tangent line on streamlines and yawed angle increasing

$y = A + Bx + Cx^2 + Dx^3$	
$L/D = 1$	A = 1.3198E+002
	B = -3.1530E+000
	C = 1.168E-001
	D = -2.2857E-003
$L/D = 2$	A = 1.1398E+002
	B = -2.3765E+000
	C = 7.3479E-002
	D = -1.3333E-003
$L/D = 3$	A = 1.0999E+002
	B = -2.6450E+000
	C = 9.8304E-002
	D = -2.1904E-003
$L/D = 3.5$	A = 1.2397E+002
	B = -3.3322E+000
	C = 7.3176E-002
	D = -8.5714E-004
$L/D = 4$	A = 1.2596E+002
	B = -1.0459E+000
	C = -1.3360E-001
	D = 3.7142E-003
$L/D = 4.5$	A = 1.3396E+002
	B = -2.0402E+000
	C = -8.8257E-002
	D = 3.0476E-003
$L/D = 5$	A = 1.3600E+002
	B = -3.5579E+000
	C = 5.3521E-002
	D = 9.5238E-005

4.2.3.7. Flow patterns

For further analysis can be investigated quantitative values. For example, changing of lift coefficient over time on two cylinders can be compared with lift coefficient of single cylinder.

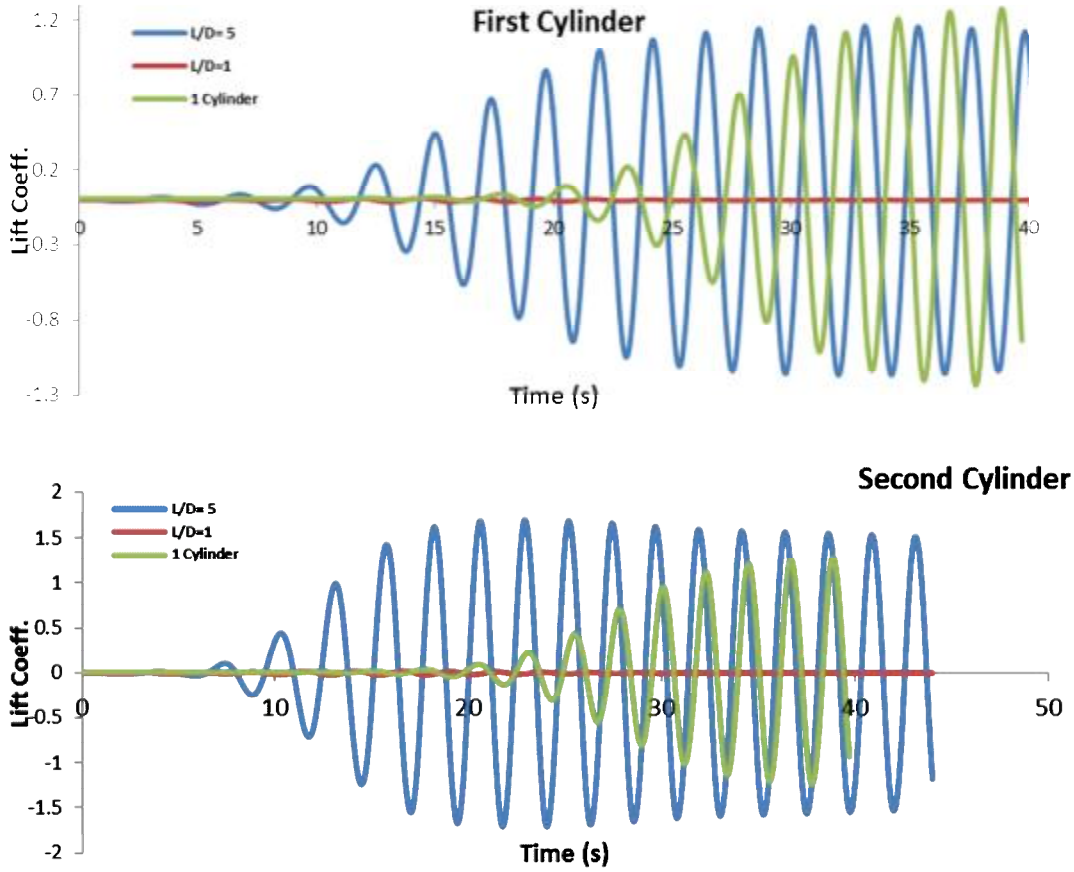

Figure 4.60. Comparing lift coefficient changes over time for two cylinder at L/D=1 and L/D=5 with single cylinder at 0˚

As can be seen, lift coefficient for both cylinders for the spacing ratio at L/D=1 was less than in comparison between single cylinder and also at the distance ratio of L/D=5. The cause of this phenomenon can be justified induced the wake structure and dimension and streamlines in this case. As the figures related to the streamlines confirmed it, which vortex dimension created in behind of downstream cylinder at ratio of L/D=1, was smaller than ratio of L/D=5, and also single cylinder. Therefore, the amount of fluctuations force was lost when occurred as an outcome of the smaller vortex. In other words, as was mentioned, in the smaller ratio of L/D, vortex formation length and near wake region were much smaller than the larger values of L/D ratio, as it was clearly visible in the figures (David summer- Page 70-72).

In the ratio of L/D=5 for the upstream and downstream cylinders, lift coefficient was very close to the amount of lift coefficient for single cylinder. With regardless of phase changes at the beginning of vortex shedding or the fluctuating of lift coefficient, alternately variation of lift coefficient was very similar to the single-cylinder's state. And this was proof that vortex shedding frequency was similar for both cases. Therefore, Strouhal number for single cylinder will be similar to upstream cylinder and also Strouhal number in the ratio of L/D=5. Also phase changes was observed at the beginning of vortex shedding phenomenon and beginning of fluctuations of lift force exerted on the downstream cylinder. But again, oscillation period of single cylinder was similar, according to this issue; Strouhal number of downstream will be similar with single cylinder. For a more detailed investigation of this phenomenon, obtained Strouhal numerical values from the experimental results (PIV) was illustrated at zero degrees of cylinders in terms of increasing of L/D ratio.

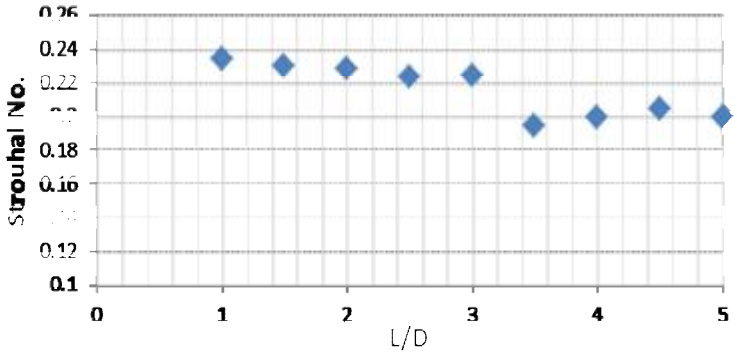

Figure 4.61. Strouhal numbers for various L/D ratios at the yaw angle of α=0˚

According to the obtained results in the figure 4.55, the outcomes were indicated with increasing ratio of L/D, Strouhal number was decreased and this value was about 0.2 for L/D>4 which it was approached to value of single cylinder.

As mentioned in the investigation and comparison at wake structure of cylinder. These phenomena was indicated which vortex shedding of downstream cylinder effected so less from upstream cylinder in this range of L/D ratio. It means with increasing spacing after the L/D=4, the effect of the upstream cylinder was lost

on the downstream cylinder. Simultaneously, with this phenomenon (with approaching frequency of vortex shedding of cylinders to 0.2), flow pattern was similar steady-state of Kármán vortex shedding between two cylinder. For small ratios of L/D=1, 1.5, it can be said instead of cylinder structure was encountered with a bluff body which was located in flow.

And according to the figure 4.47, due to difference of geometry created, some changes were seen. This phenomenon was occurred due to geometric deformation at cavity region, especially. As mentioned in the comparing the drag coefficient section and also according to sources (Zrakovich & Pridden 1977) and (David summer - Page 70-72).

With increasing spacing from each other cylinders and reaching a ratio of L/D=4, changes of drag coefficient of the upstream cylinder was very closer to drag coefficient of single cylinder with angle increase. Also the process of drag reduction with increasing angle of cylinder was observed in this spacing ratio. Also, increasing in the drag coefficient of the downstream cylinder at 15˚ which in comparison with previous spacing ratios, was more intangible than spacing ratio of L/D= 4.

5. CONCLUSIONS AND RECOMMENDATIONS

5.1. Conclusion

The aim of the present study is to investigate the effects of yaw angle on flow around single cylinder and two cylinders in tandem, at Re=5,000. Both numerical simulations and experimental measurements were performed for that purpose. The effect of spacing ratio also investigated. Results were summarized below.

For single cylinder case, the vortex shedding was suppressed as yaw angle reached to $\alpha=25^{\circ}$. This situation may be attributed to the following: At relatively small yaw angles, shear layers originating from the top and bottom side of the cylinder curled towards the base region due to the pressure difference and then rolled into the vortices. As incidence angle reached to $\alpha=25^{\circ}$, the spanwise component of the velocity become dominant on the base surface and lowered the pressure difference starting from the bottom end of the cylinder.

The lowered base pressure accompanied a reduction in time-averaged drag coefficient of single cylinder. On the other hand, suppressing the vortex shedding accompanied a sharp reduction in lift fluctuations, in other words, flow-induced vibration was diminished.

In the case of two cylinders in tandem arrangement without yaw angle, the downstream cylinder suppressed the vortex shedding from the upstream one up to spacing ratio of L/D=2.5. Hence, a pair of counter rotating vortices was formed between the rear surface of the upstream cylinder and front surface of the downstream cylinder. As a result of that, the pressure level in the wake of upstream cylinder was increased. Contrary to this, the high pressure region in the front surface of the downstream cylinder was lowered. Consequently, the time-averaged drag coefficients of the cylinders were reduced.

In this study, the investigation of the effect of gap ratio between two cylinders was carried out for spacing ratios of L / D = 1 to 5 at angle at zero degree, and it was observed that in gap ratio of L/D = 1, the geometry was changed such as a bluff body, due to be tangent two cylinders with together. Because of cavity which was created in the region of the tangent cylinders .In this ratio of gap between cylinders; there are only two small vortexes in the above and below regions (shoulders) of tangent point of cylinders. Vertex was slightly established with larger dimensions in behind of downstream cylinder. Vortex was formed by taking away from cylinders in gap between of them at the ratio of L/D= 1.5. Gradually, this vortex was grown with increasing the gap between them and it was become larger. However, the dimension of the vortex was decreased in the back of downstream cylinder at gap ratio of L/D = 3.

Another important point was at spacing ratio of L / D = 3, the distance was increased from the center vortex of upstream cylinder, but after that, a reduction of distance was observed. Vortex centers were closer to upstream cylinder.

Wake structure was similar to wake of around single cylinder in different centre-to-center gap ratios of L/D at the angle of zero degrees, only with a difference in the L / D = 1. It occurred due to forming of different body of bluff body, at least, led to create vortexes curved.

With increasing distance from center to center, wake became more similar to the wake structure of single-cylinder; even wake structure between the two cylinders became similar it, also. The effects of increasing the yaw angles of the cylinders were inducted at gap ratios of L/D= 1, 2 and 4. In comparison with the single cylinder, vortex dimension was much smaller until reaching to angle of 25 degree. Finally, the vortexes were disappeared in horizontal symmetry plan. With studying on wake structure by using three-dimensional structure, was observed which the vortex was shortened in behind of downstream cylinder with increasing yaw angle, so wake structure was changed after reaching to 30 degree.

With studding on drag coefficient of variations, it was indicated that drag coefficient was reduced with increasing the yaw angles of cylinders. In the gap ratios of between L/D= 1 and L/D=4 was observed this process. The upstream cylinder

drag coefficient was become very close to drag coefficient of single cylinder because of increasing the gap between them. It means that in greater ratio, downstream cylinder is not influence of upstream cylinder.

At least, outcomes were indicted a high accuracy of SST turbulence model in prediction and simulation of flow around cylinder, vortex shedding phenomenon, predict the transition point and deformation of wake structure.

5.2. Recommendations for Future Work

In the present project, another point which should be mentioned is about the numerical simulation, which numerical study was carried out for fixed cylinder for the range of Reynolds number, it was presented good results at this range of Reynolds number. Another method which can be used for flow analysis with using of simulation for fluid structure is Interaction of solid -fluid. This issue is for the case that the cylinder is completely fixed and the incoming oscillating forces did not have any displacement. It was worth mentioning, any fluctuation or motion of an object was made changes, especially when vibrations were close to value of the vortex frequency, it had a major effect on the formation of vortex.(Blevins, 2001)For example, the vibration of a cylinder can be made following changes:

1- Increase the strength and durability of the vortex

2. Expand the size of the wake (Vandier, J., Jong, J. 1987)

3- Vibration of cylinder can make a transition the frequency of Vortex flow to the vibration frequency of cylinder. (Vandier, J., Jong, J. 1987)

The phenomenon was called Lock-in or Synchronization. Also, if the cylinder vibration frequency was been a multiple of the frequency of vortex ,flow will develop less than other case.

4. Increase the average value of Drag cylinder. (Vandier, J., Jong, J. 1987)

5-The phase change and Vortex pattern in the wake .(Tanida, Y., 1988)

It should be mentioned, if the domain of oscillation was large, frequency of vortex could be have about 40 percent difference in comparison of current frequency of vortex for a fixed cylinder. If a cylinder fluctuates at frequencies close to the

vortex frequencies, it will affect the flow pattern and vortex phase. When the frequency of cylinder's oscillation passes from value of natural frequency of vortex flow, phase transition is created between vortex flux and movement of cylinder at about 180 degrees. Zdravkovich (1982) observed when the vibration frequency was slightly less than the natural frequency of vortex flux, vortices were produced from opposite direction of where included maximum displacement, and for frequencies were slightly higher than natural frequency of vortex flux, vortex flows from where included most movement. The vibration was amplitude of the cylinder when IT reached about half of cylinder's diameter, symmetrical pattern of vortex generated was disappears.

As shown in Fig 5.1, when oscillation amplitude was equivalent to a diameter of a cylinder, three vortices were formed per cycle of oscillation but while vibration amplitudes were low, two vortices were produced per cycle of vibration.

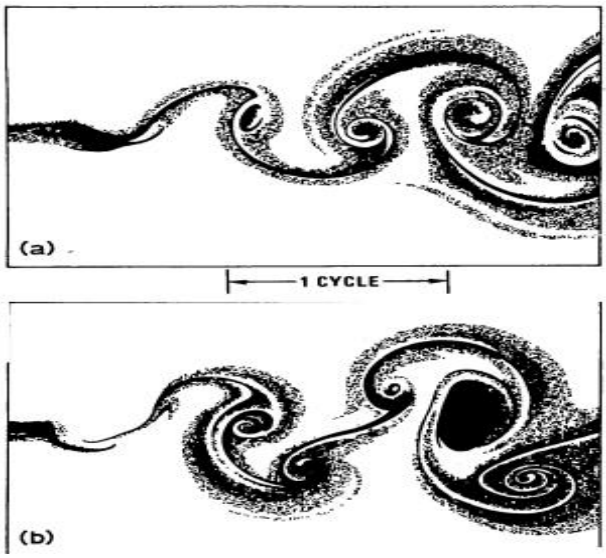

Figure 5.1. vortex path behind vibrating cylinder is in the direction perpendicular to the flow, in the figure above is amplitude ratio of diameter 0.5 and in the bottom is equal to 1 ,(Williamson, C., Roshko, A., 1989)

The average amount of drag cylindrical is a function of vibration amplitude when its vibration is near to frequency of the vortex. Drag increases with increasing at range of vibration in the vertical direction.

REFERENCES

ANDERSON, J. D., "Fundamentals of Aerodynamics", 2nd Ed. McGraw-Hill, New York, , Ch. 3: pp. 229, 1991

ATTA,C.W.,1968.Experimentsinvortexsheddingfromyawedcircularcylinders.AIAAJournal6,931–933.

BARDINA et AL- The superior performance of this model has been demonstrated in a large number of validation studies.

BEARMAN,P.W.,OWEN,J.C.,1998.Reductionofbluff body drag and suppression of vortex shedding by the introduction of wavy separation lines. Journal of Fluid and Structures12,123–130.

BIERMANN, D.,HERMRNSTEIN,W.H.,1934.The interference between strutsin various combinations.NACAReportNo.468.

BLEVINS, R., Flow induced vibration, Krieger, Florida, 2001

BLOOR, M. S. & GERRARD, J. H. 1966, Measurements on turbulent vortices in a cylinder wake. Proceedings of the RoyaJ Society of London Series A 294, 319-342.

BURSNALL,W.J.,LOFTIN,L.K.J.,1951.Experimental investigations of the pressure distribution about a yawed circular cylinder in the critical Reynolds number range.NationalAdvisoryCommitteeforAeronautics,1–34.

C. H. K. WILLIAMSON . 1988,The existence of two stages in the transition to three-dimensionality of a cylinder wake. Physics of Fluids.

C. H. K. WILLIAMSON. 1992, The natural and forced formation of spot-like vortex dislocations in the transition of a wake. Journal of Fluid Mechanics,.

C. H. K. WILLIAMSON. 1996a,Three-dimensional wake transition. Journal of Fluid Mechanics,328.

C. H. K. WILLIAMSON. 1996b, Vortex dynamics in the cylinder wake. Annual Review of Fluid Mechanics, 539.

CHOI, H.C.,JEON ,W.P.,KIM,J.S.,2008.Control of flow over a bluff body.Annual Review of FluidMechanics40,113–139.

DAREKAR, R.M.,SHERWIN,S.J.,2001.Flow past a square-section cylinder with a wavy stagnation face. Journal of Fluid Mechanics426,263–295.

DAVIS, M., "A comparison of the wake structure of a stationary and oscillating bluff body using a conditional averaging technique", Journal of fluid mechanics, Vol.75, pp.209-231.

GERRAD, J. H., 1966. The mechanics of the formation region of vortices behind bluff bodies. Journal of Fluid Mechanics 25, 401-413.

HANSON, A. R., 1966. Vortex-shedding from yawed cylinders. AIAA Journal ,738–740.

HANSON,A.R.,1966.Vortexsheddingfromyawedcylinders.AIAAJournal4,738-740.

HAYAS, T., KAWAMURA a,T.,1995.Non uniformity in a flow around a yawed circular cylinder. Flow Measurement and Instrumentation6,33–39.

HAYASHI, T.,KAWAMURA.,1995.Non uniformity in a flow around a yawed circular cylinder. Flow Measurement and Instrumentation6,33–39.

KANEKO, S., KAWAMURA ,T.,2002. Numerical study of flow around two yawed and parallel circular cylinders. Theoretical and Applied Mechanics Japan51,199–205

KAWAMURA,T., HAYASHI,T.,1994. Computation of flow around a yawed circular cylinder .JSME International Journal 37,229–236.

LAM, K.,LIN,Y.F.,2007.Drag force control of flow over wavy cylinders at low Reynolds number . Journal of Mechanical Science and Technology 21,1331–1337.

LAM, K.,LIN,Y.F.,2008.Large eddy simulation of flow around wavy cylinder at a subcritical Reynolds number. International Journal of Heat and Fluid Flow 29,1071–1088.

LAM, K.,LIN,Y.F.,2009.Effect of wave length and amplitude of a wavy cylinder in cross-flow at low Reynolds numbers. Journal of Fluid Mechanics620,195–220.

LAM, K.,WANG,F.H.,LI,J.Y.,So,R.M.C.,2004.Experimental investigation of the mean and fluctuating forces of wavy cylinders in across-flow.

LOURENCO, L.,SHIH,C.,KROTHAPALLI,A.,1992. Observations on the near wake of a yawed circular cylinder .In Proceedings of the Sixth International Symposium Lisbon,Portugal,pp.257–284.

LUCOR, D., and KARNIADAKIS, G. E., 2003, ‘‘Effects of Oblique Inflow in Vortex-Induced Vibrations,’’ Flow, Turbul. Combust., 71, 375–389.

LUCOR, D.,KARNIADAKIS,G.E.,2003. Effects of oblique in flow in vortex-induced vibrations .Flow ,Turbulence, and Combustion 71, 375–389.

M. M. ZDRAVKOVICH. 1997, Flow Around Circular Cylinders, Vol. 1 Fundamentals. Oxford University Press,.

M. M. ZDRAVKOVICH. 1997, Flow Around Circular Cylinders, Vol. 1 Fundamentals, Oxford University Press.

MARSHALL, J.S.,2003.Wake dynamics of a yawed cylinder. Journal of Fluids Engineering125,97–103

NISHIMURA,T.,1986.Flow across tube banks In:Cheremisinoff ,N.P.(Ed.),Encyclopedia of Fluid Mechanics—Flow Phenomena and Measurement ,vol.1.Gulf Publishing Company,Houston,USA,pp.763–785.

RAMBERG, S., 1983. The effects of yaw and finite length upon vortex wakes of stationary and vibrating circular cylinders. Journal of Fluid Mechanics 128, 81–107.

RAMBERG, S.E.,1983.Thee effects of yaw and finite length up on the vortex wakes of stationary and vibrating circular cylinders .Journal of Fluid Mechanics128,81–107

RAMBERG. S., Griffin, M., "Velocity correlation and vortex spacing in the wake of vibrating cable", Journal of fluids engineering, Vol.98, pp.10-18.

SCHINCHTING, H., 1979Boundary-Layer Theory, 7th ed. New York: McGraw-Hill.

SCHINCHTING, Ueno,S.,Ishida,Y.,Wakiya,S.,1984.Vortex excited oscillation of a circular cylinder in a uniform flow. Bulletin of JSME 27,1120–1126..

SCHLICHTING, H., Boundary-Layer Theory, 7th ed. New York: McGraw-Hill, 1979

TANIDA, Y., "Stability of a circular cylinder oscillating in uniform flow for wake", journal of fluid mechanics, Vol. 61, pp. 769-784, 1988.

THAKUR, A.,LIU, X.,MARSHALL,J.S., 2004.Wake flow of single and multiple yawed cylinders .ASME Journal of Fluids Engineering126, 861–870.

VAKIL A.,GREEN ,2009 ,numerical investigated yawed circular cylinders with finite aspect ratio with aspect ratios from 2 to 20Z> in the Reynolds number

VAKIL A.,GREEN, S.I.,2009. Drag and lift coefficients of inclined finite circular cylinder satmode rate Reynolds numbers. Computers& Fluids 38,1771–1781.

VAN ATTA, C. W.,1968. Experiments on vortex shedding from yawed circular cylinders. AIAA Journal 6, 931–933.

VANDIER, J., Jong, J., "The relationship between in-line and cross-flow induced vibration of cylinder", Journal of fluids and structures, Vol.1, pp. 381-399, 1987.

WILLIAMSON, C., Roshko, A., "Vortex formation in the wake of an oscillating cylinder", Journal of fluid and structures, Vol. 2, pp.355-381, 1989.

WILLIAMSON, C., ROSKKO, A., "Vortex formation in the wake of an oscillating cylinder", Journal of fluid and structures, Vol. 2, pp.355-381, 1989

WILLIAMSON, C.H.K. 1996, "Three-dimensional wake transition", Journal of Fluid Mechanics, vol. 328, pp. 345-407.

YEO, D.H.,JONES,N.P. ,2008.Investigationon 3-Dcharacteristics of flow around a yawed and inclined circular cylinder. Journal of Wind Engineering and Industrial Aerodynamics96,1947–1960.

ZDRAVKOVICH, M. M., 1982, Modification of vortex shedding in the synchronization range. ASME Journal of Fluids Engineering 104, 513- 517.

ZDRAVKOVICH, M. M., 1985, Flow induced oscillations of two interfering circular cylinders. Journal of Sound and Vibration 101 (4), 511 -521.

ZDRAVKOVICH, M. M., 1987. The effect of interference between circular cylinders in cross flow. Journal of Fluids and Structures 1, 239-261.

ZDRAVKOVICH, M. M., 1997. Flow around Circular Cylinders, vol. 1:Fundamentals. Oxford University Press, Oxford, UK.

ZDRAVKOVICH, M. M., 2003. Flow around Circular Cylinders, vol. 2: A Comprehensive Guide through Flow Phenomena, Experiments, Applications, Mathematical Models ,and Computer Simulations. Oxford University Press, Oxford, UK.

ZDRAVKOVICH, M. M., PRIDDEN, D. L., 1977. Interference between two circular cylinders; Series of unexpected discontinuities. Journal of Industrial Aerodynamics 2, 255-270.

ZDRAVKOVICH,M.M.,1993.Interstitial flow field and fluid forces. In :Au-YANG,M.K.(Ed.),Technology for the 90s :A Decade of Progress. ASME, New York, USA ,pp.594–658.

ZDRAVKOVICH,M.M.,2003.FlowAroundCircularCylinders,vol.2:Applications.OxfordUniversityPress,Oxford,UK.

ZDRAVKOVICH. M. M., 1993. Interstitial flow field and fluid forces, In Technology for the 90s: A Decade of Progress (edited by Au-Yang, M. K.),

ZDRAVKOVICH., M. M., 1977, Review of flow interference between circular cylinders in cross flow. ASME Journal of Fluids Engineering 99, 618-633.

ZHAO, M., CHENG, L., ZHOU, T., 2009. Direct numerical simulation of three dimensional flow past a yawed circular cylinder of infinite length. Journal of Fluids and Structures 25, 831-847.

ZHAO, M.,CHENG,L., T.M.,2009.Directnumericalsimulationofthree dimensional flow past a yawed circular cylinder of infinite length. Journal of Fluids and Strucutres25,831–847.

URL-1, http://www.lavision.de/en/techniques/piv.php,

URL-2, http://www.dantecdynamics.com/seeding-materials,

URL-3, http://www.dantecdynamics.com/measurement-principles-of-piv,

URL-4, http://www.piv.de/piv/measurement_principle/page_1.php,

URL5 - http://www.piv.de/images/content/piv_components.jpg,

CURRICULUM VITAE

Leila NAJAFI was born on 1979 in IRAN. She graduated from Yektayee High School, and enrolled at Tabriz University to study mechanical engineering IN 2000. She graduated with a Bachelor of Science degree in mechanical engineering from the Department of Mechanical Engineering. She began her MSc studies at the Department of Mechanical Engineering of Çukurova University2014.